



International Ocean Discovery Program Expedition 399 Preliminary Report

Building Blocks of Life, Atlantis Massif

12 April–12 June 2023

Andrew McCaig, Susan Q. Lang, Peter Blum, and the Expedition 399 Scientists

Publisher's notes

Core samples and the wider set of data from the science program covered in this report are under moratorium and accessible only to Science Party members until 3 May 2025.

This publication was prepared by the *JOIDES Resolution* Science Operator (JRSO) at Texas A&M University (TAMU) as an account of work performed under the International Ocean Discovery Program (IODP). This material is based upon work supported by the JRSO, which is a major facility funded by the National Science Foundation Cooperative Agreement Number OCE1326927. Funding for IODP is provided by the following international partners:

National Science Foundation (NSF), United States
Ministry of Education, Culture, Sports, Science and Technology (MEXT), Japan
European Consortium for Ocean Research Drilling (ECORD)
Ministry of Science and Technology (MOST), People's Republic of China
Australia-New Zealand IODP Consortium (ANZIC)
Ministry of Earth Sciences (MoES), India

Portions of this work may have been published in whole or in part in other IODP documents or publications.

Disclaimer

The JRSO is supported by the NSF. Any opinions, findings, and conclusions or recommendations expressed in this material do not necessarily reflect the views of the NSF, the participating agencies, TAMU, or Texas A&M Research Foundation.

Copyright

Except where otherwise noted, this work is licensed under the Creative Commons Attribution 4.0 International (CC BY 4.0) license (<https://creativecommons.org/licenses/by/4.0/>). Unrestricted use, distribution, and reproduction are permitted, provided the original author and source are credited.



Citation

McCaig, A., Lang, S.Q., Blum, P., and the Expedition 399 Scientists, 2024. Expedition 399 Preliminary Report: Building Blocks of Life, Atlantis Massif. International Ocean Discovery Program. <https://doi.org/10.14379/iodp.pr.399.2024>

ISSN

World Wide Web: 2372-9562

Expedition 399 participants

Expedition 399 scientists

Andrew McCaig

Co-Chief Scientist

Institute of Geophysics and Tectonics
School of Earth and Environment
University of Leeds
United Kingdom

a.m.mccaig@leeds.ac.uk

Susan Q. Lang

Co-Chief Scientist

Department of Geology and Geophysics
Woods Hole Oceanographic Institution
USA

sqlang@whoi.edu

Peter Blum

Expedition Project Manager/Staff Scientist

International Ocean Discovery Program
Texas A&M University
USA

blum@iodp.tamu.edu

Natsue Abe

Physical Properties Specialist/Downhole Measurements

Japan Agency for Marine-Earth Science and Technology
Japan

abenatsu@jamstec.go.jp

William Brazelton

Microbiologist

School of Biological Sciences
University of Utah
USA

william.brazelton@utah.edu

Rémi Coltat

Metamorphic Petrologist

Geosciences Department
Ecole Normale Supérieure Paris
France

remi.coltat54840@gmail.com

Also at

Instituto Andaluz de Ciencias de la Tierra
CSIC-UGR
Spain

Jeremy R. Deans

Physical Properties Specialist/Downhole Measurements

School of Biological, Environmental, and Earth Sciences
University of Southern Mississippi
USA

jeremy.deans@usm.edu

Kristin L. Dickerson

Physical Properties Specialist/Downhole Measurements

Department of Earth and Planetary Sciences
University of California, Santa Cruz
USA

krdicker@ucsc.edu

Marguerite Godard

Inorganic Geochemist

Department of Geosciences
University of Montpellier
France

marguerite.godard@umontpellier.fr

Barbara E. John

Structural Geologist

Department of Geology and Geophysics
University of Wyoming
USA

bjohn@uwyo.edu

Frieder Klein

Metamorphic Petrologist

Department of Marine Chemistry and Geochemistry
Woods Hole Oceanographic Institution
USA

fklein@whoi.edu

Rebecca Kuehn

Structural Geologist

Institute of Geosciences and Geography
Martin-Luther-University Halle-Wittenberg
Germany

rebecca.kuehn@geo.uni-halle.de

Kuan-Yu Lin

Igneous Petrologist

Department of Earth Sciences
University of Delaware
USA

kyklin@udel.edu

C. Johan Lissenberg

Igneous Petrologist

School of Earth and Environmental Sciences
Cardiff University
United Kingdom

lissenbergcj@cardiff.ac.uk

Haiyang Liu

Igneous Petrologist

Institute of Oceanology
Chinese Academy of Sciences
China

hyliu@gdio.ac.cn

Ethan L. Lopes

Paleomagnetist

Department of Geophysics
Stanford University
USA

ellopes@stanford.edu

Toshio Nozaka
Metamorphic Petrologist
Department of Earth Sciences
Okayama University
Japan
nozaka@cc.okayama-u.ac.jp

Andrew J. Parsons
Structural Geologist
School of Geography, Earth, and Environmental Sciences
University of Plymouth
United Kingdom
andy.parsons@plymouth.ac.uk

Vamdev Pathak
Paleomagnetist
Department of Geology
Central University of Punjab
India
vamdev.pathak@cup.edu.in

Mark K. Reagan
Igneous Petrologist
Department of Earth and Environmental Sciences
University of Iowa
USA
mark-reagan@uiowa.edu

Shore-based scientists

Ivan P. Savov
Shore-Based Scientist
School of Earth and Environment
University of Leeds
United Kingdom
i.savov@leeds.ac.uk

Outreach

Lesley Anderson
Onboard Outreach Officer
Science Planner
United States Antarctic Program
USA
lesley.science.education@gmail.com

Jordyn A. Robare
Microbiologist/Geochemist
School of Molecular Sciences
Arizona State University
USA
jrobare@asu.edu

Gordon Southam
Microbiologist
Earth and Environmental Sciences
The University of Queensland
Australia
g.southam@uq.edu.au

Fengping Wang
Geomicrobiologist
International Center for Deep Life Investigation (IC-DLI)
Shanghai Jiao Tong University
China
fengpingw@sjtu.edu.cn

C. Geoffrey Wheat
Inorganic Geochemist/Organic Geochemist
College of Fisheries and Ocean Sciences
University of Alaska Fairbanks
USA
wheat@mbari.org

Olivier J. Sissmann
Shore-Based Scientist
France
olivier.sissmann@ifpen.fr

Sarah N.R. Treadwell
Onboard Outreach Officer
Department of Communication
University of North Dakota
USA
treadwell.sarah@gmail.com

Also at
Blue Marble Space Institute
USA

Operational and technical staff

Siem Offshore AS officials

Harm Nienhuis
Master of the Drilling Vessel

Wayne Lambert
Drilling Supervisor

JRSO shipboard personnel and technical representatives

Matthew Allen
Engineer

Carel Lewis
Curatorial Specialist

Heather Barnes
Assistant Laboratory Officer

Nicholas Logan
Marine Computer Specialist

Erick Bravo Jimenez
Marine Laboratory Specialist

Maurice Martinez
Logging Engineer

Michael Cannon
Marine Computer Specialist

Zenon Mateo
Marine Laboratory Specialist

Oscar Cavazos
Marine Laboratory Specialist

William Mills
Laboratory Officer

Bridgette Cervera
Marine Laboratory Specialist

Doris Pinero Lajas
Assistant Laboratory Officer

Keith Dupuis
Publications Specialist

William Rhinehart
Operations Superintendent

Kirby Garrett
Logging Engineer

Alexander Roth
Marine Laboratory Specialist

Luan Heywood
Marine Laboratory Specialist

Johanna Suhonen
Marine Laboratory Specialist

Myriam Kars
Marine Laboratory Specialist

Kara Vadman
Marine Laboratory Specialist

Jan Kotze
Marine Instrumentation Specialist

Hai Zhao
Applications Developer

Abstract

International Ocean Discovery Program (IODP) Expedition 399 collected new cores from the Atlantis Massif (30°N; Mid-Atlantic Ridge), an oceanic core complex that hosts the Lost City hydrothermal field (LCHF). Studies of the Atlantis Massif and the LCHF have transformed our understanding of tectonic, magmatic, hydrothermal, and microbial processes at slow-spreading ridges. The Atlantis Massif was the site of four previous expeditions (Integrated Ocean Drilling Program Expeditions 304, 305, and 340T and IODP Expedition 357) and numerous dredging and submersible expeditions. The deepest IODP hole in young (<2 My) oceanic lithosphere, Hole U1309D, was drilled ~5 km north of the LCHF and reached 1415 meters below seafloor (mbsf) through a series of primitive gabbroic rocks. A series of 17 shallow (<16.4 mbsf) holes were also drilled at 9 sites across the south wall of the massif during Expedition 357, recovering heterogeneous rock types including hydrothermally altered peridotites, gabbroic, and basaltic rocks. The hydrologic regime differs between the two locations, with a low permeability conductive regime in Hole U1309D and a high (and possibly deep-reaching) permeability regime along the southern wall.

Expedition 399 targeted Hole U1309D and the southern wall area to collect new data on ancient processes during deformation and alteration of detachment fault rocks. The recovered rocks and fluids are providing new insights into past and ongoing water-rock interactions, processes of mantle partial melting and gabbro emplacement, deformation over a range of temperatures, abiotic organic synthesis reactions, and the extent and diversity of life in the subseafloor in an actively serpentinizing system. We sampled fluids and measured temperature in Hole U1309D before deepening it to 1498 mbsf. The thermal structure was very similar to that measured during Expedition 340T, and lithologies were comparable to those found previously in Hole U1309D. A significant zone of cataclasis and alteration was found at 1451–1474 mbsf. A new Hole U1601C (proposed Site AMDH-02A) was drilled on the southern ridge close to Expedition 357 Hole M0069A, where both deformed and undeformed serpentinites had previously been recovered. Rapid drilling rates achieved a total depth of 1267.8 mbsf through predominantly ultramafic (68%) and gabbroic (32%) rocks, far surpassing the previous drilling record in a peridotite-dominated system of 201 m. Recovery was excellent overall (71%) but particularly high in peridotite-dominated sections where recovery regularly exceeded 90%. The recovery of sizable sections of largely intact material will provide robust constraints on the architecture and composition of the oceanic mantle lithosphere. The deepest portions of the newly drilled borehole may be beyond the known limits of life, providing the means to assess the role of biological activity across the transition from a biotic to an abiotic regime.

Borehole fluids from both holes were collected using both the Kuster Flow-Through Sampler and the new Multi-Temperature Fluid Sampler. Wireline logging in Hole U1601C provided information on downhole density and resistivity, imaged structural features, and documented fracture orientations. A reentry system was installed in Hole U1601C, and both it and Hole U1309D were left open for future deep drilling, fluid sampling, and potential borehole observatories.

Plain language summary

The Earth's mantle is a thick (1802 miles; 2900 km) layer of dense rock that makes up most of the planet's mass. It has long been a goal to drill through the Earth's crust and into the upper mantle, but so far this has not been achieved, even in the oceans where the crust is relatively thin (6 km). In some places, mantle and lower crustal rocks have been brought to the seafloor by faulting associated with plate tectonics. One such place is the Atlantis Massif, an underwater mountain in the middle of the Atlantic Ocean. Mantle rocks are rich in the mineral olivine, and when they are altered by seawater they produce the mineral serpentine. Hydrogen is produced as a by-product of the reaction and can further fuel the generation of compounds such as methane, short-chain hydrocarbons, and organic acids in the absence of life. Hence, we can call these compounds "the building blocks of life" because when life began on Earth in the distant past, they may have been the precursors to more complex compounds, such as DNA, necessary for life to exist. At the pres-

ent day, this suite of compounds may be feeding ancient forms of microbial life far below the seafloor.

The goals of Expedition 399 were to recover rocks and fluids to provide new insights into how underwater mountains such as the Atlantis Massif form, to document the nonbiological reactions between water and rocks that may represent ancient systems that preceded life on Earth, and to assess the extent of life in the subseafloor. We deepened preexisting Integrated Ocean Drilling Program Hole U1309D by 83 m to reach a new depth of 1498 meters below seafloor and sampled fluids to understand the geochemical regime. The recovered rocks were gabbroic, typical of the lower crust, and temperatures near the bottom of the borehole were $\sim 140^{\circ}\text{C}$, similar to previous measurements. Drilling revealed a 23 m zone of fracturing and alteration.

A new Hole U1601C was also drilled on the southern wall of the massif and achieved a total depth of 1267.8 meters below seafloor with excellent overall recovery of 71%. It primarily consists of a long section of mantle rocks with intrusions of gabbro that cooled from injections of magma from depth. Previous drilling into this type of rock has not been nearly as successful and has only reached a maximum depth of 201 m. The recovery of sizable sections of largely intact mantle rocks will provide robust constraints on the structure and composition of the oceanic mantle lithosphere and the reactions that produce hydrogen. Downhole logging measurements were carried out to provide a continuous record of temperature, density, porosity, seismic velocity, and distributions of fractures. Water samples were collected from several depths within the borehole to determine the chemical and biological characteristics of fluids. Both Holes U1601C and U1309D were left open for future fluid sampling and potential borehole observatories.

1. Introduction

The Atlantis Massif oceanic core complex (OCC) (30°N ; Mid-Atlantic Ridge; Figure F1) has been investigated during four drilling expeditions (Integrated Ocean Drilling Program Expeditions 304,

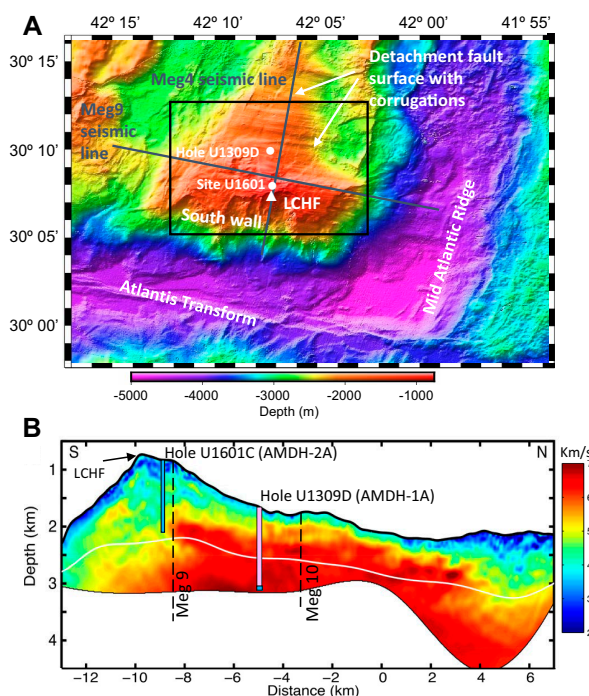


Figure F1. A. Atlantis Massif showing main structural features, location of LCHF, Hole U1309D, and Site U1601 (core recovered in Holes U1601A and U1601C). Bathymetry was collected during Expedition 357 (Früh-Green et al., 2018; Escartín et al., 2022). Box = area of Figure F2. B. Full waveform inversion of Seismic Line Meg 4 and locations of Holes U1309D and U1601C, with proposed site numbers. Blue = new core recovered during Expedition 399, pink = core from Expedition 304/305. Modified after Harding et al. (2016).

305, and 340T and International Ocean Discovery Program [IODP] Expedition 357) and numerous other cruises (Cann et al., 1997; Blackman et al., 1998; Kelley et al., 2001, 2005; Blackman et al., 2002, 2013; Karson et al., 2006; Canales et al., 2004, 2008; Lang et al., 2021). The southern wall of the massif hosts the Lost City hydrothermal field (LCHF), which has vented alkaline fluids rich in H_2 and CH_4 at temperatures of 40° – $116^\circ C$ for $>100,000$ y (Früh-Green et al., 2003; Ludwig et al., 2011; Kelley et al., 2005; Proskurowski et al., 2008; Seyfried et al., 2015). The LCHF is a model site for studying the serpentinization processes that lead to the creation of alkaline hydrothermal fluids rich in H_2 and CH_4 , which are proposed to occur on other planetary bodies. The Atlantis Massif has also been targeted by multiple expeditions to study the crustal accretion and OCC formation at slow-spreading ridges. Although previous expeditions to this site have sought to characterize these and other processes, drilling has yet to recover ultramafic rocks that are characteristic of the conditions thought to occur deep beneath the LCHF. To address these gaps in knowledge, the goal of the current expedition was to collect deeper cores from the Atlantis Massif from both Integrated Ocean Drilling Program Hole U1309D (proposed Site AMDH-01A) as well as from the southern wall in the footprint of shallower drilling carried out during Expedition 357 (Figures F1, F2, F3).

Hole U1309D in the central dome of the Atlantis Massif is located in the footwall to a large slip oceanic detachment fault system (Blackman et al., 2004; Blackman, Ildefonse, John, Ohara, Miller, MacLeod, and the Expedition 304/305 Scientists, 2006; Grimes et al., 2008) and penetrated largely gabbroic rocks to 1415 meters below seafloor (mbsf) (Figures F1, F2, F3, F4). This site contrasts with the southern wall of the massif near the LCHF, which predominantly consists of serpentinized peridotite with $\sim 20\%$ gabbroic rocks (Figures F1, F3, F5), and was extensively sampled by shallow coring during Expedition 357 (Früh-Green et al., 2018; Schroeder and John, 2004; Karson et al., 2006). At the top of the Massif is an oceanic detachment fault zone largely formed in serpentinites and minor gabbros above the southern wall and gabbros in Hole U1309D. Syntectonic diabase dikes intrude the fault rocks and are in turn deformed at both localities. Fault rocks include talc-tremolite-chlorite schists overprinting serpentinite, with fault breccias and cataclasites locally overprinting higher temperature fault rocks including amphibolites (Blackman et al., 2011; McCaig et al., 2010; McCaig and Harris, 2012).

During Expedition 399, we revisited Hole U1309D in the central dome of the massif and also drilled two new holes at Site U1601 (proposed Site AMDH-02A), within the footprint of Expedition 357 on the southern wall (Figures F1, F2, F3, F6; Table T1).

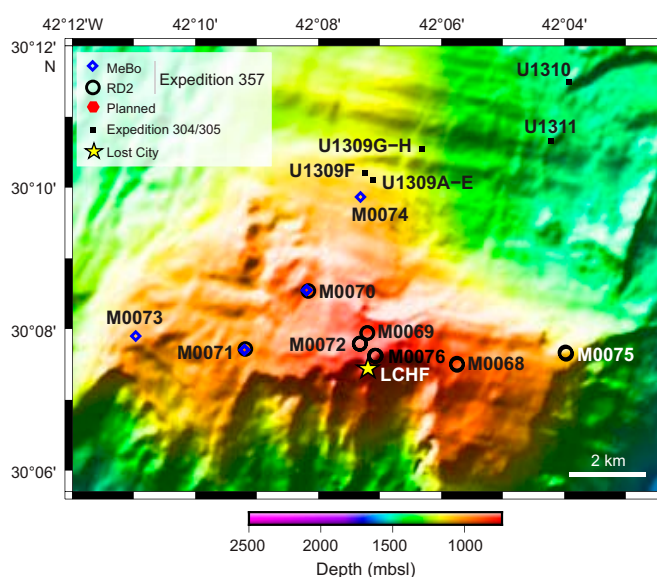


Figure F2. Location of previous drilling during Expeditions 304/305 and 357 (modified after Früh-Green et al., 2016). MeBo = Meeresboden-Bohrgerät 200 drill, RD2 = RockDrill2 drill. Expedition 399 sites are at Site U1309 (Hole U1309D; labeled U1309A–E) and between Sites M0069 and M0072 (Site U1601).

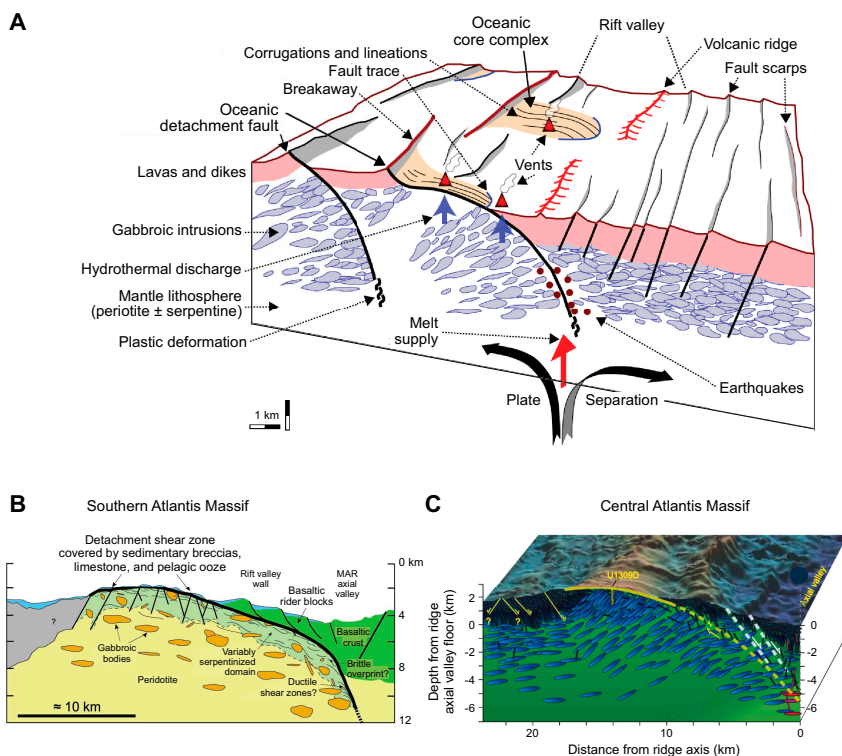


Figure F3. Conceptual sketches of tectonomagmatic evolution of heterogeneous lithosphere and denudation of mantle rocks as detachment faulting progresses (Früh-Green et al., 2016). A. Generic “detachment mode” seafloor (Escartín and Canales, 2011). B. Southern wall of Atlantis Massif is dominated by variably altered peridotites with gabbroic lenses (Boschi et al., 2006). 100 m thick detachment fault zone containing talc-tremolite-chlorite metasomatic schists is at the summit (Karson et al., 2006). MAR = Mid-Atlantic Ridge. C. In contrast, major gabbroic intrusions dominate the central dome (Grimes et al., 2008).

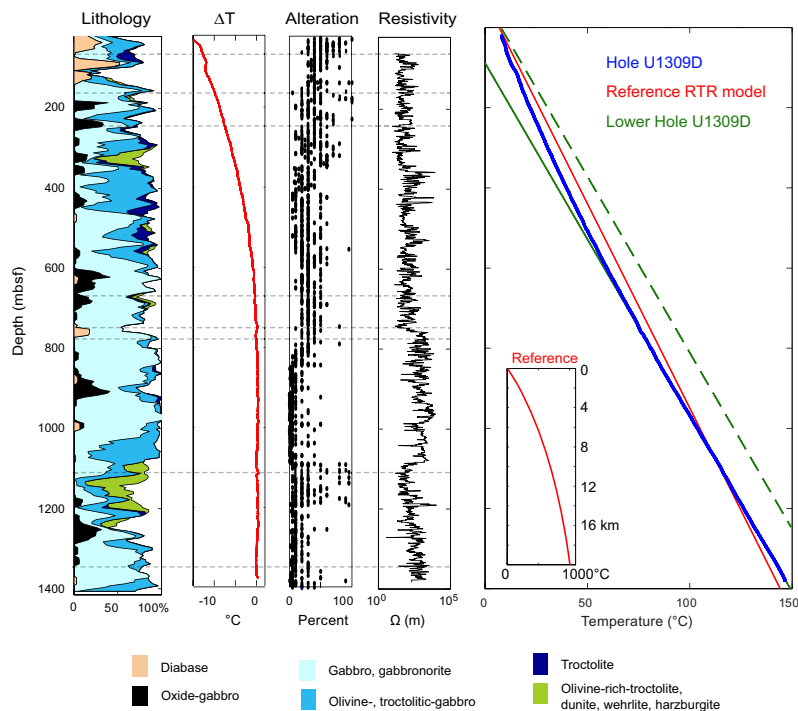


Figure F4. Lithology, temperature, and resistivity logging results, Expeditions 304/305 and 340T and Hole U1309D (after Blackman et al., 2014). ΔT = difference between observed temperature and an extrapolation of conductive gradient at depth to the surface. Minor excursions in temperature are interpreted to be zones of fluid flow at 746 mbsf, where temperature gradient changes from convective to conductive, and 1107 mbsf, near a zone of olivine-rich troctolite.

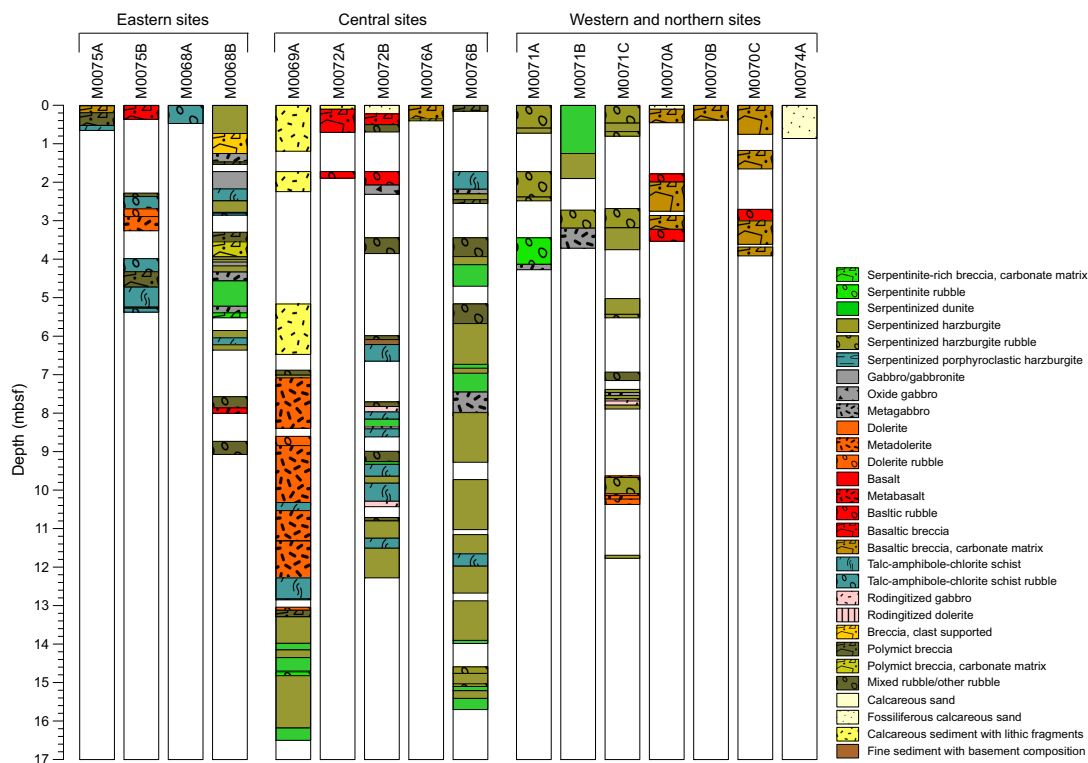


Figure F5. Lithologic summaries from Expedition 357 holes along southern wall of Atlantis Massive (from Früh-Green et al., 2016, 2018). Site U1601 is close to Hole M0069A, where metadolerite (metadiabase) intrudes into talc-tremolite-chlorite schists, both of which are brecciated and underlain by a subhorizontal brittle fault zone at ~13 mbsf. Below this fault are little-deformed serpentinized harzburgite and dunite. Beneath the soft-sediment layer, hole recovery was excellent.

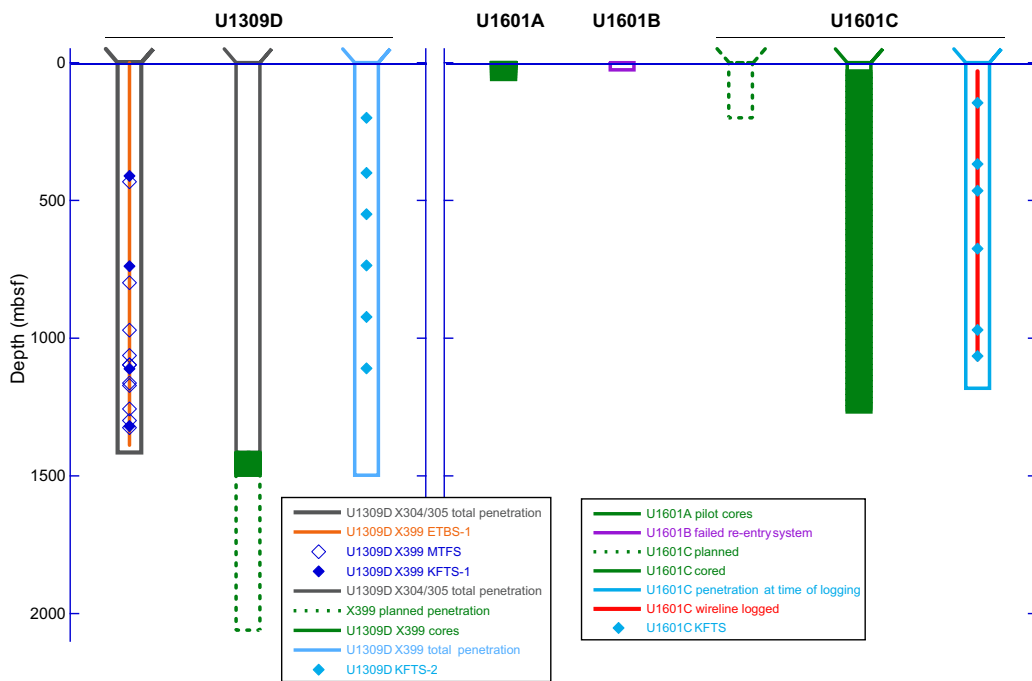


Figure F6. Expedition 399 operations summary. X = expedition. KFTS-1 = first KFTS deployment, KFTS-2 = second KFTS deployment.

Table T1. Expedition 399 operations summary. DSF = drilling depth below seafloor. RCB = rotary core barrel. MTFs = Multi-Temperature Fluid Sampler, ETBS = Elevated Temperature Borehole Sonde, KFTS = Kuster Flow-Through Sampler.

Hole	Latitude	Longitude	Water depth (m)	Total penetration DSF (m)	Cored interval (m)	Recovered length (m)	Recovery (%)	Drilled interval (m)	Drilled interval (N)	Total cores (N)	RCB cores (N)	Other cores (N)
399-												
U1309D	30°10.1195'N	42°7.1131'W	1644.9	82.5	82.5	48.93	59		0	17	17	1
U1601A	30°7.9260'N	42°7.2255'W	850.0	60.6	60.6	14.52	24		0	12	12	0
U1601B	30°7.9339'N	42°7.2171'W	850.0	26.0			0	26.0	1	0	0	0
U1601C	30°7.9417'N	42°7.2072'W	850.0	1267.8	1244.8	886.03	71	23.0	1	257	257	1
Expedition 399 totals:				1436.9	1387.9	949.48		49.0	2	286	286	2

Hole	Temperature and fluid sampling with MTFs-ETBS	Temperature and fluid sampling with dual KFTS-ETBS	Geophysical wireline logging	Date started (Expedition 399)	Start time UTC (h)	Date finished (Expedition 399)	End time UTC (h)	Time on hole (d)
399-								
U1309D	1 coreline run	5 coreline runs		25 Apr 2023	0715	4 Jun 2023	0430	8.08
U1601A				19 Apr 2023	0545	22 Apr 2023	1730	3.49
U1601B				22 Apr 2023	1730	25 Apr 2023	0715	2.54
U1601C		4 coreline runs	5 tool strings	1 May 2023	2245	2 Jun 2023	1800	31.80
								45.91

The data summarized in this report are based on shipboard sample curation and core descriptions. Because of shipboard circumstances, the Hole U1601C cores were recurated and re-described at the Gulf Coast Repository (College Station, Texas [USA]) during the fall/winter of 2023 by a shore-based team of technicians and scientists, leading to changes in reported lithology, alteration petrology, and structural features and adjustments to stratigraphic intervals. Sample names and depths in this report are not updated to reflect these changes; they will be reflected in the more detailed Expedition Reports section of the Expedition 399 *Proceedings of the International Ocean Discovery Program* volume.

2. Background

2.1. Previous holes in basement rocks

Several previous Deep Sea Drilling Project (DSDP)/Ocean Drilling Program (ODP)/Integrated Ocean Drilling Program/IODP expeditions have succeeded in drilling holes deeper than 100 m into the igneous basement, and they highlight the scientific value of both the recovered material and the borehole itself (Figure F7). The deepest is DSDP Hole 504B, which succeeded in drilling into the sheeted dike complex in the Nazca Plate. Hole 504B has been visited repeatedly for water sampling and hydrogeology experiments (Magenheim et al., 1995; Becker et al., 2004; Teagle, Alt, Umino, Miyashita, Banerjee, Wilson, and the Expedition 309/312 Scientists, 2006).

Two deep boreholes, ODP Hole 735B and IODP Hole U1473A, were drilled into gabbro on the Atlantis Bank, SW Indian Ridge (Table T2; Natland and Dick, 2002; Dick et al., 2017). The second deepest is Hole U1309D in the Atlantis Massif, which is by far the deepest basement hole in young (<2 Ma) lithosphere (Blackman et al., 2011). Most successful drilling has occurred in OCCs or slow-spread crust because the gabbroic layer in fast-spread crust has proved very hard to reach, the exceptions are ODP Leg 147 Hole 894B (Gillis, Mével, Allan, et al., 1993) and Integrated Ocean Drilling Program Hole U1415P, which recovered layered gabbros near the base of the faulted rift wall of the Cocos Plate at Hess Deep (Gillis et al., 2014).

Very few expeditions have recovered significant lengths of mantle rocks. Two holes from ODP Leg 147 to Hess Deep Rift (Holes 895D and 895E) penetrated 93.7 and 87.6 m, respectively (Gillis, Mével, Allan, et al., 1993). Six holes were started at this site, coring 272.9 m but recovering only 64.6 m. All the other boreholes drilled into mantle rocks are located on the slow-spreading Mid-Atlantic Ridge, including ODP Leg 153 Holes 920B and 920D (23°N; Mid-Atlantic Ridge; Cannat, Karson, Miller, et al., 1995) and ODP Leg 209 Holes 1271B, 1272A, 1268A, and 1274A (12°–16°N;

Mid-Atlantic Ridge; Kelemen, Kikawa, Miller, et al., 2004). At 200.9 m, Hole 920D is the deepest hole drilled in mantle rocks prior to this expedition. Peridotite can only be exposed on the seafloor by faulting, and drilling fault rocks has contributed to the poor recovery and penetration of previous holes.

Previous holes in serpentinized peridotite have often hosted significant thicknesses of gabbroic rock and have led to important insights into the nature of slow-spread lithosphere (Cannat, 1996) and processes such as melt-rock reaction, deformation, and serpentinization (Coogan et al., 2000a, 2000b; Karson et al., 1997). However, poor recovery has hampered systematic study of relationships, and drilling a deep hole into serpentinized and fresh peridotite was one of the main aims of Expeditions 304 and 305 in the Atlantic Massif (Blackman et al., 2004). This aim was frustrated when 1415 m of gabbroic rocks was recovered instead.

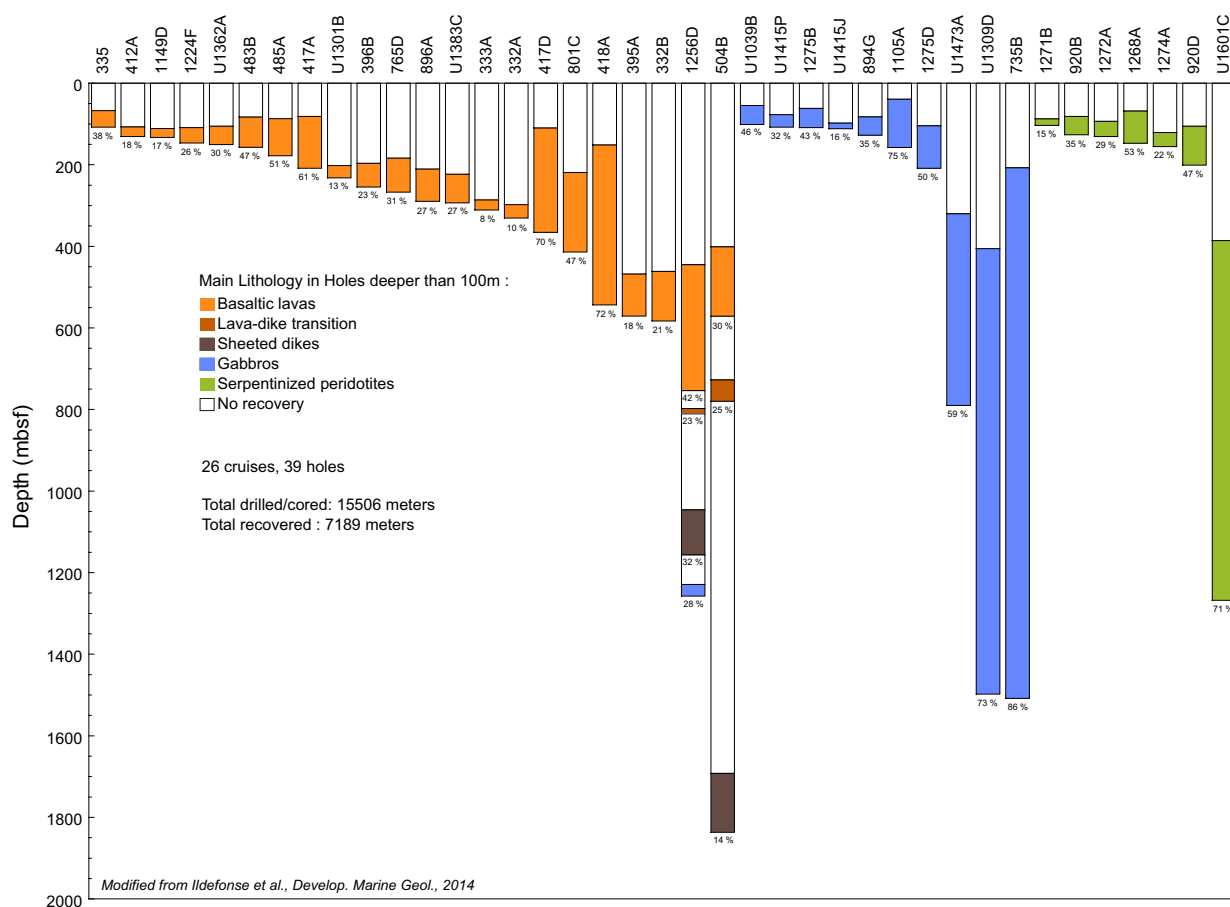


Figure F7. Summary of all DSDP/ODP/IODP holes with >100 m basement penetration (modified after Ildefonse et al., 2014), with Hole U1309D updated to reflect additional penetration during Expedition 399 and Hole U1601C added.

Table T2. Summary of holes drilled >750 m into oceanic lithosphere.

Hole	Depth (mbsf)	Total bit runs (including logging)	Leg/Expedition	Site name	Latitude	Longitude
U1473A	790	24	IODP Expedition 360	Atlantis Bank, Southwest Indian Ridge	32°42.340'S	57°16.691'E
U1601C	1267	8	IODP Expedition 399	Atlantis Massif	30°7.942'N	42°7.207'W
U1309D	1498	12	Integrated Ocean Drilling Program Expeditions 304 and 305 and IODP Expedition 399	Atlantis Massif	30°10.120'N	42°7.113'W
735B	1508	14	ODP Legs 118 and 176	Atlantis Bank, Southwest Indian Ridge	32°43.395'S	57°15.959'E
1256D	1522	62	ODP Leg 206 and Integrated Ocean Drilling Program Expeditions 309, 312, and 335	Guatama Basin	6°44.16'N	91°56.06'W
504B	2111	98	DSDP Legs 69, 70, 83, and 93 and ODP Legs 111, 137, 140, and 148	Costa Rica Rift	1°13.611'N	83°43.818'W

2.2. Geologic setting

The Atlantis Massif is an inside corner high on the right-stepping, sinistral, Atlantis I transform fault at 30°N on the Mid-Atlantic Ridge (Figure F1). The massif formed within the last 1.2–2 My (Grimes et al., 2008; Escartín et al., 2022). It was the first corrugated massif identified as an OCC (Cann et al., 1997), and it is capped by a domal detachment fault with corrugations parallel to the spreading direction (Figure F3). To the east, the detachment surface disappears beneath a hanging wall composed of fresh basaltic rocks and is truncated by steep east facing median valley faults. Recent interpretations (Escartín et al., 2022) suggest that a relic of the detachment fault has been trapped in the bottom of the axial valley by a westward ridge jump. To the west, a breakaway is assumed to be present but has never been unequivocally located. The shallowest part of the massif is at the top of the south wall, with a depth <700 meters below sea level (mbsl), and the detachment fault slopes north toward the central massif, where Site U1309 is located. To the north, the detachment is inferred to disappear beneath faulted blocks of basalt.

Early work on the massif concentrated on dredging and submersible studies along the south wall and to a lesser extent the dome (Figure F3B), which is dominated by serpentized peridotite with inclusions of gabbro (Cann et al., 1997; Blackman et al., 1998, 2002). This slope is a transform fault wall degraded by slope failure, and it may be the substrate supporting the LCHF (Kelley et al., 2001, 2005). Geophysical surveys include a refraction experiment (Detrick and Collins, 1998) and multichannel seismic (MCS) profiles (Canales et al., 2004). High velocities were inferred from the refraction data and interpreted to be fresh peridotite at shallow depths. However, Hole U1309D (drilled during Expeditions 304 and 305 in 2004 and 2005) showed that the central massif was floored predominantly by gabbro to at least 1415 mbsf (Figures F3, F4), requiring reevaluation of the internal structure of the Atlantis Massif and the geophysical interpretation (Blackman et al., 2011). Canales et al. (2008) reprocessed the MCS data in terms of *P*-wave tomography, showing high velocities in the central massif and lower velocities under the South Ridge, with a steep contact between a gabbroic domain and a serpentinite domain to the south. Further processing of the MCS data by Henig et al. (2012) improved the resolution of the imaging, and full waveform inversion (Figure F1B) by Harding et al. (2016) produced sharper and more detailed images, groundtruthed by the deep Hole U1309D (Figure F4). It remains very difficult to resolve variably serpentized peridotite from variably altered gabbro beneath the South Ridge, but an irregular intrusive contact between gabbro and partially serpentized peridotite seems likely.

Hole U1309D was revisited during Expedition 340T (Blackman et al., 2013, 2014), which carried out an extensive wireline logging program, including a vertical seismic profile (VSP) and a temperature profile. The temperature gradient was nearly linear below 750 mbsf, indicating a conductive thermal gradient in the lower part of the hole.

Paleomagnetic data from Hole U1309D frequently show multicomponent remanences, mainly in the upper part of the hole (Morris et al., 2009; John et al., 2009). Inclinations of the primary remanence are shallower than expected at 30°N, and integration of paleomagnetic data with Formation MicroScanner (FMS) logging has allowed the declination of primary remanence to be constrained, indicating at least 45° of anticlockwise rotation about a ridge-parallel axis (Morris et al., 2009; Pressling et al., 2012). The section sampled in Hole U1309D was therefore likely dipping at <45° west when it formed, and interpretation of all high temperature events should be interpreted in terms of distance from an originally steep detachment fault at depth, rather than the seafloor (cf. McCaig and Harris, 2012)

Expedition 357 was a mission-specific platform expedition during which a series of 17 shallow holes were drilled (to a maximum of 16.4 mbsf) at 9 locations in the southern part of the massif using seabed drills (Figures F1, F2, F5) (Früh-Green et al., 2017, 2018). The majority of the sites were located along an 8.5 km east–west profile perpendicular to the plate spreading on the Mid-Atlantic Ridge, accessing lithosphere of distinct ages. Two sites were drilled on the eastern part, closest to the spreading center (Sites M0068 and M0075), three sites were drilled in the central section north of the LCHF (Sites M0069, M0072, and M0076), and two sites were drilled on the western end (Sites M0071 and M0073). Excellent sections were collected of heterogeneous rocks through fault and alteration zones from these drill sites. The cores from the central sites at the top

of the massif and closest to Lost City were predominately composed of pervasively serpentinized harzburgite. Mafic rocks were less prevalent in these central locations compared to Hole U1309D, suggesting a different mode of melt accumulation. Two additional locations were drilled closer to the central dome of the massif (Sites M0070 and M0074) to target the mafic, plutonic domain drilled at Site U1309, but with limited recovery of only surficial material.

2.3. Igneous petrology

Rocks recovered from Hole U1309D include a sequence of gabbro and olivine gabbro (Figures F4, F8) with intervals of troctolite and olivine-rich troctolite and several diabase intrusions in the uppermost 100 m of the hole (Blackman, Ildefonse, John, Ohara, Miller, MacLeod, and the Expedition 304/305 Scientists, 2006; Blackman et al., 2011). Back-correcting for rotation, the diabase intrusions in the detachment zone could represent a lateral dike–gabbro transition (McCaig and Harris, 2012). Olivine-rich troctolites are interpreted to be mantle rocks modified by melt–rock reaction (Drouin et al., 2009, 2010; Ferrando et al., 2018); less modified mantle rocks are confined to very short intervals (<1 m) at shallow depths. The petrology and geochemistry of these mantle peridotite derived samples were studied by Tamura et al. (2008). The gabbro contains many internal contacts (Suhr et al., 2008; John et al., 2009) and local igneous layering. Plutonic rocks recovered from Hole U1309D are amongst the most primitive ever recovered from the ocean floor in Holes U1309B and U1309D (Godard et al., 2008) (Figure F8). Unlike other drilled plutonic sections (Pacific Ocean: DSDP Hole 147 and ODP Hole 1256D; Indian Ocean: ODP Holes 735B and 1105A and IODP Hole U1473A), many of the Atlantis Massif plutonic rocks are in equilibrium with mid-ocean ridge basalt (MORB), with some primitive enough to have formed directly from primary mantle melts. Furthermore, they record significant isotopic heterogeneity, attesting to the delivery of individual batches of mantle melt to the plutonic section (Lambart et al., 2019). Hence, the Atlantis Massif offers a unique opportunity to study the compositions of melts delivered to the crust from their mantle source and how they evolve to MORB. This is paramount; crustal evolution of melt is now recognized to be significantly more complicated than previously realized, involving not only fractional crystallization but also in situ crystallization and reactive porous flow (Lissenberg and MacLeod, 2017). Hence, interpreting MORB compositions and implications for the upper mantle is highly nonunique, unless melt evolution processes in the lower crust are quantified (Godard et al., 2009).

The sequence of rocks on the south wall of the Atlantis Massif beneath Lost City has been summarized by Karson et al. (2006) and consists largely of highly serpentinized peridotites with gabbroic intervals (Figure F3). Gabbros here and in Expedition 357 cores have an uncertain relationship to the main gabbro farther north. They may be intrusions of different age or level of exhumation, or

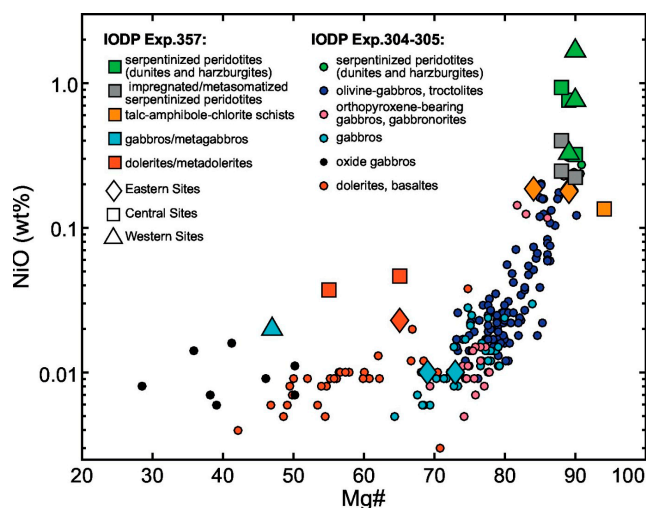


Figure F8. Summary of bulk rock igneous compositions, Hole U1309D (Expedition 304/305; Godard et al., 2009) and Expedition 357 core samples (Früh-Green et al., 2018). Note very primitive compositions of many of the gabbroic rocks compared to the diabase (dolerite) dikes, which are similar to MORB at 30°N in the Atlantic. $Mg\# = 100 \times Mg/(Mg + Fe)$.

they may be satellites of the larger body. Establishing the genetic relationship between these bodies is important.

2.4. Structural and alteration history of the massif

The overall structure of the Atlantis Massif is domal, with much of the top showing spreading-parallel corrugations identified as a low angle detachment fault. To the east the detachment fault plunges beneath hanging wall basalts, and locally dips toward the transform valley to the south (Escartín et al., 2022). Holes drilled in the top of the massif are expected to pass through the detachment fault zone, estimated by Karson et al. (2006) to be ~100 m thick (Figure F3).

The Hole U1309D section is remarkable for the paucity of high-temperature crystal-plastic fabrics compared to the only other deep holes into the footwall of OCCs, including the Atlantis Bank (Dick et al., 2017; Ildefonse et al., 2007; McCaig et al., 2010). However, significant breccia intervals occur in the uppermost 100 m of Holes U1309B and U1309D (Blackman et al., 2011). These both deform and are cut by syntectonic diabase intrusions common in the same interval (Figures F4, F5). Brecciation is inferred to have occurred over a wide range of temperatures up to >700°C (McCaig and Harris, 2012). Alteration is pervasive in the upper part of Hole U1309D, and isotopic data show the detachment fault zone to be highly altered by seawater-derived fluids at temperatures similar to black smoker fluids (McCaig et al., 2010). Greater intensities of crystal-plastic deformation were found in gabbroic lenses in peridotite on the south wall of the massif (Schroeder and John, 2004) and in the shallow cores from Expedition 357 (Früh-Green et al., 2018).

Intense alteration in the shallow Expedition 357 cores (Früh-Green et al., 2018; Rouméjon et al., 2017) is generally consistent with previous work on the south wall (Boschi et al., 2006). Early serpentine replacing olivine is locally overprinted by talc-tremolite-chlorite assemblages frequently associated with mafic intrusions and/or shearing. Carbonate veining is surprisingly rare and almost exclusively observed at the drill sites closest to the LCHF (Ternieten et al., 2021). Extensive water-rock interaction at variable temperatures is further reflected in heterogeneous sulfur isotope compositions (Liebmann et al., 2018). These document a complex evolution of the hydrothermal system with episodes of low-temperature serpentinization and incorporation of seawater sulfate facilitating microbial activity and episodes of high-temperature water-rock interaction controlled by the intrusion of microgabbroic veins, accompanied by considerable mass transfer.

Alteration in Hole U1309D records progressive fluid influx during cooling from magmatic to ambient temperatures. It is pervasive above 300 mbsf, with olivine-plagioclase reactions forming amphibole and chlorite in characteristic corona textures, reflecting temperatures above 500°C (Nozaka and Fryer, 2011). Deeper, the corona texture is restricted to the vicinity of fault zones and lithologic contacts, but partial serpentinization of olivine is common in many intervals and frequently accompanied by prehnite and hydrogarnet replacing plagioclase (Frost et al., 2008). Serpentinization reactions are complex, including early brucite-antigorite veins followed by more pervasive lizardite-magnetite (Beard et al., 2009). Olivine alteration in gabbros at low temperatures often produces saponite (Nozaka et al., 2008). Saponite in harzburgite has been observed to host nitrogenous compounds, including the amino acid tryptophan, which may be synthesized abiotically (Ménez et al., 2018). Alteration of Sr isotope ratios by seawater-derived fluids is common in the upper part of the hole but decreases below 350 mbsf and is mainly present in serpentine-rich intervals where the primary Sr content is low and the seawater signal may be carried by carbonates (McCaig et al., 2010). Alteration of oxygen isotope ratios away from primary igneous values is more persistent, but also reduces downhole, affecting only visibly altered rocks. $\delta^{18}\text{O}$ is almost always <5.7‰ (the average composition of unaltered mantle and ocean crust), indicating that the dominant reactions were at temperatures >200°–250°C (McCaig et al., 2010), where the fractionation between rock and water is <5.7‰.

Reaction porosity and permeability produced by dissolution of minerals at the grain scale or greater is common in the upper part of Holes U1309B and U1309D and has been found in chloritized gabbros in Expedition 357 cores (McCaig et al., 2022). Rapid dissolution of primary minerals can occur if far from equilibrium hot fluid is in excess, as is likely in the upflow zone of a black smoker system (Cann et al., 2015).

Initial cooling of the massif was rapid, based on paleomagnetic (Morris et al., 2009), geochronological, and thermochronological data (Grimes et al., 2008; Schoolmeesters et al., 2012) and diffusion timescales (Ferrando et al., 2020). This may have been linked to circulation of black smoker fluids in the detachment fault zone (McCaig et al., 2010; McCaig and Harris, 2012) in an early phase of circulation compared to the current phase of lower temperature venting at the LCHF.

2.5. Present day thermal structure and hydrothermal circulation

Expedition 340T (Blackman et al., 2014) found that the temperature profile in Hole U1309D was conductive below 750 mbsf, with a gentle curvature suggesting slow downflow of fluid above that depth (Figure F4). Minor excursions in downhole temperature at 750 and 1100 mbsf suggest fluid influx into permeable fault zones. To vent at temperatures up to 116°C, the LCHF must mine fluid to several kilometers depth, based on inferences of circulation temperatures from fluid chemistry (Kelley et al., 2005; Allen and Seyfried, 2004, 2005; Foustoukos et al., 2008; Lang et al., 2012; Seyfried et al., 2015) and hydrothermal modeling (Titarenko and McCaig, 2016; Lowell, 2017). Close to the seafloor, the LCHF is localized by faulting (Denny et al., 2016); whether more diffuse or multichannel flow occurs at depth or whether there is shallow recharge and mixing is very important for the chemical and hence microbiological evolution of the system and therefore underpins all of our main objectives. The LCHF may be driven in part by exothermic serpentinization reactions (Früh-Green et al., 2004), but this is not certain because a lateral permeability change could stabilize and sustain the LCHF over long periods of time (Titarenko and McCaig, 2016). New measurements of the thermal structure and fluid flow at depth at Site U1601 close to Lost City can provide important constraints on the hydrogeology of the Atlantis Massif.

2.6. Potential for abiotic organic synthesis

It is axiomatic that before life could begin on Earth or other worlds in the solar system, precursors of DNA, RNA, proteins, and other biologically relevant macromolecules must have been synthesized without biological intervention (Stüeken et al., 2013). The LCHF and Atlantis Massif have many features that make these synthesis reactions favorable; these locations have therefore been proposed as a model for the early Earth settings where prebiotic chemistry may have led to life (Kelley et al., 2002b; Martin et al., 2008). Serpentinization and abiotic organic synthesis reactions play a major role in generating H₂ and organic carbon molecules that are carried with fluids, including methane, ethane, propane, and small carboxylic acids such as formate (Kelley et al., 2001, 2005; Proskurowski et al., 2008; Lang et al., 2010, 2018; Wang et al., 2018; Klein et al., 2019). In samples recovered from nearby Hole U1309D, the amino acid tryptophan and additional carbonaceous material have been identified in association with iron-rich saponitic clays and proposed to be synthesized abiotically (Pisapia et al., 2018; Ménez et al., 2018).

A major driving factor for organic synthesis reactions is the production of H₂ in association with serpentinization reactions, which makes the reduction of CO₂ thermodynamically favorable (McCullom and Seewald, 2007, 2013). H₂ is likely to be generated from the reduction of H₂O in circumstances where the average Fe³⁺/Fe²⁺ ratio of secondary minerals is higher than that of primary minerals (McCullom and Bach, 2009; Klein et al., 2009; Andreani et al., 2013). Experiments suggest generation rates are highest around 300°C (McCullom et al., 2016). Hydrogen has been detected in the water column widely across the Atlantis Massif, even in locations not associated with the focused circulation pathway of the LCHF (Lang et al., 2021).

Temperature and lithology are likely additional major controls on the type and abundance of organic compounds synthesized at the Atlantis Massif. Some reduced compounds, such as methane and short-chain alkanes, are believed to form through Fischer-Tropsch-type reactions at temperatures well above the known limit to life (Proskurowski et al., 2008; Wang et al., 2018; Klein et al., 2019), perhaps catalyzed by Fe-, Ni-, and Cr-bearing minerals (Foustoukos and Seyfried, 2004). These compounds may form at high temperature, trapped in fluid inclusions, and be mobilized into circulating fluids when the system is at lower temperatures (Kelley and Früh-Green, 1999, 2001; Klein et al., 2019). In contrast, the formation of carboxylic acids, amino acids, and carbonaceous material likely proceeds at lower temperatures (<400°C), including within thermal regimes

conductive to life (Lang et al., 2010; 2018; McDermott et al., 2015; Ménez et al., 2018; Klein et al., 2019; Andreani et al., 2023).

One goal of Expedition 399 was to examine abiotic organic synthesis in multiple settings spanning distinct thermal and geochemical regimes. Hole U1309D contains core material that never experienced temperatures lower than 140°C. Site U1601 was targeted as a location that could potentially recover material currently undergoing active serpentinization. In addition to recovering core material, we aimed to collect fluid samples from within the boreholes to provide critical insights into volatile and elemental distributions.

2.7. Thermal limits of life and the deep biosphere in the oceanic crust

To date, there is very little information about the existence of a deep biosphere in subseafloor serpentinizing systems. The warmest, highest pH domains of carbonate chimneys from the LCHF are dominated by a single clade of Lost City Methanosarcinales (Schrenk et al., 2004). Chimney exteriors are mixing zones between seawater and anoxic alkaline fluids and create gradients conducive to biochemical and microbial activity (Summit and Baross, 2001; McCollom and Seewald, 2007; Lang and Brazelton, 2020). DNA sequencing and lipid biomarker analyses have identified communities involved in H₂, CH₄, and sulfur cycling (Bradley et al., 2009; Brazelton and Baross, 2010; Brazelton et al., 2010, 2006; Méhay et al., 2013; Lang et al., 2018). A portion of the community actively cycles formate, an organic acid formed abiotically, deep in the circulation pathway (Lang et al., 2018; McGonigle et al., 2020).

Insights into the constraints on life in the subseafloor and the metabolic strategies that the small numbers of inhabitants employ can be gained in part through characterization of the endolithic communities. Distinguishing endemic microbial taxa from those introduced from seawater or contamination is a major challenge requiring multiple strategies to overcome (Kallmeyer, 2017; Sylvan et al., 2021; Pendleton et al., 2021). Nonetheless, the signatures of endolithic communities have been successfully identified from the subseafloor of the Atlantis Massif during both Expeditions 304 (Mason et al., 2010) and 357 (Motamedi et al., 2020; Goordial et al., 2021; Quéméneur et al., 2019) (Figure F9). Despite the widespread dominance of communities that cycle H₂ and CH₄ in the Lost City hydrothermal chimneys (Schrenk et al., 2004, 2013; Brazelton et al., 2006), genes associated with H₂ and CH₄ metabolisms were rare or absent in the Atlantis Massif subseafloor (Goordial et al., 2021). In general, the genes necessary for autotrophic carbon fixation pathways were rare, whereas those associated with heterotrophy were regularly identified (Quéméneur et al., 2019; Motamedi et al., 2020; Goordial et al., 2021). Enrichment experiments also primarily identified microorganisms that rely on heterotrophy (Quéméneur et al., 2019). Although early indications suggested that alkane degradation may be an important metabolic strategy in the gabbroic-dominated Hole U1309D (Mason et al., 2010), genes associated with alkane degradation

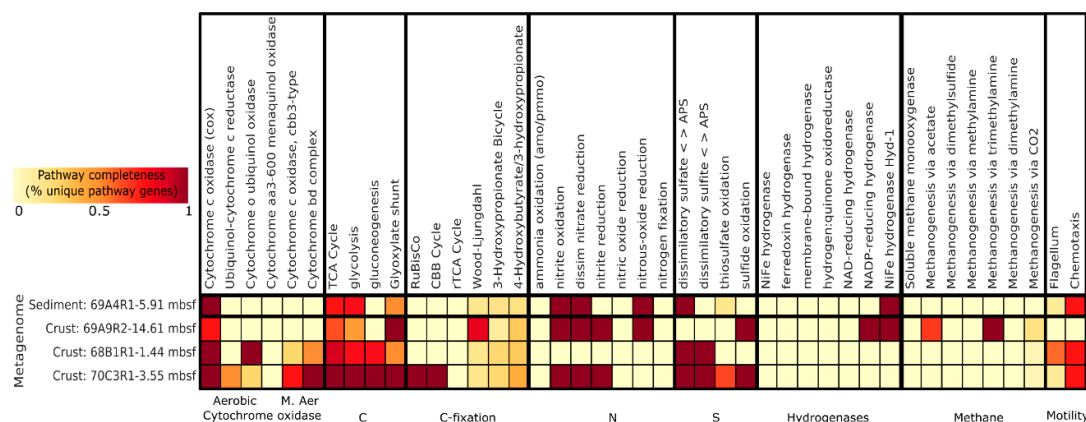


Figure F9. Metabolic potential of microbial communities isolated from subsurface sediments and crust from Atlantis Massif Expedition 357 samples based on metagenomes. Genes associated with autotrophy, including methanogenesis and methanotrophy, and alkane degradation were rare. Identified genes were associated with heterotrophy, aerobic carbon monoxide, and formate cycling. M. Aer oxidase = microaerobic cytochrome oxidase. From Goordial et al. (2021).

were not detected in metagenomic studies of the more ultramafic Expedition 357 cores (Goordial et al., 2021). Using high-pressure incubations, a strictly anaerobic, mesophilic bacterium that relies on fermentation of organic compounds for growth was successfully isolated from Expedition 357 Hole M0070C (Quéméneur et al., 2019).

Together, these data point to communities that are adapted to the Atlantis Massif seafloor and quite distinct from those that inhabit the chimneys of the LCHF. Instead of capitalizing on the abundant thermodynamic energy available for autotrophy from the co-occurrence of H_2 , CH_4 , and SO_4 (Lang and Brazelton, 2020), they appear to rely instead on organic molecules that are either transported with seawater or synthesized in situ. Collecting deep samples from an actively serpentinizing system will allow us to explore the hypothesis that something (pH, low carbon dioxide availability, water availability, etc.) limits the biosphere in this subsurface system. It will also help us constrain the source of the organics that these communities require and determine whether they consume the abiotic organic molecules created as a result of serpentinization reactions.

3. Scientific objectives

The Atlantis Massif is one of the best studied near-ridge sites in the ocean floor; this allows our objectives to be driven by process and hypothesis rather than exploration. Operations during Expedition 399 were designed to address the following objectives.

3.1. Objective 1: characterizing the life cycle of an oceanic core complex and the links among igneous, metamorphic, structural and fluid flow processes

Previous work summarized above shows that the massif is <2.0 Ma old and has been exposed by detachment faulting. A full range of processes including partial melting, intrusion of gabbros and melt-rock reaction, alteration and hydration by seawater over a wide range of temperatures, and deformation both within the detachment fault zone and at greater depths have occurred over this short time interval. This includes structure rotation by $\sim 45^\circ$ during the faulting process. The new data and samples collected as part of the expedition can provide insights into these ancient processes recorded in the rocks. In turn, fluid sampling and borehole temperature measurements can constrain the current thermal and hydrological structure of the massif and ongoing processes of fluid-rock interaction.

3.2. Objective 2: accessing the chemical kitchen that preceded the appearance of life on Earth

Environments that are actively serpentinizing have been proposed as potential locations for the origin and evolution of early life because water-rock reactions produce alkaline conditions that are favorable for prebiotic chemistry, H_2 that can drive the reduction of CO_2 to organic molecules, and gradients of redox and pH that promote biochemical reactions (Martin and Russell, 2006; Sojo et al., 2016). A consensus is emerging that serpentinization related reactions play a major role in generating H_2 , CH_4 , short-chain hydrocarbons, organic acids, amino acids, and reduced carbonaceous material (Kelley and Früh-Green, 1999; Proskurowski et al., 2008; McCollom and Bach, 2009; McCollom and Seewald, 2013; Klein et al., 2013, 2019; Lang et al., 2010, 2018, 2021; McDermott et al., 2015; Ménez et al., 2018; Andreani et al., 2023). These compounds can become mobilized and available for microbial activity at lower temperatures around vent systems such as the LCHF, potentially the type of location where life evolved on the early Earth (Kelley et al., 2002a). The geochemical signatures of modern serpentinizing systems can provide important insights to the ancient processes that may have occurred, but modern overprints such as reactions with oxygen and active microbial communities obscure signals.

An open question is what the rates of serpentinization, hydrogen generation, and organic synthesis may be. A major goal of the expedition was to link abundances of H_2 and organic molecules with the physical, chemical, and temporal conditions that lead to their synthesis. A second major goal was to leave both the deepened Hole U1309D and the new peridotite-hosted hole at Site

U1601 in a condition such that future expeditions could relog them for temperature and conduct fluid sampling.

3.3. Objective 3: characterize the deep biosphere and limits for life in the Atlantis Massif, in particular the impact of lithologic substrate, porosity, permeability, temperature, fluid chemistry, and reactive gradients

Results from shallow (<16.4 mbsf) coring on the southern wall during Expedition 357 indicate that the crustal subseafloor at the Atlantis Massif is a very low biomass ecosystem (Figure F10) compared to other crustal subsurface systems (Früh- Green et al., 2018). However, the depth of coring may not have been sufficient to intersect with large fluid flux pathways. Sampling for microbiological studies during Expedition 357, and during Expeditions 304 and 305 where low cell counts were also noted from Hole U1309D, did not specifically target the porous and permeable zones most likely to contain more substantial biomass. Despite low biomass, communities adapted to in situ conditions have been identified in recovered core material, including successful enrichment cultures (Mason et al., 2010; Quéméneur et al., 2019; Motamedi et al., 2020; Goordial et al., 2021). A target for Expedition 399 was to preferentially sample zones of higher porosity and permeability to test whether these regimes are associated with higher cell abundances. The highest cell counts recovered from Expedition 357 were adjacent to highly chloritized gabbro with relict reaction porosity, which was infilled with chlorite down to conditions of <100°C (McCaig et al., 2022). Increased porosity, a less alkaline local fluid, or chemical gradients between serpentinite and gabbro may have promoted microbial growth. A major aim of drilling at Site U1601 was to recover samples that are similarly vuggy or in zones with mixed lithology or fluid chemistry.

The thermal structure of the Atlantis Massif offers a unique opportunity to study the temperature limits of a deep life in a crustal system because fluid temperatures in Hole U1309D (Figure F4) are expected to cross both the known upper thermal limit for life in laboratory cultures (122°C) and the lower suspected temperature limit (~80°–90°C) for life in energy-limited subsurface crustal systems (Heuer et al., 2020). Because many portions of the Atlantis Massif subseafloor are not energy limited, evidence of active life may be present even at the higher thermal limits only previously reached in laboratory cultures.

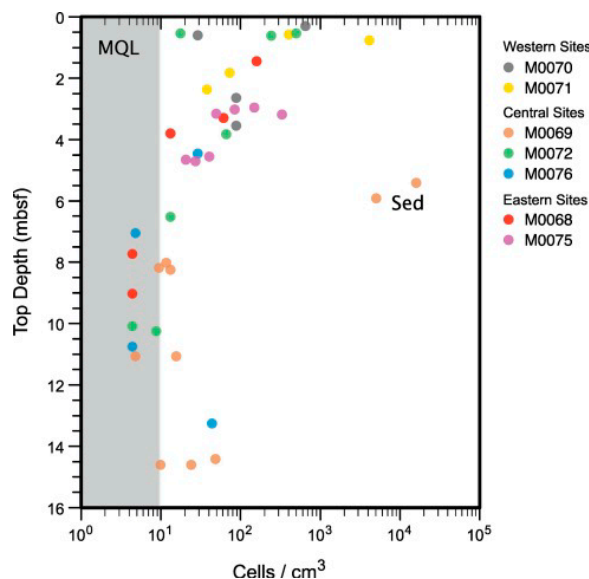


Figure F10. Cell counts from interior portions of whole-round cores, Expedition 357. Shaded area = minimum quantification limit (MQL) of 9.8 cells/cm³. Sediment (Sed) samples from Site M0069 have higher cell counts than other samples from similar depths. Cell counts are generally low; serpentinites at the base of Hole M0069A are the deepest samples with significant cell counts. From Früh-Green et al. (2018).

4. Site summaries

4.1. Site U1309

4.1.1. Background and objectives

4.1.1.1. Previous drilling at Site U1309

Site U1309 is located on the central dome of Atlantis Massif, 14–15 km west of the median valley axis of the Mid-Atlantic Ridge, and ~5 km north of the LCHF. The seafloor is interpreted to be a gently sloping, corrugated detachment fault surface (Figures F1, F2). The site was established during Expeditions 304 and 305 in 2004–2005, when the two main Holes U1309B and U1309D were drilled as well as 5 shallow and failed holes (Blackman, Ildefonse, John, Ohara, Miller, MacLeod, and the Expedition 304/305 Scientists, 2006; Blackman et al., 2011).

Expedition 304 established a hard rock reentry system comprising 25 m of 13 $\frac{3}{8}$ inch casing in Hole U1309D using a hammer drill. During that operation, 4.5 m of casing was left protruding from the seafloor and a reentry cone was successfully dropped onto the casing. The hole was then deepened to 131 mbsf. After carrying out operations at Sites U1310 and U1311, Hole U1309D was deepened to 401 mbsf and logged. Expedition 305 followed directly after Expedition 304 and deepened Hole U1309D to 1415 mbsf in two stages, with logging runs in the middle and at the end of coring. Hole U1309D was reentered and logged during Expedition 340T in 2012 and had remained undisturbed from 25 February 2012 until operations during Expedition 399.

Hole U1309D sampled a continuous sequence of gabbroic rocks including troctolite and olivine-rich troctolite, olivine gabbros, oxide gabbros, and rare leucocratic intrusions (Figures F4). A few minor screens of mantle harzburgite are present in the upper 300 m of the section. Diabase/basalt intrusions with chilled margins form ~40% of the top 120 m of the sequence, with rare occurrences at greater depths. Many igneous contacts are present within the section, with units varying from centimeters to tens of meters in thickness (John et al., 2009). More evolved units generally (but not always) intrude into more primitive units.

Crystal-plastic deformation is restricted to narrow zones in the section, mainly above 300 mbsf. Cataclasis and fault breccia are present in several strands in the upper 80 m of the section, a fault zone at ~160 mbsf, and a prominent 6 m thick fault zone at 744–750 mbsf within a damage zone from 742 to 761 mbsf (Michibayashi et al., 2008; John et al., 2009). A crystal-plastic deformation zone at 1100 mbsf is suggested by temperature logging and has a weak signal in the core.

Alteration is most extensive in the upper 300 m of the section, where clinopyroxene is usually at least partly altered to amphibole (hornblende and actinolite) in both gabbro and diabase. In olivine-bearing rocks, chloritic tremolite and chlorite form at the expense of olivine and plagioclase. Below 300 mbsf, this reaction only goes to completion around faults and gabbro contacts (Nozaka and Fryer, 2011) and rodingitization of plagioclase to prehnite \pm hydrogarnet driven by serpentinization of olivine is seen (Frost et al., 2008). The latest reactions and veins contain saponite and zeolites (Nozaka et al., 2008) and may be forming in near ambient conditions.

Temperature logging occurred at the end of Expedition 305 and again during Expedition 340T, 7 y later (Blackman, Ildefonse, John, Ohara, Miller, MacLeod, and the Expedition 304/305 Scientists, 2006; Expedition 340T Scientists, 2012). During Expedition 305, the temperature gradient was strongly affected by drilling, with a steep rise in the lowest part of the hole and a maximum temperature of 118.9°C at 1415 mbsf. During Expedition 340T, the temperature profile in the borehole water was assumed to have equilibrated with the rock and reached 146.2°C at 1405 mbsf. Below ~750 mbsf, the temperature gradient is linear, and a conductive regime is inferred. Above 750 mbsf, the temperature profile is curved, suggesting slow downward movement of fluid in the rock mass (Blackman et al., 2014). Small excursions in temperature, seen at ~750 and 1100 mbsf, are inferred to be the result of influx of colder fluid.

Samples for microbiology were taken from a range of lithologies and depths during Expeditions 304 and 305 (Blackman, Ildefonse, John, Ohara, Miller, MacLeod, and the Expedition 304/305 Scientists, 2006; Mason et al., 2010). Cell counts were below detection limit (<10³ cells/cm³ rock).

Microbial diversity was assessed using cloning and sequencing, terminal restriction fragment length polymorphism, and a microarray for metabolic genes (“GeoChip”). The low-diversity microbial communities consisted of lineages closely related to bacteria from hydrocarbon-dominated environments and known hydrocarbon degraders (Mason et al., 2010).

Figure F1 (Harding et al., 2015) shows the most recent processing of the seismic data collected more than 20 y ago and used to select the location for Site U1309. Seismic velocities increase with depth, with velocities of 7 km/s below 1000 mbsf, consistent with fresh gabbro (Blackman et al., 2011). At higher levels, lower velocities reflect alteration of gabbro and increased fracturing consistent with slow fluid circulation inferred from the temperature profile (above). Physical properties measured on the ship and logging data including VSPs collected during Expeditions 305 and 340T are consistent with the lithologies collected and were used in processing the full waveform inversion model shown in Figure F1 (Harding et al., 2015).

4.1.2. Objectives of Site U1309 revisit

- To sample fluids and obtain temperature data in the undisturbed borehole and study geochemistry and microbiology of fluids at temperatures above and below the current known limit of life;
- To mill out a caliper arm lost during Expedition 340T and believed to be in the bottom of Hole U1309D, leaving the hole in good condition for further operations;
- To deepen the hole by ~650 m to reach temperatures of ~220°C, where active serpentinization reactions might be occurring and where increasing amounts of mantle rock might be expected within the gabbroic sequence; and
- To drill an additional single bit hole at Site U1309, with the aim of sampling zones of fault-induced and reaction porosity for microbiology, which were not collected during Expedition 304.

Although our first two objectives were realized, Hole U1309D was only deepened by 83 m and a new shallow hole was not drilled. In light of the unexpectedly good results at Site U1601, the Science Party decided that achieving a deep hole in peridotite (the original aim of Expeditions 304 and 305) at Site U1601 should be prioritized.

4.1.3. Operations

4.1.3.1. Hole U1309D (first visit)

After the failure of releasing the reentry system in Hole U1601B on 24 April 2023, the rig crew needed time to assess the situation, identify an alternative method for deploying a reentry system at Site U1601, and build that system. We decided that while this was happening, we would move to Hole U1309D to conduct the fluid sampling program and, depending on conditions, initialize coring (Table T1; Figure F6).

4.1.3.1.1. Bit Run 1: temperature logging and fluid sampling

The ship began its 2 nmi dynamic positioning (DP) move to Hole U1309D at 2353 h on 24 April and arrived at 0116 h on 25 April. A bottom-hole assembly (BHA) was assembled with a 9¼ inch clean-out bit (4½ inch inner diameter) and without a float valve to deploy the novel Multi-Temperature Fluid Sampler (MTFS), the Kuster Flow-Through Sampler (KFTS), and the Elevated Temperature Borehole Sensor (ETBS) on the coring line. The drill string was lowered at 0830 h, and the subsea camera with Niskin water sampling bottles attached to its frame was deployed at 1115 h. The ship was offset ~20 m from Hole U1309D to pump the “pig” tool to clean rust from the inside of the newly deployed drill string. The bit reentered Hole U1309D at 1455 h. The reentry cone was partly filled and blocked by a soft particulate deposit that was easily displaced upon bit entry into the cone. The Niskin bottles were triggered, and the camera frame with the bottles was returned to the rig floor by 1620 h. The MTFS and ETBS were prepared on the catwalk, rigged up, and lowered down the drill pipe at 1815 h. The MTFS assembly descended in the open hole at a rate of 10 m/min, with 3 min temperature check stops every 100 m. The tool string tagged the bottom at 1389 mbsf, indicating a 26 m thick fill at the bottom of Hole U1309D, and then ascended at a rate of 15 m/min in the borehole and 30 m/min in the water column. The tools arrived back on the rig floor at 0043 h on 26 April.

The tools were rigged down, and the ETBS was removed from the MTFs and connected to the two KFTSs. The two KFTS clocks were set to sample at 411 mbsf (0310 h) and 739 mbsf (0330 h). The tool assembly was lowered down the drill pipe at 0207 h and was back on the rig floor at 0500 h. A second run of the KFTS-ETBS assembly was configured to sample at 1111 mbsf (0823 h) and 1320 mbsf (0846 h). It was lowered down the drill string at 0706 h and was back on the rig floor at 1225 h. On descent, the tool string traveled at a rate of 20 m/min, slowing to 15 m/min within 40 m of the desired sample depth to minimize hole disturbance. The tool was recovered at a rate of 10 m/min with 3 min stops every 100 m for temperature check measurements. The drill string was retrieved with the bit clearing the rig floor at 1620 h on 26 April, ending BHA Run 1 in Hole U1309D during Expedition 399.

4.1.3.1.2. Bit Run 2: milling

Next, we needed to remove a few tens of meters of fill from previous drilling in Hole U1309D during Expeditions 304 and 305, as well as a logging caliper arm presumed to have been left in the hole at the end of Expedition 340T. A BHA was made up with a 9 $\frac{1}{8}$ inch concave mill and two junk baskets and lowered to the seafloor at 1845 h. At 2120 h, the subsea camera and two Niskin water samplers were deployed. At 0000 h on 27 April, Hole U1309D was reentered for the second time during this expedition. The camera and Niskin water sample bottles were recovered, and the drill string was further run into the hole. At 0800 h, the bit tagged the top of the fill at 1379 mbsf (~37 m of fill). Milling and washing downhole proceeded expeditiously, the first 7–8 m at 8 m/h and the remainder at 30 m/h. At 1007 h, the bit was ~1.5 m above the previously reported bottom of Hole U1309D (1415.5 mbsf). The first 10 min of milling near the bottom indicated erratic torque, presumed to be the result of encountering metal pieces lost during a previous expedition. The subsequent 3.5 h of milling indicated low and steady torque. The pipe was raised and lowered repeatedly for 1 h to fill the junk baskets, and a 30 bbl mud sweep completed cleaning operations in Hole U1309D. Retrieval of the drill string began at 1515 h, and at 2200 h, the mill bit arrived at the rig floor where the junk baskets were emptied. Amongst dozens of rock pieces and bags of cuttings created during previous drilling on Expeditions 304 and 305, the junk baskets also recovered several metal pieces, including three 5 cm \times 5 cm chunks. The metal pieces were identified as parts from the Versatile Seismic Imager (VSI) wireline logging tool that was damaged during Expedition 340T ~11 y ago.

4.1.3.1.3. Bit Run 3: coring

At 2315 h, the rig crew began assembling the rotary core barrel (RCB) BHA with a new C-7 bit, which was complete at 0130 h on 28 April. The drill string and subsea camera were deployed, and at 0525 h, Hole U1309D was reentered for the third time during this expedition. The camera was retrieved, and the bit was lowered until it reached a hard tag at 1410.0 mbsf. We dropped a core barrel, washed to 1415.5 mbsf, and began deepening Hole U1309D from where Expedition 305 had ended. Coring proceeded until 1 May, when the bit had accumulated 50 h at the bottom, and we decided to retrieve it. This coring bit run advanced Hole U1309D by 82.5 m, from 1415.5 to 1498.0 mbsf. Cores 399-U1309D-279R through 313R recovered a total of 48.9 m, with core recovery ranging 26%–98% (average recovery of 59%). Every ~5 m 30 bbl mud sweeps were pumped to keep the hole clean. At 1145 h, we began retrieving the drill string, and the bit cleared the seafloor at 1620 h.

This was a good opportunity to test the ETBS, which had malfunctioned during previous runs and had been worked on since. With the bit several meters above the seafloor, we installed the top drive again, installed the sinker bars, and deployed the ETBS to the end of the pipe for ~10 min. The test results were negative and required additional repair efforts. At 1900 h, we continued to retrieve the drill string, and the bit cleared the rig floor at 2245 h on 1 May, ending bit Run 3 in Hole U1309D for this expedition.

During this first period of operations in Hole U1309D, the crew had established a plan and prepared equipment for a second attempt at setting a reentry system at Site U1601. Operations therefore continued in Hole U1601C from 1 May to 2 June.

4.1.3.2. Hole U1309D (second visit)

On 2 June 2023, the ship returned to Hole U1309D for the last operations of Expedition 399 to take more borehole fluid samples from Hole U1309D using the KFTS and then flush the hole rigorously. The ship had already moved over to Hole U1309D in DP mode by 1612 h on 2 June while the drill string was being retrieved from Hole U1601C. A BHA was assembled with a clean-out bit, no float valve, and an oversized landing ring (logging configuration). At 1915 h, the drill string was lowered to the seafloor, the subsea camera was deployed at 2130 h, and Hole U1309D was reentered for the fourth time during Expedition 399 at 2317 h. At 0045 h on 3 June, the drill string was positioned at 32 mbsf. Two KFTS bottles were assembled with the ETBS and the Conductivity-Temperature-Depth (CTD) tool. The first run on the coring line was deployed at 0100 h, and it was back on the rig floor at 0315 h. The borehole water samples were taken at 200 and 400 mbsf. The tool string was retrieved and disassembled, the water samples and data were retrieved, and the tools were reassembled for the second run. The CTD was not included on subsequent runs because its temperature rating would have been exceeded at the deeper sampling stations. The second sampling run from 0400 to 0645 h triggered one KFTS at 550 mbsf and one at 736 mbsf. Ample time was available to redress the tools and conduct a third run from 0736 to 1100 h. During this final run, the tools were not able to pass an obstruction at 1024 mbsf and the samples were taken at 923 and 1110 mbsf instead of a deeper planned station. After the conclusion of the sampling runs, the drill string was lowered to 1421 mbsf and washed down to the bottom of the hole at 1498 mbsf. Next, the hole was flushed with seawater seven times the borehole volume to leave behind as clean as possible a hole for potential future water sampling and temperature measurement operations. Final retrieval of the drill string from Hole U1309D began at 1945 h on 3 June and was completed with the bit clearing the rig floor at 0324 h on 4 June. The rig was secured for transit, and the vessel was underway at 0430 h, ending operations at Site U1309 and for Expedition 399. The vessel arrived in Ponta Delgada, Azores (Portugal), on 8 June, with the first line ashore at 0748 h.

4.1.4. Principal results

4.1.4.1. Igneous petrology

Deepening Hole U1309D from 1415 to 1489 mbsf during Expedition 399 recovered predominantly gabbroic rocks (Figure F11): gabbro (27%), olivine-bearing gabbro (59%), and olivine gabbro (12%), with small proportions of crosscutting diorite and diabase (1% and 2%, respectively). As was observed for the 1415 mbsf interval drilled during Expeditions 304 and 305, olivine-bearing rocks are abundant in the newly drilled interval. However, the proportion of gabbro below 1415 mbsf is significantly higher and the proportion of olivine gabbro is significantly lower than above that interval. In addition, many of the rock types recovered at shallower levels in Hole U1309D were not recovered during Expedition 399, including ultramafic rocks, troctolite, tonalite, trondhjemite, and oxide gabbros.

The main recovered gabbro body has internal gradational contacts between rocks with different grain sizes, mineral modes, and textures (subophitic to ophitic to poikilitic). This indicates that the

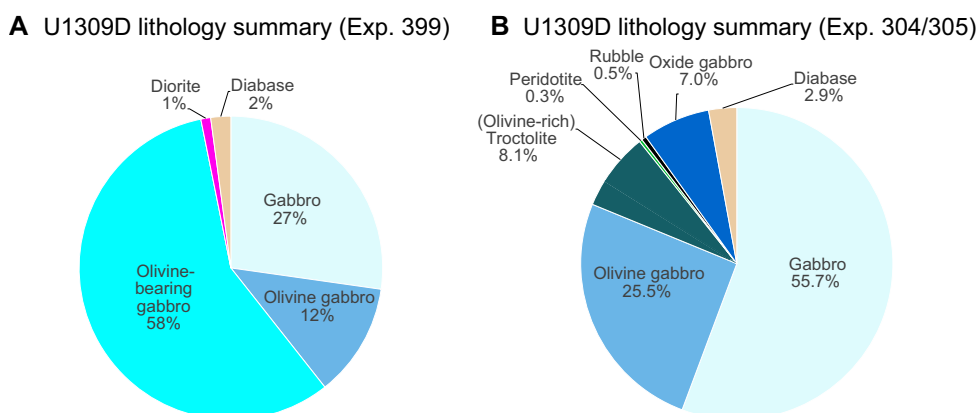


Figure F11. Recovered lithology, Hole U1309D. A. 1415–1498 mbsf (Expedition 399) B. 0–1415 mbsf (Expedition 304/305).

different subunits form part of a continuum of crystallization within a single plutonic body rather than representing discrete intrusions. In general, olivine was first to crystallize, followed by plagioclase and clinopyroxene. Crystallization continued as melt compositions evolved. This is evidenced by the common presence of zoning in plagioclase and late-stage crystallization of orthopyroxene. The general lack of the characteristic assemblage of amphibole + Fe-Ti oxide indicates that this late-stage melt did not generally evolve to the point of oxide saturation.

Following the accretion of the gabbroic units, two stages of additional magmatism occurred. First, diorite veins intruded, forming sutured and reactive contacts, which indicate that intrusion occurred when the gabbroic rocks were still at elevated temperatures. The final igneous activity is marked by the diabase dikes. The chilled margins of the diabase dikes with the gabbros attest to intrusion in a relatively cold environment. Furthermore, the thin section observations of entrainment of hydrothermally altered microxenoliths indicate that at least some diabase intrusions occurred after the host gabbroic rocks had already experienced hydrothermal alteration.

4.1.4.2. Alteration petrology

Gabbroic rocks recovered from Hole U1309D during Expedition 399 show a low extent of alteration (<20 vol% secondary replacement) that slightly decreases downhole. An exceptionally high extent of alteration occurs at intervals where localized alteration associated with cataclastic deformation, prominent hydrothermal or magmatic veining, and patchy bleaching took place (Figure F12). Alteration minerals appear to have formed under static conditions, except for amphibole formation associated with localized deformation in cataclastic zones.

Zeolite, amphibole, chlorite, and composite amphibole-chlorite veins frequently occur throughout cores without systematic downhole distribution. Crosscutting relationships of veins indicate a sequence of generation stages from older to younger: (1) magmatic veins; (2) amphibole, chlorite, or amphibole-chlorite veins; and (3) prehnite-carbonate and zeolite veins.

Primary minerals in gabbroic rocks are variably altered to secondary minerals along grain boundaries, microcracks, or cleavage surfaces. In some cases, particularly in proximity to hydrothermal veins, complete replacement yields pseudomorphs after primary minerals. Olivine is replaced by serpentine + oxide/sulfide, talc + sulfide/oxide, clay + oxide/sulfide, and amphibole + oxide +

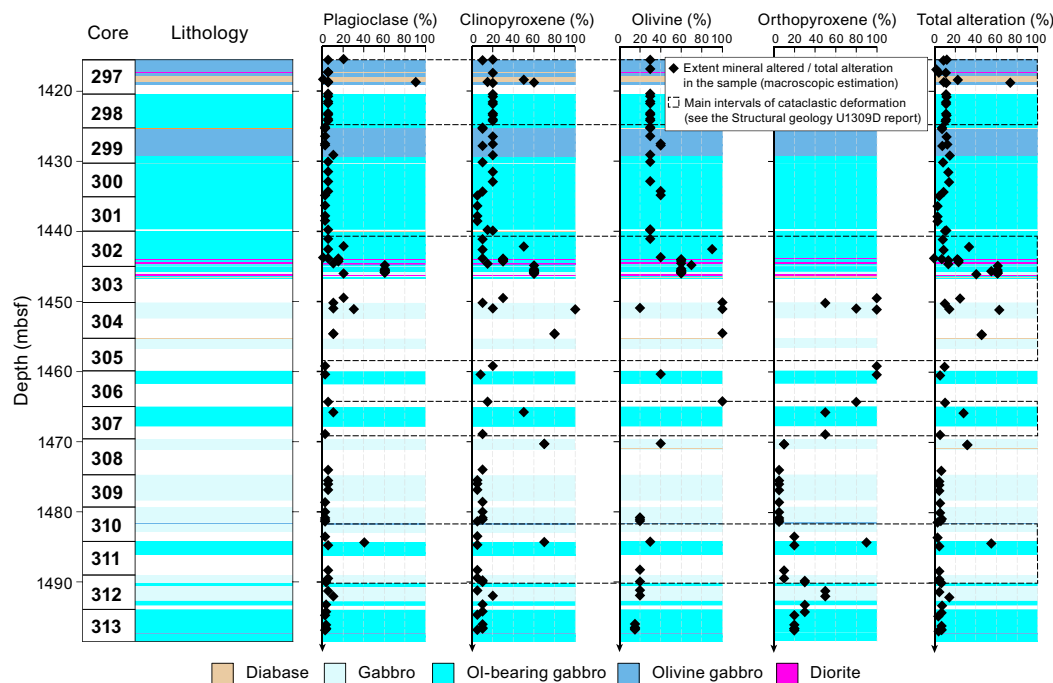


Figure F12. Downhole variation of percentage of alteration extent of each mineral and percentage of total alteration intensity in gabbroic rocks, Hole U1309D below 1415 mbsf. See Figure F4 for total alteration intensity from 0 to 1415 mbsf (Expedition 304/305). Ol = olivine, Opx = orthopyroxene.

chlorite. Fluid inclusions in olivine are locally abundant. Clinopyroxene and orthopyroxene are altered to amphibole, chlorite, and/or talc. Plagioclase is altered to chlorite, amphibole, secondary plagioclase, prehnite, and zeolite.

The observations of mineral assemblages, microscopic textures and fluid inclusions, and crosscutting relationships of the alteration assemblages and hydrothermal veins indicate that sequential alteration and deformation took place at conditions ranging from amphibolite through greenschist to subgreenschist facies.

4.1.4.3. Structural geology

Structural analysis of Cores 399-U1309D-297R through 313R (1415–1498 mbsf) recovered during Expedition 399 reflects a temporal and spatial overlap in magmatism and semibrittle to brittle deformation processes in the footwall of an oceanic detachment system.

Magmatic fabrics in the recovered gabbroic rocks are dominantly isotropic, with grain size variations and rare diffuse contacts between grain size domains. Rare magmatic foliations, shown by a shape preferred orientation of plagioclase or pyroxene, have gentle to subvertical dips.

Rare crystal-plastic deformation was only observed microscopically. Gabbroic rocks that appear undeformed at the macroscale infrequently display very low strain crystal-plastic deformation (twinning and/or subgrains) in plagioclase. Localized fault rocks can display subgrain development and minor grain boundary bulging dynamic recrystallization in plagioclase related to brittle to semibrittle deformation of relict igneous plagioclase.

Brittle to semibrittle deformation is concentrated in two strands of a semibrittle shear zone between 1451 and 1460 mbsf (Sections 399-U1309D-304R-2 to 306R-1) and between 1464 and 1474 mbsf (Sections 307R-1 to 308R-1), with relatively undeformed rocks in sections above and below these intervals. The shear zones are characterized by brittle to semibrittle deformation over a significant range of intensities from fractures and microfaults, faults and fault breccia, to formation of zones of cataclasite and phyllonite. Microscopic analysis of high intensity deformation zones shows localized plagioclase-amphibole cataclasite and amphibole phyllonite fault cores. Reverse shear sense was determined in rare cases where structural orientation was preserved in recovered intervals. Diabase dikes in some cases cut cataclastic zones (Figure F13).

The most abundant vein types include amphibole, chlorite, and zeolite veins and minor prehnite and carbonate veins, formed across a broad range in temperature. Crosscutting relationships and vein deformation record that amphibole and chlorite veins are pre-/syn- and postdeformational. Additionally, amphibole-chlorite alteration of fractured rocks is typically undeformed. Low-temperature zeolite, prehnite, and carbonate veins are undeformed and therefore postdate deformation. Collectively, the deformation mechanisms in plagioclase and amphibole, taken with crosscutting relations between deformation, alteration, and vein generation, demonstrate that semibrittle deformation occurred at lower amphibolite to greenschist facies conditions.

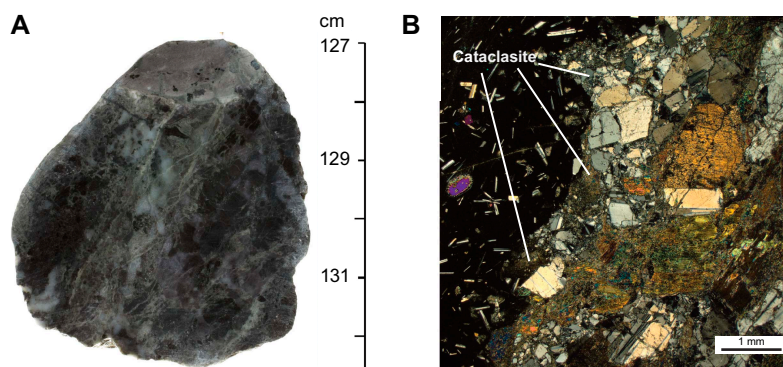


Figure F13. A. Diabase cutting fractured olivine-bearing gabbro (399-U1309D-303R-1, 126–132 cm). Diabase is at 127–128 cm. B. Chilled margin of undeformed diabase against zone of cataclasis in isotropic olivine gabbro (297R-2, 97–100 cm, TS22; cross-polarized light).

The cores reflect a down-temperature history from crystallization of gabbroic rocks, cooling with very limited deformation to lower amphibolite–upper greenschist facies conditions, followed by semibrittle deformation in a shear zone at lower amphibolite to greenschist facies conditions along shear planes with present-day dips of 10°–30°. Because the depth of the interval is 1415 to 1498 mbsf, it is unlikely that the reported semibrittle shear zone is directly related to the detachment fault exposed at the seafloor. The greenschist facies conditions of deformation suggest that Atlantis Massif continued to deform during the later stages of exhumation, followed by a phase of magmatism (diabase).

4.1.4.4. Geochemistry

Geochemical analyses were carried out on rock samples selected by the geochemistry and microbiology teams and fluids collected during the two separate water sampling campaigns. A total of 29 rock samples from Hole U1309D were analyzed for major and trace element concentrations and for their volatile element concentrations. These samples comprised (1) 1 diabase, 1 leucocratic diorite, 3 olivine gabbro, and 15 gabbro (including 10 olivine-bearing gabbro) collected for rock geochemical studies and (2) 1 olivine gabbro sample and 8 olivine-bearing gabbro samples analyzed as part of an interdisciplinary study of rock samples collected primarily for microbiological studies.

The analyzed samples do not display systematic chemical variations with depth except for those associated with the crosscutting diabase at 1417.9 mbsf and leucocratic diorite at 1443.8 mbsf.

Expedition 399 olivine gabbros and gabbros have major and trace element compositions similar to those of the most primitive gabbros and the most evolved olivine gabbros recovered at Site U1309 during Expeditions 304 and 305. They overlap in composition and are characterized by high Mg# (74–80) and Ca# (73–82) and low TiO₂ concentrations (0.26–0.50 wt%). Except for some microbiology samples that have H₂O up to 2.17 wt%, they have low H₂O contents similar to Hole U1309D gabbroic rocks sampled below 850 mbsf. The presence of H₂O indicates the replacement of primary minerals by hydrous minerals during hydrothermal alteration and weathering. The major and trace element compositions of Expedition 399 olivine gabbros and gabbros provides no evidence of elemental remobilization associated with H₂O concentration variations, even for fluid mobile elements.

The analyzed leucocratic sample is the from the felsic part of the diorite sample recovered at ~1444 mbsf. Its composition is that of an An₄₅ plagioclase, and, except for Sr, an element typically enriched in plagioclase, it is depleted in almost all trace elements. In that respect, it differs significantly from the previously analyzed Site U1309 leucocratic veins and dykes that represented the most enriched end-members of the rocks recovered during Expeditions 304 and 305. The fine-grained diabase intruding the gabbroic rocks at 1417.9 mbsf has a basaltic composition characterized by high Mg# (69) and low TiO₂ concentrations (0.79 wt%). It represents one of the most primitive, depleted, and least altered basaltic intrusions of the MORB magmatic suite at Site U1309.

Based on their major and trace element compositions, Expedition 399 Hole U1309D diabase and gabbroic rocks form a coherent suite with the diabase, basalt, and gabbroic rocks sampled at the same site during Expeditions 304 and 305, indicating a cogenetic origin for these mafic rocks.

In the initial fluid sampling campaign in Hole U1309D, the inaugural deployment of the MTFS (Figure F14) successfully recovered fluids from four depths and the KFTS recovered fluids from an additional four depths. Both samplers returned with abundant solid material that was likely a mixture of drilling mud, cuttings from the borehole, bottom fill, and grease. The fluids appear to be a mixture of seawater, formation water, and a fluid that reacted with fill at the base of the hole. The second fluid sampling campaign at the end of the expedition collected an additional three KFTS samples with full volumes and three samples with incomplete recovery. The samplers did not return large amounts of solid material from these deployments, and the fluids were notably clearer.

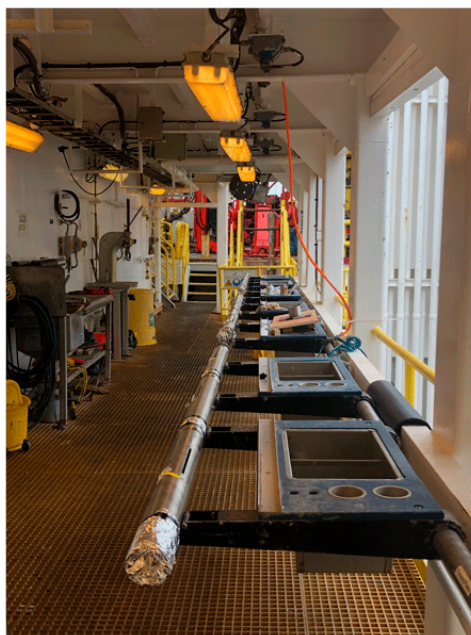


Figure F14. MTFS assembled and ready for deployment on catwalk during IODP Expedition 385T (Wheat et al., 2020).

4.1.4.5. Microbiology

Microbiological investigations in Hole U1309D were designed to explore potential signs of recent or past life at extreme temperatures, in particular the shallowest rocks that may have been exposed to borehole water during the 18 y since Expedition 305. Microbiology samples were collected for traditional analyses such as cell counts, cultivation, and DNA sequencing, as well as organic geochemistry analyses intended to document the presence of organic compounds including lipids, organic acids, and amino acids. A total of nine microbiology whole-round (WR) samples were collected from Cores 399-U1309D-297R through 313R. Eight of the samples are olivine-bearing gabbro, and one sample is olivine gabbro.

Each of the nine samples was rinsed, photographed, and separated into exterior and interior sections according to our standard methodology. Perfluorocarbon tracer (PFT) levels in the interior sections of all nine samples were below detection or at very low levels (maximum of 0.1 ppb). In contrast, PFT was detectable in the exterior shavings of all microbiology WR samples except one, ranging from trace levels to 22 ppb. The consistent reduction of PFT levels from exterior shavings to interior zones affirms the efficacy of our procedures for limiting contamination into the interior zones of the core samples.

Subsamples from each of the nine samples were collected for cell counts, DNA sequencing, lipid characterization, and organic carbon analyses. Subsamples for single-cell activity assays were collected from six of the nine samples. Stable isotope tracer experiments were conducted with four of the samples. Subsamples for virus counts, enrichment cultivations, and scanning electron microscope imaging were collected from the first five samples. High-pressure cultivation experiments were conducted with subsamples collected from Cores 399-U1309D-297R and 298R.

Water samples collected with Niskin bottles, the MTFS, and the KFTS were subsampled for microbiological analyses intended to characterize the extent, diversity, and activity of microbial communities within Hole U1309D. Subsamples for cell counts and single-cell activity assays were collected from all four of the high-volume MTFS samples (Bottles 1, 2, 4, and 5) and all KFTS and Niskin samples. In addition, MTFS Bottle 2 was subsampled for virus counts, enrichment cultivations, high-pressure cultivations, and stable isotope tracer experiments. Water from MTFS Bottle 4 (260 mL), the three KFTS bottles (250 mL each), and all Niskin bottles (3–5 L) were filtered through a 0.2 μm Sterivex filter cartridge intended for DNA sequencing.

4.1.4.6. Petrophysics

The petrophysical properties of gabbro in Hole U1309D were characterized through natural gamma radiation, magnetic susceptibility, and gamma ray attenuation density measurements on WR cores from Cores 399-U1309D-297R through 313R (1415–1498 mbsf). Discrete measurements were completed on cubes and included wet mass, dry mass, and dry volume for the calculation of density and porosity and *P*-wave velocity. Core pieces from section halves were selected for thermal conductivity measurements. Downhole temperature logs were completed. No other petrophysical logging was attempted in this hole.

Bulk density from WR measurements ranges 2.6–2.9 g/cm³ and generally increases with depth. Some intervals deviate from this trend, including a general downhole decrease in density in Cores 399-U1309D-302R through 303R (1441–1445 mbsf), which is also mirrored in the grain density measured on discrete cube samples.

A total of 31 discrete cube samples were analyzed. Grain density ranges 2.87–3.03 g/cm³, with an average of 2.94 ± 0.08 g/cm³. Grain density and bulk density generally increase with depth. Grain density is negatively correlated with porosity, with porosity generally decreasing with depth. Porosity ranges 0.5%–2%, with an average of $1.27 \pm 0.79\%$. The highest porosity is measured in Cores 399-U1309D-302R through 305R (1441.2–1455.0 mbsf), which also includes an altered felsic dike that has a grain density of 2.55 g/cm³ and a porosity of 5%.

P-wave velocity was measured on 30 discrete cube samples (1 diabase, 3 olivine gabbro, and 26 gabbro) along the three principal directions *x*, *y*, and *z* in the core reference frame (CRF). The average *P*-wave velocity of the three-axis on each sample ranges 4964.7–5894.6 m/s, the average is 5476.0 m/s, and the apparent anisotropy of *P*-wave velocity ranges 4.1%–7.0%.

Magnetic susceptibility is relatively low, reflecting a relatively low proportion of magnetite in these rocks. Pass-through loop magnetic susceptibility (MSL) is typically under 500 instrument units (IU), and point magnetic susceptibility (MSP) is typically below 1000 IU. The highest values for MSL and MSP are in Section 399-U1309D-311R-1, with a value of ~1500 IU for MSL and ~6500 IU for MSP, indicating more abundant magnetite.

Natural gamma radiation is very low with most values <0.5 counts/s. Thermal conductivity was measured on 17 archive-half core pieces >10 cm in length. Samples of representative lithologies for the hole were measured. Values for all pieces range 2.14–2.63 W/(m·K) with a mean of 2.35 ± 0.14 W/(m·K). No obvious trend with depth or lithology exists.

Borehole fluid temperatures were measured in Hole U1309D prior to coring. The best results were recorded with the first run down the hole, with the ETBS attached to the MTFS. Values for the entire borehole during the down run range from 6.7°C at the seafloor to 139.6°C near the bottom of the hole. The resulting profile shows slight curvature in the upper ~580 mbsf, transitions into a more linear gradient deeper than 580 mbsf, and continues linearly to the bottom of the hole. The profile in the deeper half of the hole indicates a gradient of ~114°C/km. The temperature profile is very similar to that recorded during Expedition 340T, indicating no significant changes in hydrological or heat flow regime in the last 11 y.

4.1.4.7. Paleomagnetism

Remanence measurements were made on archive section halves from Hole U1309D, adding to the breadth of knowledge for the preexisting hole. These measurements generated 6,281 new measurement points downhole. The mean natural remanent magnetization (NRM) inclination was determined to be $-25.7^\circ \pm 12^\circ$. Stronger alternating field (AF) steps of 10–15 mT shift and narrow the distribution toward the expected geocentric axial dipole (GAD) value of -49° . At the AF step of 50 mT, the mean inclination became -34.4° . This shallower inclination value relative to the expected value is consistent with previous work on the hole. The cause for shallowing was interpreted to be the result of tectonic rotation.

Archive section half data were complemented by discrete sample measurements. Both paleomagnetic and physical properties cube samples were analyzed using AF demagnetization, thermal demagnetization, isothermal remanent magnetization acquisition, and isothermal remanent mag-

netization backfield methods. Additionally, paleomagnetic cube samples were pretreated with liquid nitrogen dunking as a way of reducing the drilling overprint. Multiple remanence directions were recorded, but the direction of the most coercive components was consistent with the mean inclination direction, as put forth by the archive section half analysis. The bulk remanence of these rocks is carried by magnetite. The intensity of magnetic remanence varies downhole, ranging 0.02–3.81 A/m with a mean of 0.90 A/m, indicating varying distributions of magnetite. Results from the isothermal remanence experiments provide evidence for predominantly multidomain and minimal single domain magnetite grain populations.

Anisotropy of magnetic susceptibility (AMS) data indicate predominantly oblate magnetic fabrics. The clustering of the shortest magnetic axis (K_{\min}) around the vertical indicates that the direction of magnetic flow was horizontal. The degree of anisotropy (P_j) averages 1.121 ± 0.075 ($n = 50$) with low and high values ranging 1.029–1.424. The average value of P_j indicates that most susceptibility tensors are moderately anisotropic but significantly higher degrees of anisotropy are noted in many coarse-grained gabbroic samples.

4.2. Site U1601

4.2.1. Background and objectives

Site U1601 (proposed Site AMDH-2A) is located on a flat region near the southern wall at the top of the Atlantis Massif at a water depth of 850 m. Mass wasting along the southern edge of the massif has created steep cliffs that expose a 3000 m cross section of the internal structure. The southern wall is predominately composed of variably altered peridotite with intermittent mafic plutonic intrusions (Blackman et al., 2002; Schroeder and John, 2004; Schroeder et al., 2002; Früh-Green et al., 2003, 2018; Boschi et al., 2006; Karson et al., 2006).

The location of Site U1601 was chosen in part based on the success of drilling in this region during Expedition 357. The central Sites M0069A, M0072B, and M0076B were drilled to 12.4–16.4 mbsf, with recoveries ranging 52%–75% (Früh-Green et al., 2017). Recovered cores contained diverse lithologies with upper layers that included calcareous sediment, basalt, and dolerite. Serpentinized harzburgite was recovered in the deeper sections of all three boreholes (Früh-Green et al., 2017), and water column concentrations of H_2 were elevated to ~ 40 nM above these locations (Lang et al., 2021), suggesting that deeper drilling may encounter rocks undergoing active serpentinization. It was also hoped that a hole at this site would recover a complete section through the detachment fault zone, suggested to be ~ 100 m thick. Several of the shallow holes of Expedition 357 had recovered fault rocks including cataclasites and talc-tremolite-chlorite schists. Thus, a hole located near one of the central sites could address many of the primary goals of the expedition.

Hole M0069A was specifically targeted because it had some of the best recovery during Expedition 357. It was also the location of the deepest serpentinite sample subjected to microbiological analyses (14.6 mbsf), revealing cell densities of 10–24 cells/cm³ (Früh-Green et al., 2018). Genes from putative indigenous subsurface organisms were identified from Core 357-M0069A-92R (Goordial et al., 2021) and other nearby drilling locations (Motamedi et al., 2020).

4.2.2. Operations

4.2.2.1. Port call and transit to Site U1601

Expedition 399 (Building Blocks of Life, Atlantis Massif) began in Ponta Delgada, Portugal, at 0800 h on 12 April 2023 with the R/V *JOIDES Resolution* tied up at the Dock 12, NATO Berth. Port call activities were minimal because most of the activities occurred during the tie up in Tarragona, Spain. All oncoming scientists and *JOIDES Resolution* Science Operator (JRSO) staff boarded the vessel on 13 April. All personnel received a Coronavirus Disease 2019 (COVID-19) self-test kit the night before to be used before joining the group and boarding the bus to the ship. The COVID-19 Mitigation Protocols Established for Safe JR Operations (COPE) were followed, which included daily antigen tests and mask wearing for all personnel for at least 6 days. Once on board, general welcome and introductions, including ship and laboratory safety presentation and tours were conducted. One member of the Science Party disembarked the vessel. At 1400 h on 15 April, after a first lifeboat drill, the voyage to Site U1601 began. We arrived at Site U1601 at 0530 h on 19 April, completing the 937 nmi transit from Ponta Delgada with an average speed of 10.7 kt. The ship was

in DP mode by 0551 h, starting operations at Site U1601. The COVID mitigation period ended at 1815 h.

4.2.2.2. Hole U1601A

The objective at Site U1601 was to core a 200 m deep hole through the detachment fault at the Atlantis Massif. We chose IODP Site M0069 as a reference location, which was drilled in 2015 with the British Geological Survey RockDrill2 during Expedition 357 on the *RSS James Cook*. The operational plan called for a reentry system installation, which required drilling a ~50 m deep pilot hole to assess the formation (Table T1; Figure F6).

On 19 April 2023, the rig crew assembled a BHA with an RCB and C-7 drill bit and deployed it to 854 meters below rig floor (mbrf) near the seafloor. The subsea camera was deployed for a brief seafloor survey. Site M0069 was immediately located thanks to several meters of pipe sticking out of the 2015 hole as well as various skid marks and sampling spots left by the remotely operated vehicle (ROV) *Jason* in 2018. Our survey line extended 60 m southwest of Site M0069 and showed sand waves along the seafloor, which were also seen more clearly on the 2018 ROV footage. No prohibitive obstructions or hazards were identified. As was true for most deployments of the subsea camera, two Niskin bottles attached to the camera frame were triggered to collect bottom water samples before the frame was retrieved. The seafloor was tagged at 861 mbrf. Operations in the pilot Hole U1601A began by pushing the bit into the sediment with minimal rotation (5 rpm) and minimal pump (5 strokes/min) for 2.4 m. The core barrel for Core 399-U1601A-1R was retrieved at 2045 h and was empty. Core 2R was advanced 9.7 m, and subsequent Cores 3R–12R, recovered on 20 and 21 April, advanced 4.8 or 4.9 m each to a total depth of 60.6 mbsf. Recovery ranged 1%–72%, with an average of 26%, and increased downhole. At 1245 h on 21 April and at 56.3 mbsf, the bit became stuck. The rig crew tried to free the bit for the remainder of the day, without success. At 0045 h on 22 April, the decision was made to deploy the Schlumberger pipe severing tool. The first two severing attempts failed, and the third attempt at 1243 h succeeded in severing the pipe at 10.1 mbsf. The drill string was retrieved, and the end of the pipe cleared the rig floor at 1730 h, ending operations in Hole U1601A.

4.2.2.3. Hole U1601B

Assembly of the drill-in casing system began late on 22 April 2023. The upper guide horn was removed to create the space in the moonpool area needed to assemble the ~22 m long 13 $\frac{3}{8}$ inch casing string, hydraulic release tool (HRT), landing platform, and free-fall funnel (FFF). The stinger BHA, including a mud motor, underreamer, and 12 $\frac{1}{4}$ inch bit, were assembled and tested. The reentry system was lowered to the seafloor and drilling in Hole U1601B began at 1455 h on 23 April. Sepiolite mud sweeps were pumped every ~4 m. At 1215 h on 24 April, we reached the target depth of 26.0 mbsf. The “go-devil” trigger tool used to release the HRT from the reentry system was dropped and pumped down the drill string with 25 strokes/min until it landed, with a pressure drop indicating that the release had occurred. However, several attempts to pull the stinger subassembly out of the casing subassembly were unsuccessful despite turning the pumps on and off several times to work the underreamer. At 1430 h, the decision was made to retrieve the subsea camera and then the entire reentry assembly back to the rig floor. The rig crew started to disassemble the reentry system, with the stinger bit at the rig floor at 2353 h on 24 April. The mud motor was severely damaged: the lower section of the housing holding the bearing support, a 12 inch long cylindrical piece, had broken off and was missing.

The rig crew needed time to assess the situation, identify an alternative method for deploying a reentry system at Site U1601, and build that system. We decided that while this was happening, we would move to Hole U1309D to conduct the fluid sampling program and, depending on conditions, initialize coring.

4.2.2.4. Hole U1601C

After operating at Site U1309D from 25 April to 1 May 2023, we returned to Site U1601 to deploy a reentry system in a new hole (U1601C). This was a different system from the one we were not able to release in Hole U1601B. It did not have a mud motor, underreamer, or a casing release tool. Instead, the plan was to drill a 14 $\frac{3}{4}$ inch ~22 m deep hole, reenter the hole with a 9 $\frac{7}{8}$ inch coring bit, drop a casing-cone assembly by letting it free fall into the hole using the drill string as a guide, and begin coring (Table T1; Figure F6). By 2254 h on 1 May, the ship had moved the 2 nmi from

Hole U1309D to Hole U1601C in DP mode. Hole U1601C is located 20 m northeast of Hole U1601B.

4.2.2.4.1. Summary of bit runs with coring bit

The following is a summary of the bit runs in Hole U1601C, with the following information for the coring runs (bit runs with a coring bit): the number of hours the bit was cutting core at the bottom of the hole, the cores retrieved, the interval cored in meters below seafloor, and the average recovery:

- Bit Run 1: drill casing hole.
- Bit Run 2: coring Run 1 (50 h, Cores 399-U1601C-2R through 55R, 23–284.9 mbsf, and 60% recovery).
- Bit Run 3: coring Run 2 (54 h, Cores 56R–132R, 284.9–658.4 mbsf, and 84% recovery).
- Bit Run 4: coring Run 3 (50 h, Cores 133R–197R, 658.4–973.6 mbsf, and 74% recovery).
- Bit Run 5: coring Run 4 (50 h, Cores 198R–240 R, 973.6–1182.2 mbsf, and 62% recovery).
- Bit Run 6: wireline logging and water sampling.
- Bit Run 7: milling.
- Bit Run 8: coring Run 5 (44 h, Cores 242R–259R, 1182.2–1267.8 mbsf, and 63% recovery).

4.2.2.4.2. Bit Run 1: drill casing hole

At 0130 h on 2 May 2023, assembly of the BHA with a 14 $\frac{3}{4}$ inch drilling bit was complete. After reinstalling the upper guide horn once more, deployment of the drill string began at 0315 h, was paused at 0400 h for general rig servicing, and was complete at 0630 h. Drilling the initial 14 $\frac{3}{4}$ inch wide and 23 m deep hole progressed slowly but steadily and was complete at 0615 h on 3 May. The drill string was retrieved, with the bit clearing the rig floor at 1025 h.

4.2.2.4.3. Bit Run 2: install casing and first coring run

Two joints of 10 $\frac{3}{4}$ inch casing, with a 10 $\frac{3}{4}$ to 13 $\frac{3}{4}$ inch crossover at the top, were welded together and staged in the moonpool area. An RCB BHA with a new 9 $\frac{7}{8}$ inch C-7 bit was made up and deployed through the casing, starting at 1345 h. The subsea camera was launched at 1610 h. While the ship was maneuvered to the Hole U1601C coordinates, we passed Hole U1601B, which had a hole in the center of a cuttings cone. At the Hole U1601C coordinates 20 m northeast, a “pond” of white sepiolite slurry came into sight but the hole was not visible. After a short period of poking into the pond, the bit reentered Hole U1601C at 1925 h and reached the bottom of the hole without detecting any fill. The bit was raised 8.7 m, and the camera frame was retrieved. The rig crew installed the FFF around the drill string and attached it to the top of the 13 $\frac{3}{4}$ inch casing crossover. At 2334 h, the casing-cone assembly was dropped into the moonpool and down the drill string. At 0005 h on 4 May, the subsea camera was launched to confirm that the reentry assembly had properly landed in the predrilled 23 m deep hole, which was visually confirmed. The camera frame and Niskin samples were retrieved, and the first core barrel was dropped. Unusually high pressure was indicated, which could have resulted from plugged jet nozzles. A second barrel was dropped without incident, and coring began. Coring progressed remarkably well, far exceeding expectations by reaching 284.9 mbsf in the first coring run. The subsea camera was launched once more while the drill string was being retrieved to confirm a clean exit of the bit from the reentry cone, confirming that the reentry system installation was fully successful. With the camera near the seafloor, we also briefly navigated over Holes U1601A and U1601B, identified the cutting cones, and confirmed that the seafloor was clear of any artifacts. The drill string was retrieved, clearing the rig floor at 1830 h.

4.2.2.4.4. Bit Runs 3–5: coring Runs 2–4

Despite having exceeded the planned penetration of 200 m at this site with the first coring run, the Science Party decided repeatedly to continue deepening Hole U1601C. Three more coring runs were completed from 8 to 25 May 2023, followed by bit Runs 6 and 7 for wireline logging and water sampling and for milling junk at the bottom of the hole, respectively. A fifth and final coring run with bit Run 8 was conducted from 29 May to 2 June.

All 4-stand coring BHAs were equipped with new C-7 coring bits. All reentries were successful. Approximately 20–30 m of soft bridges or hole fill were tagged after each reentry and never posed a significant problem to wash down. Down to Core 399-U1601C-178R (881.5 mbsf), 30 bbl mud

sweeps were pumped every ~10 m of coring. Subsequent sweeps used 20 bbl of mud every ~10 m to conserve mud. Likewise, the final 50 bbl sweep at the end of each run was reduced to 30 bbl below that depth. Mud sweeps were followed with 2–7 times the open hole volume of seawater at the end of each run. The bit used for Run 4 (coring Run 3) returned with 16 tungsten carbide teeth missing, a degree of wear considered acceptable and not traceable to any particular event. The bit used for Run 5 had lost the tips of all four roller cones. One of the cones had kicked inward, losing parts of the bearing, including the plug seal. Dozens of tungsten carbide teeth were missing or damaged. This led to the decision to conduct the milling bit Run 7.

After bit Run 4, we tested the ETBS, which malfunctioned during previous deployments and had been repaired in the meantime. The test deployment inside the drill string returned valid temperature data, closely following the temperature profile measured by the CTD tool ~6 h later outside the drill string.

After bit Run 5, the hole was replaced with freshwater (drilling water) (5550 bbl; 4710 strokes) to improve the resistivity contrast during subsequent wireline logging. When the drill string was retrieved to 55.5 mbsf, another 20 bbl of freshwater were pumped to top off the hole.

4.2.2.4.5. Bit Run 6: wireline logging and water sampling

We decided to conduct a full suite of wireline logging operations as well as borehole water sampling in Hole U1601C before attempting a final coring run in this hole. The intent of this sequencing was to minimize the various risks of not gathering the logging data for this >1 km deep legacy hole. On 26 May 2023, a 3-stand BHA with a logging bit was assembled, without a floating valve and including a large bore landing saver. The rig was serviced, the drill string was deployed, the subsea camera was launched, and Hole U1601C was reentered for the fifth time at 0406 h. The bit was positioned at 30.9 mbsf, and the camera was retrieved.

The first wireline logging tool string was assembled including the Schlumberger logging equipment head-mud temperature (LEH-MT) for borehole and tool temperature, Hostile Environment Natural Gamma Ray Sonde (HNGS) tool, and Hostile Environment Litho-Density Sonde (HLDS) for bulk density and photoelectric factor. We also added the IODP ETBS to the bottom of the tool string. The ETBS does not transmit data in real time. Logging started at 0715 h and ended at 1530 h on 26 May. The downward pass tagged hard at 1077 mbsf (105 m above the bottom of the hole). During both the downward and the upward passes, the tool string was held every 100 m for 10 min for the ETBS to acquire temperature equilibration time series.

The second logging tool string, including the neutron Accelerator Porosity Sonde (APS), High-Resolution Laterolog Array (HRLA) resistivity tool, and Ultrasonic Borehole Imager (UBI), started at 1700 h and was completed at 0225 h on 27 May. The tool string tagged at 1071.5 mbsf, slightly shallower than the first run. Logging with the third tool string, including the HNGS and the Magnetic Susceptibility Sonde (MSS), began at 0300 h and ended at 0830 h. This run reached 1075.5 mbsf. For the fourth tool string, including the VSI, we targeted the daylight hours to comply with marine wildlife protection protocols. At 1030 h, the protected species watch and preparation of the air guns began. At 1400 h, the logging attempt was aborted and postponed because of issues with cabling or software. Instead, we deployed the FMS and Dipole Shear Sonic Imager (DSI) as the fourth logging tool string. This run began at 1445 h and ended at 2350 h with two upward passes completed. This fourth run reached 1070.0 mbsf. The tools were rigged down at 0045 h on 28 May.

We still had the postponed VSI to run as the fifth and final logging tool string. However, this required daylight, so we proceeded with borehole water sampling objectives instead. The plan was to deploy both KFTSs in series, with the ETBS at the bottom, using the coring line. We planned to do this three times for a total of 6 sampling stations down the borehole. The first run started at 0205 h on 28 May and ended at 0340 h. After laying out the tools, removing the water samples, and resetting the tools, the second deployment started at 0515 h and ended at 0725 h. The third deployment started at 0830 h and ended at 1225 h.

The prior issues with the VSI had been resolved, and the rig was again readied for wireline logging. The protected species watch began at 1430 h on 28 May, and the fifth logging tool string was

deployed at 1435 h. An issue with the telemetry head required retrieval of the VSI string at 1515 h and replacement of the telemetry head. The air guns were prepared, and at 1640 h the tool string was redeployed to 1069 mbsf. Given the remaining daylight hours, the measurement stations on the upward pass were set at 100 m intervals. The run was completed at 2105 h.

We decided to conduct a fourth water sampling run because one of the samplers from a previous run only recovered ~5% of the chamber volume and because the results from the other water samples were encouraging. The dual KFTS and ETBS configuration was deployed once more at 2215 h and was back on deck at 0055 h on 29 May. We retrieved the drill string equipped with the logging bit, which cleared the rig floor at 0335 h. This ended the wireline logging and water sampling bit Run 6. The borehole water sampling effort in Hole U1601C yielded a total of 8 samples at 6 targeted depths intervals: 146, 368, 465, 675 (sampled twice with ~5% and 100% recovery, respectively), 970, and 1074–1065 mbsf (repeated at 1065 mbsf to avoid mud sampled at 1074 mbsf).

4.2.2.4.6. Bit Run 7: milling

Before the next attempt to deepen Hole U1601C, we needed to clear the hole of metal debris left behind by previous coring runs, particularly the last one leaving behind a cone bearing. A BHA was assembled with two junk baskets and a 9 $\frac{1}{2}$ inch junk mill. The drill string was lowered to the seafloor at 0430 h on 29 May 2023, filling the pipe every 15 stands from the rig. The subsea camera was launched at 0527 h, and Hole U1601C was reentered for the sixth time at 0704 h on 29 May. The bit was further lowered in the hole, and a hard tag was encountered at 1074 mbsf. While washing down to the bottom of the hole at 1182.2 mbsf, hard spots were encountered at 1084, 1094, 1123, and 1145 mbsf. Milling, which included slowing circulation and rotating and lifting the pipe twice an hour, was carried out from 1430 to 1945 h. The hole cleaning action ended with pumping a 30 bbl mud sweep with two times the hole volume of seawater. At 1945 h, we began retrieving the drill string, with the mill back on the rig floor at 0050 h on 30 May. The junk baskets contained several metal pieces among the rock cuttings, and some were clearly parts of the lost cone bearing.

4.2.2.4.7. Bit Run 8: coring Run 5

A BHA with a new C-7 coring bit was assembled. At 0330 h on 30 May 2023, after rig maintenance, the drill string was deployed to the seafloor, and Hole U1601C was reentered for the seventh time at 0554 h. The drill string was lowered in the hole and encountered a bridge at 1053.6 mbsf. After washing down to the bottom at 1182.2 mbsf, including a 30 bbl mud sweep, the wash core barrel was retrieved (“ghost” Core 399-U1601C-241G) and a new barrel was dropped. At 1445 h, coring in Hole U1601C resumed with Core 242R. Coring continued until the bit had accumulated 43.8 h on the bottom, and we decided to end coring with Core 259R at 1267.8 mbsf on 2 June. Cores 242R through 259R recovered 53.9 m of the 85.6 m cored, with core recoveries ranging 31%–97% (average recovery of 63%). Mud sweeps of 20 bbl were pumped every ~10 m, with a final 30 bbl mud sweep followed by pumping 7 \times the hole volume of seawater. The last core barrel was retrieved at 1230 h, and the pipe was retrieved with the bit clearing the rig floor at 1800 h. This concluded operations in Hole U1601C, and the ship returned to Hole U1309D (see [Hole U1309D \(second visit\)](#)).

4.2.2.5. Changes to shipboard processing on recognition of chrysotile

While completing coring operations in Hole U1601A in late April 2023, core describers identified and reported the presence of chrysotile veins in the recovered serpentinized peridotite cores. Chrysotile (one of three polymorphs of serpentine) has long been recognized as a common alteration mineral in serpentinized mantle rock, but in most cases in low concentrations. Chrysotile is a type of asbestos, and asbestos is an acknowledged health hazard in asbestos mining and asbestos abating jobs, at industrial concentrations. Regulations for exposure to airborne asbestos emphasize the danger of longtime exposure to significant asbestos dust (defined by most regulations as 0.1 fiber/cm³ as an 8 h time-weighted average in a specific microscopic size range).

During Expedition 399, the occurrence of white vein material of >1 mm thickness, in a few cases up to a size where fibers could be seen with the naked eye, led to concerns by the technical support staff handling cores that their health might be at risk. These concerns were communicated to shore management and Texas A&M University Environmental Health and Safety (TAMU EHS) officials. Consequently, throughout May, core handling, including splitting, sampling, imaging,

description, etc., became a major challenge. Precautionary procedures for core handling were implemented, but continued concerns and slow communications between ship and shore led to stop and go core processing that significantly compromised shipboard scientific data analysis.

After a conversation with shore management on 6 May, shipboard processing of cores at various stages was suspended. On 9 May, after a pause of 5 days, splitting of core sections resumed (regarded as the most hazardous procedure) under special safety protocols approved by TAMU EHS, including utilization of special personal protective equipment (PPE). Scientists and operations personnel participated in the splitting to catch up with the backlog and to allow people who remained concerned about exposure to not carry out these tasks. Rapid core description methods were established to manage the confluence of backlog and continued rapid core recovery. By 15 May, core splitting had caught up with core recovery, and rapid core description had caught up with splitting the next day. This allowed us to discuss, both on the ship and with shore management, strategies for reestablishing sampling. It was decided to start describing the working halves rather than the archive halves, so that shipboard samples could be identified each day without excessive core handling and sampled after shrink wrapping but before storage in the hold. On 19 May, sampling of section halves for shipboard analysis resumed using the special procedures. A limited number of thin section billets of serpentinized peridotite were cut for processing on shore instead of being prepared shipboard. Therefore, the material of greatest scientific interest that constituted the vast majority of the core could not be fully described shipboard. Personal sampling for scientists was restricted to residues of microbiology samples that had been processed in a controlled environment.

On 24 May, JRSO management received the detailed review and advice from TAMU EHS and forwarded it to the ship. The document stated "...Though widespread or significant contamination aboard the vessel is unlikely at this time..." and recommended that "If any ongoing assessment of workspaces positively identifies asbestos contamination, associated activities should cease immediately until additional review can determine the likely cause, potential for exposure, and the feasibility of resuming work..." On 25 and 26 May, over fifty swab samples of laboratory surfaces and floors were collected by JRSO staff and images of putative chrysotile fibers were sent to shore. Because cleaning of many parts of the laboratories had been suspended as a precaution, it is not clear whether these fibers accumulated before or after the precautionary core handling protocols were put in place. This led to the halt of all core handling including splitting, description, and sampling, so that procedures could be reassessed. On 29 May, per instruction from shore, all core splitting and sampling stopped. Starting with Core 399-U1601C-242R, sections were cut and sampled for microbiology on the catwalk, capped, measured with the Whole-Round Multisensor Logger and Natural Gamma Radiation Logger, described through the core liners, and then boxed. These protocols were applied to all cores, including those consisting entirely of gabbro. The expedition was shortened by 4 days to allow professional cleaning of parts of the ship in Ponta Delgada. The cleaning company analyzed 24 air and tape samples taken from the ventilation system and various surfaces in the core splitting room; core, downhole, and chemistry laboratories; and elevator before and after cleaning. Their report concluded that "The investigations show no sign of asbestos fibres".

To summarize, treatment of the Hole U1601C core was as follows (see Table **T3** and Figure **F15** for further details):

- Sections 2R-1 through 7R-1: normal splitting, sampling, and description, but the samples were not fully processed.
- Sections 8R-1 through 130R-4: splitting with additional precautions and rapid description with less measurements made to clear the backlog; sampling only of a few purely gabbro cores (22R, 23R, 35R, and 36R).
- Sections 131R-1 through 234R-3: splitting with regular sampling of gabbros and serpentinites, but only gabbros were fully processed on the ship; some serpentinite samples were cut on the ship for thin-section billets (TSBs) and other analyses, and some samples were marked up to be cut on shore.
- Sections 235R-1 through 259R-2: suspension of all cutting other than microbiology samples; description of whole-round sections through the liner; whole-round core logging continued.

Table T3. Status of Hole U1601C core curation, description, and sampling work. Shipboard core curation, description, and sampling work was limited on *JOIDES Resolution*. Work will be completed on shore at Gulf Coast Repository (GCR) in late 2023 under mandated safety precautions. Compare with Figure F15 for an illustration of the depth intervals. TS = thin section. ICP = inductively coupled plasma spectroscopy, MAD = moisture and density, PMAG = paleomagnetism.

	Work completed on ship					Work to be completed at GCR					Comment	
	Top section	Top depth (mbsf)	Bottom section	Bottom depth (mbsf)	Number of sections	Top section	Top depth (mbsf)	Bottom section	Bottom depth (mbsf)	Number of sections		
	399-U1601C-		399-U1601C-			399-U1601C-		399-U1601C-				
Curation	Section preparation and registration	2R-1	23.0	259R-2	1265.3	773	155R-1	765.1	240R-3	1181.3	?	May need to create/register a few new sections when binning!
	Section splitting	2R-1	23.0	234R-3	1151.6	709	235R-1	1153.1	259R-2	1265.3	64	Includes binning of section halves.
	Section half binning (re-curation)	2R-1	23.0	154R-3	764.3	494	155R-1	765.1	240R-3	1181.3	228	Existing sample and description intervals will have to be shifted.
Imaging	Whole-round section imaging	2R-1	23.0	36R-2	190.4	220	235R-1	1153.1	259R-2	1265.3	64	The GCR is currently not equipped for this task.
	Archive section half imaging	2R-1	23.0	130R-4	648.9	414	8R-1	52.1	259R-2	1265.3	763	Essentially all images to be repeated on the re-curated and dry section halves.
	Working section half imaging	2R-1	23.0	234R-3	648.7	295						No further imaging on working section halves.
Description	Archive section halves described (and imaged)	2R-1	23.0	130R-4	648.9	414	2R-1	23.0	36R-2	190.4	73	Structural descriptions should be integrated in final template.
	Working section halves described (and imaged)	131R-1	648.9	234R-3	1151.6	295	131R-1	648.7	154R-3	764.3	79	Ideally re-describe in archive half (lower priority).
	Sections described through liner	155R-1	765.1	234R-3	1151.6	215	155R-1	765.1	234R-3	1151.6	215	Redescribe after binning/re-curating.
Sampling	Sections described through liner	235R-1	1153.1	259R-2	1265.3	64	235R-1	1153.1	259R-2	1265.3	64	Describe archive section halves after splitting/binning.
	TS batch 1: completed on board (mainly gabbroic rock types)	22R-1	121.0	36R-1	189.2	9	8R-1	52.1	259R-2	1265.3	~200?	Starting with Core 8R, sampling was restricted in various ways based on changing core processing protocols as well as by type of lithology. This applied not only to TS, but also to other shipboard sampling and measurements (e.g., ICP, MAD, and PMAG).
		131R-1	649.1	211R-1	1037.2	44						
	TS batch 2: billets cut on board (mainly serpentinite)	2R-2	24.5	6R-2	43.8	6						
133R-1		659.0	188R-1	925.8	20							
TS batch 3: billets marked, not cut (mixed rock types)	162R-1	799.0	218R-3	1074.5	14							

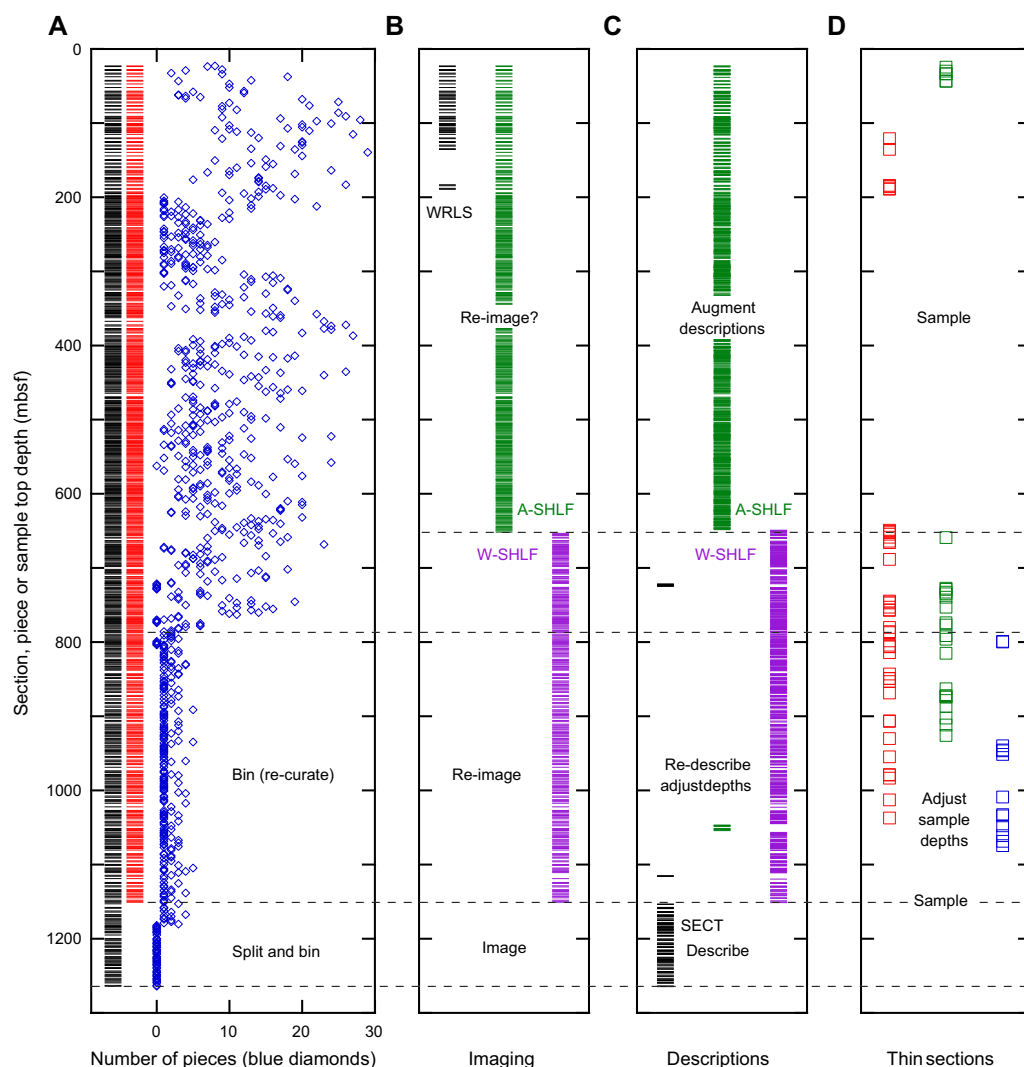


Figure F15. Shipboard core curation, imaging, description, and sampling work was limited on *JOIDES Resolution*; work will be completed on shore at Gulf Coast Repository in late 2023 under mandated safety precautions. See Table T3 for detailed section and depth information. A. Status of curation of sections from Hole U1601C: black = top depths of all core sections, red = top depths of all section halves (i.e., sections split on ship), blue = number of pieces curated for each section. Drop-off at ~800 mbsf means that sections were no longer adequately curated. B. Status of imaging: black = whole-round sections imaged (discontinued because of core processing restrictions), green = archive section halves imaged (standard procedures), purple = working halves imaged (result of special procedures). C. Status of core description for igneous petrology team's descriptions: green = descriptions made on archive halves (standard procedures), purple = descriptions made on working halves (to accommodate special core handling procedures), black = descriptions made on whole-round sections through liners (forced by ultimate restrictions). D. Status of thin section subsampling: red = "Batch 1," subsampling completed on ship (mainly gabbroic rock types); green = "Batch 2," TSBs cut on ship and sent to commercial service (mainly serpentinite); blue = "Batch 3," TSBs marked but not cut on ship (mixed rock types). Thin sections are critical for overall description of cores. Other regular shipboard sampling for physical and magnetic properties and geochemistry was similarly limited.

4.2.3. Principal results

4.2.3.1. Igneous petrology

The primary igneous and mantle lithologies are summarized here without regard to changes induced by deformation and alteration. Drilling at Site U1601 recovered in situ sections of mantle rocks with subordinate igneous intrusions. Combined, Holes U1601A and U1601C are dominated by serpentinitized peridotites, with 56% harzburgite, 9% orthopyroxene-bearing dunite, and 3% dunite. Gabbroic lithologies constitute approximately one third of the total and have a range of scales, from millimeter-sized veins to bodies tens of meters in size. Diorite, diabase plus basalt, and ultramafic veins are rare (<1% total).

4.2.3.1.1. Hole U1601A

Hole U1601A cores are mostly peridotites (harzburgite to dunite) with subordinate basalt, gabbro, and diorite. Six lithologic units were defined within the sequence, primarily based on changes in lithology. Subunits were defined in some of these units where mineral modes changed or where veins crosscut a unit.

The uppermost unit is a microcrystalline aphyric basalt with filled vesicles (Subunit 1A) and segregation veins (Subunit 1B). Below the basalt is a series of peridotites with primary textures severely overprinted by alteration and deformation. The uppermost peridotite unit (Unit 2) is a highly altered and weathered harzburgite. The unit below is a dunite (Unit 3) with patches and trails of Cr-spinel. The dunite is mostly pyroxene-poor (Subunit 3A) but grades into an interval of orthopyroxene-bearing dunite (Subunit 3B). The dunite is underlain by two narrow intervals of highly deformed and altered gabbro (Unit 4), separated by a single pebble of dunite (Subunit 4B).

The rest of Hole U1601A is dominated by harzburgite. At shallow levels, it is highly altered and weathered (Unit 5) and becomes slightly fresher below 27.7 mbsf (Unit 6). Unit 6 peridotite has variable proportions of pyroxene and associated variations in texture. Orthopyroxene proportions vary at the scale of a few to tens of centimeters, ranging 10%–25%. Locally, orthopyroxene proportions are below 10% and the harzburgite grades into orthopyroxene-bearing dunite (Subunit 6D). From Section 399-U1601A-10R-1 (49 mbsf), two different orthopyroxene morphologies are present, granular and interstitial, indicative of a multistage petrogenetic history (Subunit 6E). Clinopyroxene is relatively rare (< 3%) and mostly confined to the upper 23 m of the unit. The Unit 6 harzburgite contains a narrow interval of deformed gabbro (Subunit 6B) and is crosscut by a centimeter-wide diorite vein (Subunit 6C).

Hole U1601A was drilled in the general footprint of Expedition 357, and the igneous stratigraphy of this hole is similar to nearby Expedition 357 Hole M0069A. The aphyric and microcrystalline nature of the basalt recovered at the top of Hole U1601A resembles the diabase found in Hole M0069A. Like Hole M0069A, a series of harzburgite and dunite was recovered below the basalt/diabase, with the dunite containing Cr-spinel. No gabbroic rocks were recovered in Hole M0069A, although narrow (tens of centimeters) metagabbro and oxide gabbro intervals were observed in Holes M0072B and M0076B located within ~600 m of Hole U1601A. Further, in contrast to the three Expedition 357 central sites (Holes M0069A, M0072B, and M0076B) no talc-amphibole-chlorite schists or breccias were recovered in Hole U1601A. Whether this is a genuine geologic difference or it relates to the low recovery (~8%) during drilling the shallowest sections of Hole U1601A is uncertain.

4.2.3.1.2. Hole U1601C

Recovery of cores in Hole U1601C began beneath casing at 23 mbsf and terminated at 1268 mbsf. Unit 1 of this hole consists of microcrystalline to aphyric basalt. A long in situ section of mantle rocks with subordinate igneous intrusions is below. Unit 2 comprises the primary peridotite lithologies. Subunit names for these lithologies are primarily based on the relative proportions of olivine and orthopyroxene because the recovered mantle lithologies are dominated by clinopyroxene-poor varieties. Subunit 2A is harzburgite, Subunit 2B is orthopyroxene-bearing dunite, and Subunit 2C is dunite. Each gabbroic body encountered has a unit name unless nearby intervals have similar magmatic features even if separated by another unit (e.g., an interval of peridotite).

The distribution of the various rock types in the section is uneven. In the top 180 m, dunite is relatively abundant. Gabbroic intrusions are relatively common between ~120 and ~195 mbsf. Between 200 and 640 mbsf, the section is dominated by harzburgite, with rare dunite and gabbro. The proportion of gabbroic rocks gradually increases again from ~640 mbsf, and gabbros are particularly prevalent below ~950 mbsf.

Minor amounts of other ultramafic lithologies were recovered in the upper 600 m of Hole U1601C. These rocks show a range of modal abundances, ranging from websterite and olivine websterite to orthopyroxenite and wehrlite. They are typically found as veins in olivine-rich peridotite hosts.

Gabbroic bodies are found throughout Hole U1601C and are particularly concentrated toward the bottom of the hole (>950 mbsf). In total, we have recorded 438 intrusive bodies, comprising 301 units. Most individual gabbroic bodies are millimeter- to centimeter-sized veins, with progressively fewer intrusions in the 10 cm–1 m, 1–10 m, and >10 m categories. By volume (as measured on the section half surface and uncorrected for unit dips), approximately three quarters of the gabbro bodies are >1 m thick, and approximately one quarter of the gabbro bodies are thicker than 10 m.

Lithologically, the gabbroic rocks are dominated by gabbro, with lesser gabbronorite and olivine gabbro (Figure F16). Other gabbroic lithologies (e.g., troctolite and oxide gabbro/gabbronorite) are relatively rare. Gabbro and gabbronorite have a wide range of thicknesses, whereas troctolite is present only as components of larger gabbroic bodies (0.1–10 m). Oxide gabbro and gabbronorite typically occur in centimeter- to decimeter-scale intervals within gabbroic bodies with less abundant oxide. Texturally, the gabbroic rocks in Hole U1601C are dominated by coarse average grain sizes and granular textures.

Contacts between gabbroic rocks (veins aside) and their host peridotites are generally sutured, and gabbroic rocks are commonly separated from the surrounding peridotite by a centimeter-scale zone of troctolite or olivine gabbro (Figure F17). Some gabbros have multicentimeter long clinopyroxene crystals at the contacts with peridotites.

U1601C-180R-1, 45–49 cm



Figure F16. Cut surface showing discrete gabbronorite vein in harzburgite (399-U1601C-180R-1, 45–49 cm).

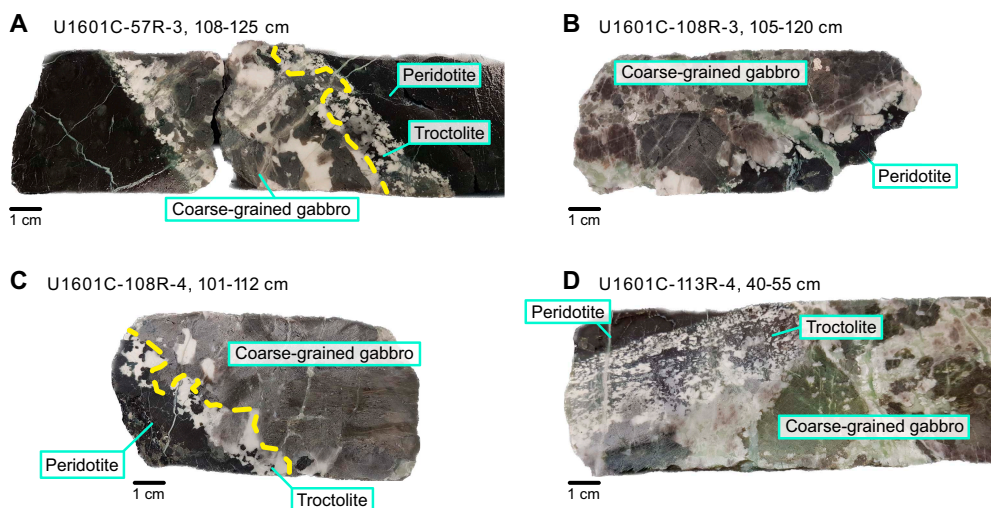


Figure F17. Troctolite contacts between coarse-grained gabbros and peridotites, Hole U1601C. A. Troctolite is present along contacts on both sides between gabbro intrusion and peridotite, with one side thicker than the other (57R-3, 108–125 cm). Note interstitial habit of olivine in the troctolite. B. Relatively thin troctolite contact between gabbro and peridotite, with euhedral plagioclase crystal growing across contact (108R-3, 105–120 cm). C. Granular olivine in mixed olivine gabbro to troctolite contact between coarse-grained gabbro and peridotite (108R-4, 101–112 cm). D. Thick troctolite with olivine-rich areas at gabbro-peridotite contact (113R-4, 40–55 cm).

Other minor lithologies in Hole U1601C are diorite and diabase. Diorite occurs as minor components in larger gabbroic bodies and is usually composed of plagioclase and hornblende, commonly with oxides. The diorite has textures suggesting that it intruded into and reacted with gabbro after the gabbro was largely or entirely crystallized. Diabase is present as 3 cm to 2.1 m dikes crosscutting gabbros.

4.2.3.2. Alteration petrology

Variably altered peridotites and gabbroic rocks were recovered from Site U1601. Peridotites include highly serpentinized (>50 vol% of the total rock volume is serpentine) harzburgite and minor dunite, as well as orthopyroxene-rich harzburgite that is exceptionally fresh (with ~20–50 vol% serpentinization) in some intervals. In serpentinized peridotites, olivine is highly altered to serpentine, magnetite, and traces of sulfides or alloy(s), as well as iowaite after brucite in Hole U1601A. Because of changes in the operational procedures, the presence of iowaite could not be verified in Hole U1601C. Orthopyroxene is partially to completely altered to serpentine in bastite texture, in which talc and/or chlorite can be locally abundant. These observations, while preliminary, suggest that serpentinization did not result in a major loss of Mg, Si, or Fe, and therefore the addition of water during serpentinization likely resulted in a significant volume increase (Malvoisin et al., 2020; Klein and Le Roux, 2020). The presence of magnetite and sulfides and/or alloy(s) in rocks from Site U1601 is indicative of reducing conditions (Klein and Bach, 2009; Beard et al., 2009; Andreani et al., 2013). Fluid inclusions, locally abundant in olivine from Hole U1601A, may contain gaseous methane and molecular hydrogen.

In shallow intervals, magnetite is locally oxidized to reddish brown iron oxide and iron oxyhydroxide minerals, indicative of less reducing conditions near the seafloor (Klein et al., 2017). At greater depths, magnetite seems less altered. Locally, in zones where serpentinized peridotite is juxtaposed with gabbroic lithologies, disseminated sulfide minerals, with unclear genetic relation with magnetite, were observed in mesh.

In addition to variably altered magmatic veins, most serpentinized peridotites are cut by two vein generations: an earlier generation composed of antigorite and/or lizardite and magnetite and a later generation composed of chrysotile or picrolite, suggesting that several serpentinization events occurred (cf. Rouméjon et al., 2017). Cu-Fe-sulfide veins associated with various proportions of carbonate and serpentine occur locally in the proximity of gabbroic rocks and provide evidence for carbon, sulfur, and base metal mobility between mafic and ultramafic rocks.

Gabbroic rocks, including gabbro, gabbro-norite, olivine gabbro, troctolite, and oxide gabbro, show a slight (~3%–20%) to moderate (~20%–50%), and locally high (>50%) degree of alteration. Gabbro is more extensively altered in intervals with a high degree of ductile and brittle deformation, high density of hydrothermal veins, and at contacts with serpentine. The main types of veins include amphibole, chlorite, talc, carbonate, and zeolite. Brown amphibole coexisting with recrystallized clinopyroxene in deformed gabbroic rocks is possibly of magmatic origin. Localized static alteration associated with hydrothermal veining resulted in the replacement of primary minerals by secondary ones (i.e., olivine by amphibole, talc, serpentine, magnetite, clay minerals, and sulfides; pyroxene by amphibole, talc, chlorite and/or clay minerals; and plagioclase by secondary plagioclase, chlorite, prehnite, and zeolite). Fluid inclusions in olivine, possibly containing reduced volatile species, are locally abundant.

The observations of mineral assemblages, microscopic textures and fluid inclusions, and crosscutting relationships of the alteration assemblages and hydrothermal veins indicate that sequential alteration and deformation of rocks at Site U1601 took place at conditions ranging from amphibolite through greenschist to subgreenschist facies.

Although these results are preliminary, the inferred alteration conditions have implications for mass transfer between hydrothermal fluid, mafic, and ultramafic rocks, the interplay between alteration and deformation, and the energy landscape of a serpentine-hosted subseafloor biosphere in the vicinity of the LCHF.

4.2.3.3. Structural geology

The structural evolution of the 1.2 km section cored at Site U1601 varies with recovered rock type. Holes U1601A and U1601C show similar structural geology in their overlapping intervals between 0 and 55 mbsf, both characterized by rare intervals of crystal-plastic and brittle deformation. Below 55 mbsf, all structural observations are recorded from Hole U1601C, as summarized below.

Magmatic veins are common throughout Hole U1601C, cutting both harzburgite and older host gabbro, and showing variable dips that steepen with depth. Thicker intervals of gabbro display rare magmatic foliations, with 75% of measured fabrics restricted to more evolved gabbro and gabbro-norite. Isotropic grain size layering/domains are common, with modal layering less common. Domain contacts are typically diffuse and irregular in shape.

Mantle fabrics and serpentine foliation hosted in peridotite vary in intensity, with subhorizontal to moderate dips, barring the interval 630–800 mbsf, where steep mantle fabrics and contacts are noted. In most cases, mantle fabrics and serpentine foliation are misoriented with respect to each other.

Crystal plastic deformation is limited in extent above 630 mbsf. Below 630 mbsf, protomylonitic to ultramylonitic crystal plastic deformation is localized in five 25–50 m thick high strain shear zones and one zone of distributed deformation separated by zones of little deformation. A total of 95% of crystal-plastic deformation occurs in gabbroic rocks, and it is typically concentrated adjacent to gabbro-peridotite contacts with contact-subparallel dips (Figure F18). Macroscopically, undeformed gabbroic rocks commonly display minor dynamic recrystallization of plagioclase. Mylonitic gabbro samples are dominated by dynamic recrystallization of plagioclase and to a lesser extent, pyroxene and amphibole. All five shear zones display reverse sense deformation. Shear Zones 1 (630–675 mbsf), 3 (950–975 mbsf), and 5 (1125–1150 mbsf) also show local normal shear sense. Where present, normal sense mylonitic foliation is steeper ($>50^\circ$) than reverse sense fabrics; steep mylonitic fabrics overprinted by late shallow mylonitic fabrics are infrequently observed. Rare diabase/microgabbro intervals display both pre- and postdeformation relationships with crystal-plastic fabrics, some of which are crystal-plastically deformed; others are crosscutting mylonitic fabrics. Amphibole and chlorite veins cut mylonitic fabrics. Microstructural fabrics, mineral assemblages, and crosscutting relationships suggest mylonitization occurred at granulite through amphibolite facies conditions.

Sparse occurrences of brittle deformation (fracturing, brecciation, and cataclasis) overprint each crystal-plastic shear zone, as well as some intervals within the low strain zones, including the interval 420–580 mbsf, and is commonly associated with hydrothermal veins. Total strain accommodated by brittle deformation is low. Slickenfibers record dominantly reverse sense shear. Brecciated diabase is observed.

Hydrothermal veins are more common between 0 and 300 mbsf and between 400 and 750 mbsf, with variable dips. Thin white chrysotile veins are a common feature of the serpentized harzburgite, and typically mimic the orientation of local serpentine foliation. Talc veins observed in gabbroic intervals, particularly at gabbro-peridotite contacts, are commonly sheared but can both cut mylonitic foliation in gabbro or be undeformed.

Fault rocks clearly linked to detachment faulting were not recovered at Site U1601, although some fabrics in gabbroic rocks might be formed during related footwall deformation. In particular, no talc-tremolite-chlorite schists, which were recovered from multiple Expedition 357 holes (Früh-Green et al., 2016, 2017), were recovered. Poor recovery in Hole U1601A and casing to ~22 mbsf in Hole U1601C means that unrecovered fault rocks cannot be ruled out in the top 25 m of Site U1601.

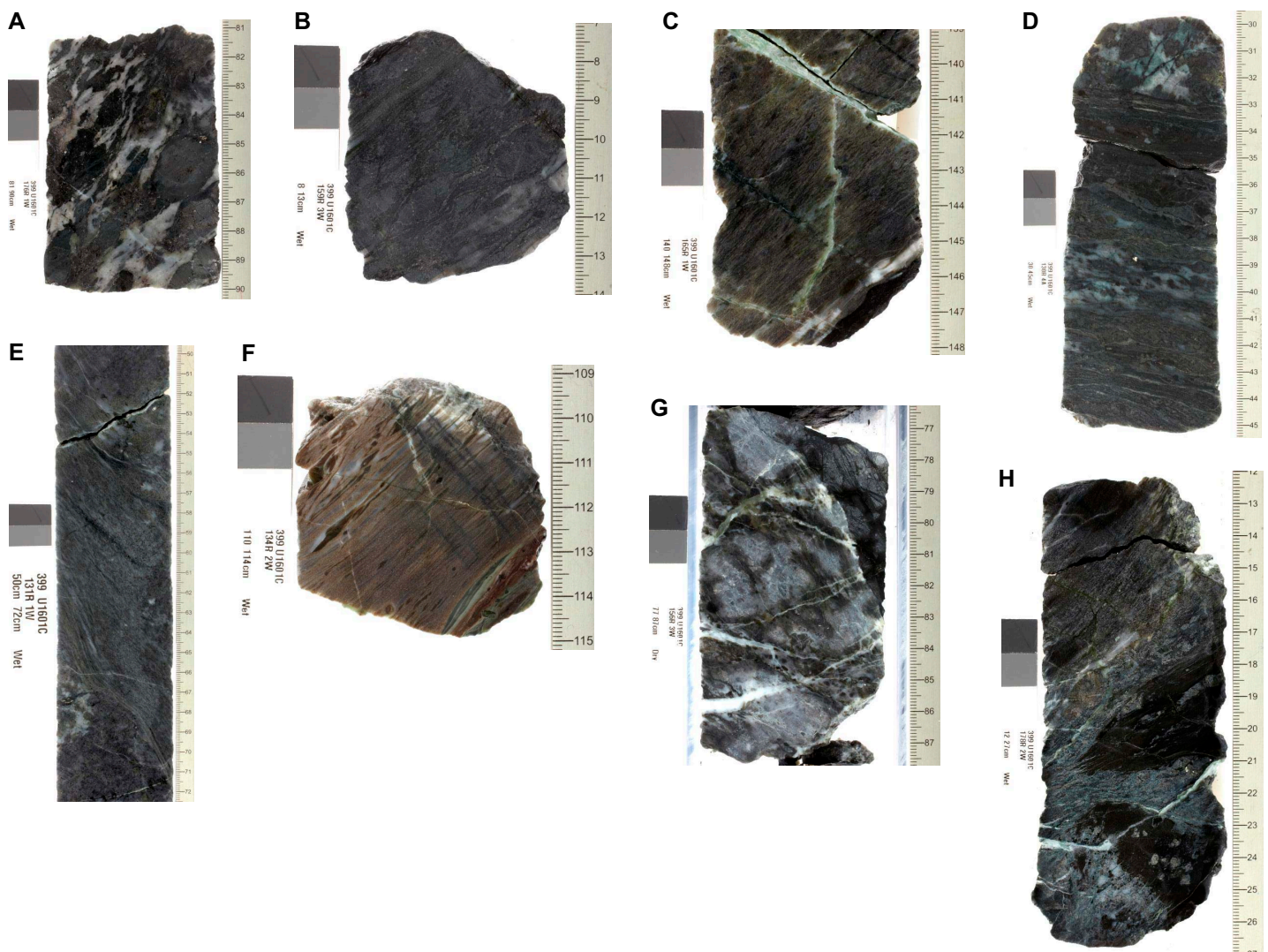


Figure 18. A. Gabbroic protomylonite (399-U1601C-176R-1, 81–90 cm; wet image). B. Oxide-gabbro protomylonite (159R-3, 8–13 cm; wet image). C. Gabbroic mylonite to ultramylonite in contact peridotite (dark brown, bottom right), reverse shear sense; undeformed talc \pm carbonate \pm prehnite veins cut mylonite (176R-1, 81–90 cm; wet image). D. Oxide-gabbro with protomylonitic, mylonitic, and ultramylonitic domains, controlled by variability of protolith grain size and/or lithology (130R-4, 30–45 cm; wet image). E. Gabbroic mylonitic to ultramylonitic discrete shear zone, normal shear sense (131R-1, 50–72 cm; wet image). F. Gabbroic ultramylonite (134R-2, 100–114 cm; unoriented, wet image). G. Irregular sheared contacts between mylonitic gabbroic rock (gray) and protomylonitic peridotite (dark brown); alteration veins cut mylonitic fabric (178R-2, 12–27 cm; wet image). H. Sheared contact between protomylonitic gabbroic rock (gray) and protomylonitic peridotite (dark brown-gray, top left); green-white talc \pm carbonate \pm prehnite alteration and veins overprint and cut mylonitic fabric (156R-3, 77–78 cm; wet image).

4.2.3.4. Geochemistry

Whole rock chemical analyses (major and trace element concentrations, total carbon and hydrogen, and inorganic carbon) were performed on 220 samples from Site U1601 for geochemical (hereafter referred to as CHEM samples) and microbiological (hereafter referred to as MBIO samples) studies. In Hole U1601A, 7 serpentinized peridotites and 1 diabase were collected as CHEM samples and 7 serpentinized peridotites and 1 basalt were collected for MBIO studies. In Hole U1601C, 144 serpentinized peridotites and serpentine veins, 44 variously altered gabbroic rocks, and 3 diabase and crosscutting carbonate veins were sampled as MBIO samples and 21 gabbroic rocks and 8 serpentinized peridotites were selected as CHEM samples. The 8 CHEM serpentinized peridotite samples will be processed and measured on shore.

MBIO samples have highly variable compositions compared to CHEM samples. This is likely the result of a sampling bias toward collecting material hypothesized to host more abundant microbial biomass including (1) more altered samples with higher prevalence of veins and/or (2) rocks with mixed mafic–ultramafic lithologies.

The composition of the serpentinized peridotite samples overlaps the field of refractory serpentinized peridotites previously collected during Leg 209 at the 15°20' Fracture Zone (also known as the Fifteen Twenty Fracture Zone [FTFZ]; Kelemen, Kikawa, Miller, et al., 2004; Godard et al., 2008). There is evidence of melt/rock interactions in dunites (iron enrichment) and harzburgites (possible refertilization and melt impregnation).

The composition of Site U1601 gabbroic rocks overlaps with the full range of Site U1309 gabbroic rocks. Gabbro recovered from the bottom of Hole U1601C is more evolved than gabbro from Site U1309. Gabbros at the bottom of Hole U1601C are also the least altered mafic plutonic rocks of Sites U1309 and U1601.

The serpentinized peridotites, gabbroic rocks, and other lithologies collected at Site U1601 contain variable amounts of carbon, mostly hosted in Ca-carbonates, in contrast to the low abundance of carbon in rock samples recovered at Site U1309.

Fluids collected from the series of KFTS runs shortly after logging operations were a mixture of the fresh drill water used to flush the hole, seawater, and possibly formation fluids. Eight cores were returned with significant volumes of fluid due to obstructions between the core and the plastic liner. The geochemistry of these samples was similar to the surface seawater used to flush the hole during drilling, with some samples that had slightly higher pH values. Borehole fluids collected with the KFTS contained detectable H₂ and CH₄ concentrations that increased with depth. Small fluid volumes that were recovered from the core catcher of most cores contained highly variable H₂ concentrations that did not increase or decrease with depth.

4.2.3.5. Microbiology

Microbiological investigations at Site U1601 were intended to explore the potential for life in the shallow subsurface of the Atlantis Massif at a site where serpentinized rocks were expected to be prevalent. Initial observations of cores from Hole U1601A were consistent with this goal. The surprising depth of Hole U1601C provided the unexpected opportunity to document the distribution of life through >1.2 km of the Atlantis Massif, possibly spanning environmental conditions from highly favorable to too extreme for life. Microbiology samples were collected for traditional analyses such as cell counts, cultivation, and DNA sequencing, as well as organic geochemistry analyses intended to document the presence of organic compounds including lipids, organic acids, and amino acids.

A total of eight MBIO WR samples were collected from Cores 399-U1601A-2R through 12R. Six of these samples are serpentinized harzburgite, plus one diabase and one serpentinized dunite.

A total of 191 MBIO WR samples were collected from 172 different cores from Hole U1601C. These samples were chosen with the goal of assembling a sample collection that is balanced with respect to apparent biological potential and geological representation while avoiding pieces that are geologically unique. Most samples are serpentinized harzburgite (60%), followed by serpentinized orthopyroxene-bearing dunite (14%), gabbro (12%), and serpentinized dunite (5%).

PFT assays were conducted with (1) samples of loose rubble collected during the core shake-out, (2) chiseled shavings of the exteriors of MBIO WR samples, and (3) crushed interior zones after the exteriors were removed by chiseling. PFT levels in loose rubble samples were in the range of 1–10 ppb in most samples and reached 10–25 ppb in 20 samples. A few extreme outliers up to 257 ppb were the result of accidental increases in the rate of PFT delivery during drilling. The fairly consistent and high levels of PFT in loose rubble samples confirmed the successful delivery of PFT during drilling. In contrast, PFT was absent or present at only trace levels in nearly all samples of crushed interiors. These results indicate that surface contamination, as measured by PFT, was largely removed from the interior samples.

The 191 MBIO WR samples from Hole U1601C were subsampled for up to 16 different microbiological and biogeochemical analyses, including microscopy (synchrotron-based microscopy, scanning electron microscopy, and counts of cells and viral-like particles), sorting of single cells, and analyses of DNA, lipids, and organic compounds. A wide range of cultivation experiments were also conducted, including incubations of crushed interiors in filter-sterilized seawater (157 sam-

ples), enrichment incubations (88 samples with different temperatures and nutrients), high-pressure incubations (5 samples), and stable isotope tracer experiments (33 samples).

Samples of borehole water from Hole U1601C were collected with the KFTS to characterize the extent, diversity, and activity of microbial communities within Hole U1601C. In addition, small volumes of fluids collected from the core catcher and analyzed for H₂ concentrations were also used for microbiological analyses, including single-cell activity and sorting experiments and DNA sequencing.

4.2.3.6. Petrophysics

The petrophysical properties of rocks at Site U1601 were characterized through measurements on WR cores, including measurements of natural gamma radiation, magnetic susceptibility and gamma ray attenuation bulk density. Discrete measurements were completed on rock cubes and cuttings of MBIO samples and included wet mass, dry mass, dry volume, and *P*-wave velocity. Bulk density, grain density, and porosity were calculated from the mass and volume measurements. *P*-wave measurements were also completed on archive-half pieces when rock cube samples were not available in Hole U1601C. Additionally, archive section half core pieces >10 cm in length were selected for thermal conductivity measurements. Downhole temperature logs were completed in Hole U1601C. A total of five wireline logging tool strings were deployed in Hole U1601C. The diameter of the borehole from caliper measurements is quite regular and is close to the bit size (9.73 inch) with a few larger diameter intervals. The hole is deviated a total of 10° from vertical in a northeast direction at the maximum logging depth (~1060 mbsf).

4.2.3.6.1. Density and porosity

The bulk density measured on discrete samples of serpentized peridotites ranges 2.34–2.72 g/cm³, and averages 2.55 ± 0.08 g/cm³. The grain density ranges 2.52–2.97 g/cm³, and averages 2.66 ± 0.05 g/cm³. Bulk density and grain density increase slightly downhole. Bulk density in gabbros ranges 2.5–3.24 g/cm³. The bulk density was measured downhole using the HLDS during logging Run 1. The bulk density has a baseline value of ~2.6 g/cm³, which best fits serpentized peridotites. Inflections with higher bulk density values are indicative of gabbro.

The porosity of serpentized peridotites ranges 1.7%–20.4%, and averages of 7.0% ± 3.7%. The porosity in gabbro has a range of 0.3%–to 13.6%, and averages 3.7% ± 3.5%. Porosity in serpentized peridotites and in gabbros is lower at shallower depths, higher between 200 and 300 mbsf, and then decreases with depth.

4.2.3.6.2. Sonic velocity

Sonic velocity on cube samples was measured along the three principal directions *x*, *y*, and *z* in the CRF. The average velocity of serpentized ultramafic rocks is 4480 m/s, ranges 3442 m/s (serpentized harzburgite; Section 399-U1601C-49R-4; 255.2 mbsf) to 5960 m/s (serpentized dunite; Section 193R-1; 950.8 mbsf). The average velocity in gabbroic rocks is higher than that in serpentized ultramafic rocks and is 5906 m/s, ranging from 4187 m/s (gabbronorite; Section 52R-2; 267.0 mbsf) to 6532 m/s (olivine gabbro; Section 32R-2; 170.3 mbsf). The apparent anisotropy of sonic velocity ranges from 0.5% (gabbro; interval 22R-1, 56.5–58.5 cm; 120.6 mbsf) to 11.8% (serpentized harzburgite; interval 148R-3, 113–115 cm; 734.9 mbsf). Sonic velocity was measured downhole using the DSI during logging Run 4. A baseline of *P*-wave velocity of ~4000 m/s and a baseline *S*-wave value of ~2000 m/s are reflective of the high proportion of serpentized peridotites in Hole U1601C. Velocity overall increases with depth.

The VSI was deployed on logging Run 5. A total of 13 stations spaced 100 m apart were measured. *P*-wave velocity measured using the VSI matches the velocities from the DSI. The average velocity across all stations is ~4500 m/s with a range of 3638 m/s at the shallowest depth (~58 mbsf) to 5299 m/s in the deepest part of the hole (~1070 mbsf). This is broadly comparable with existing seismic data.

4.2.3.6.3. Magnetic susceptibility

Magnetic susceptibility measured on the cores ranges 1,000–15,500 IU in serpentized peridotites. Gabbros have magnetic susceptibility values that range 0–23,500 IU. The vast majority of gabbros have very low to zero magnetic susceptibility values (<100 IU). The main exceptions are

Fe-Ti oxide gabbros that have the highest values of any rock type. Magnetic susceptibility was measured downhole with the MSS during logging Run 3. Magnetic susceptibility values are variable downhole, with the highest value matching the higher magnetic susceptibility measured in serpentinized peridotite cores. Downhole variations in magnetic susceptibility measured on cores and downhole match well.

4.2.3.6.4. Natural gamma radiation

Natural gamma radiation (NGR) is low overall with both gabbros and serpentinized peridotites having values of <1 counts/s. The highest values of 3–13 counts/s occur in serpentinized peridotites. NGR was measured downhole using the HNGS during logging Runs 1, 3, and 4. Downhole values are low below ~185 mbsf, with a baseline value of ~0.5 American Petroleum Institute gamma radiation units (gAPI). Between 30 mbsf (right below the logging bit) and ~185 mbsf, values are variable and as high as 35 gAPI. Standard spectral analysis by the commercial software yielded <0.1 wt% ⁴⁰K, ~2 ppm ²³⁸U, and ~0.6 ppm ²³²Th, with some negative values indicating that the lower counts are below the threshold required to compute accurate K, U, and Th concentrations.

4.2.3.6.5. Electrical resistivity

Electrical resistivity was measured using the HRLA tool during Run 2 and returned a baseline value of ~3.7 Ωm for the deep penetration. Gabbro is in general more resistive than serpentinized peridotite.

4.2.3.6.6. Borehole imaging

The UBI was employed during logging Run 2, and the FMS was used during logging Run 4. The FMS logs are of good quality and cover the depth interval 72–1072 mbsf. Serpentinized peridotites have a mottled appearance, likely reflecting the different resistivities of phases present. Gabbros have a more consistent resistivity response. At least four distinct planar features can be identified including conductive planes (darker color, likely fractures), resistive planes (light color, likely veins), and contacts (different textures), and fabrics.

4.2.3.6.7. Thermal conductivity

Thermal conductivity was measured on 48 archive section half samples selected from representative lithologies of Hole U1601C. A total of 38 ultramafic samples were measured with thermal conductivity values ranging 2.20–3.56 W/(m·K) and a mean of 3.02 ± 0.26 W/(m·K). Ultramafic samples from Hole U1601C generally show higher thermal conductivity compared to those recovered from Hole U1601A (averaging 3.02 and 2.56 W/[m·K], respectively). A total of 20 gabbroic samples have generally lower thermal conductivity than the ultramafic samples, averaging 2.63 ± 0.54 W/(m·K), and contain much higher variability, ranging 2.04–4.09 W/(m·K).

4.2.3.6.8. Downhole temperature logging

Borehole fluid temperatures were measured several times in Hole U1601C. Five runs of the ETBS were conducted. Maximum temperatures recorded at the bottom of the borehole change over time, as fluids were warmed by the surrounding formation. Logging Run 1 reached the bottom of the borehole (997.6 mbsf) ~17 h after flushing the hole with cool freshwater had ceased and recorded a maximum temperature of 70.3°C. Logging Run 4 measured a maximum temperature of 88.6°C at similar depths (1009 mbsf) ~64 h after flushing. Logging Run 5 recorded a maximum fluid temperature of 91.3°C at the bottom of the borehole (1060 mbsf) ~78 h after flushing.

4.2.3.7. Paleomagnetism

Remanence measurements were made on archive section halves from Holes U1601A and U1601C. These measurements generated 2,967 and 168,296 data points for Holes U1601A and U1601C demagnetization data sets, respectively, which helped determine the NRM of the rocks. Although the greater parts of the holes had NRM inclination values that generally clustered around an expected reversed geomagnetic polarity direction, the inclination values were quite variable. For Hole U1601A, the mean NRM inclination is $-22.2^\circ \pm 13.5^\circ$, whereas for Hole U1601C the NRM inclination is $-26.7^\circ \pm 32.8^\circ$. A low-coercivity drilling-induced component was removed by AF demagnetization steps of 10–15 mT, shifting the distribution closer to the expected GAD value of -49° . However, stronger AF steps ($>40^\circ$) shift the inclination distribution toward the present-day polarity, which suggests that the rocks contain multiple component directions, thus capturing a

complex remanence history. The timing of these remanence inducing events (e.g., tectonic rotation and hydrothermal synthesis of magnetite) cannot be uniquely determined from these data and will require further synthesis of geological data.

Archive section half data were complemented by discrete sample measurements. Both paleomagnetic and physical properties cube samples were analyzed using AF demagnetization, thermal demagnetization, isothermal remanent magnetization acquisition, and isothermal remanent magnetization backfield methods. Additionally, paleomagnetism cube samples were pretreated with liquid nitrogen dunking as a way of reducing the drilling overprint. Analysis of these data supported the variable nature in magnetic properties. The numerous high-quality discrete samples measured corroborate the variable inclination and intensity values of the archive section half data set. Although the bulk remanence of these rocks was carried by magnetite, some samples showed a significant magnetic contribution from gyro remanent minerals, likely some species of iron sulfide. Magnetite populations vary in terms of coercivity, likely indicating variable grain size and oxidation downhole for each hole.

AMS data were predominantly characterized by oblate magnetic fabrics. The relatively low recovery of Hole U1601A limited this type of analysis; thus, most of the AMS results were only meaningful for Hole U1601C. For Hole U1601C, the clustering of the shortest magnetic axis (K_{\min}) around vertical indicates that the direction of magnetic flow was subhorizontal. Particular regions, however, display elongated fabrics, or regions of greater anisotropy. The regions of magnetic elongation correspond well with the depths of recovered deformed gabbro units (200 and 600 mbsf). These observations suggest that different interval depths experienced different tectonic and/or alteration histories.

5. Preliminary scientific assessment

5.1. Operations

Expedition 399 consisted of 46 operational days on station over the time frame from 12 April to 12 June 2023. By almost any measure, drilling operations during Expedition 399 were incredibly successful. Although we did not reach our preexpedition target depth of ~2060 mbsf in Hole U1309D, the lack of progress was entirely due to decisions by the Science Party to prioritize the continued successful drilling in Hole U1601C where our scientific targets were far exceeded. In doing so, we drilled the deepest hole ever initiated for a single oceanic hard rock scientific expedition, previously accomplished during IODP Expedition 360 in Hole U1473A (789.7 mbsf) (Tables **T1**, **T2**). Previous holes drilled to >1000 mbsf required 12–98 bit runs over 2–8 expeditions (Table **T2**) to reach the full depth. In comparison, Hole U1601C was drilled with only 8 total bit runs (5 coring runs) and had remarkable core recoveries over the entire hole averaging 71%, with 24% of cores achieving recoveries >90%. Access to a continuous record through extended sections of the hole will provide robust constraints on the architecture and composition of the oceanic mantle lithosphere.

Three water sampling campaigns recovered high quality borehole fluids from both Holes U1601C and U1309D, including the inaugural deployment of the MTFs, which provided larger volumes at each depth and was designed for chemical compatibility for geochemical species of interest. The success rate of water sampler deployments was overall ~50% for the MTFs and 70% for the KFTS, which compares well to previous expeditions in Hole 504B and at Brothers Volcano (de Ronde et al., 2019).

A full suite of logging operations carried out in Hole U1601C obtained high quality data to complement and extend the data from recovered cores. The thermal profile of the hole was documented as it rebounded after extensive flushing, while magnetic susceptibility will provide further constraints on the distributions of gabbro and serpentinized peridotite downhole. Image logs can be used to reorient contacts of collected cores.

Significant challenges were encountered during shipboard processing of cores. The high recovery and rapid drilling rates imposed a significant strain on the technical staff and Science Party whose

numbers were already limited because of COVID-19 restrictions and the absence of two members for last-minute personal reasons. From 6 to 22 May 22, 5 m core intervals with almost complete recoveries were recovered every 1 h and 45 min with only a few longer breaks during bit changes. Coring rates eventually slowed when intervals dominated by gabbroic lithologies were encountered.

The recognition of chrysotile in hydrothermally altered peridotite cores triggered a halt of many core processing activities. After consultation with shore-based management and TAMU EHS, some activities resumed with new protocols designed to minimize airborne chrysotile. These protocols remained in place for several weeks before activities were again severely curtailed. Deviations to regular core processing activities included the following (Table T3; Figure F15):

- Many core sections were not split at sea and instead were capped wet on the catwalk and stored in their liners. For these cores, some WR core measurements were carried out, and descriptions were performed through the core liners.
- The majority of WR cores from Hole U1601C were not imaged prior to splitting.
- The majority of split cores from Hole U1601C were imaged wet through plastic sheeting and were not measured for spectral reflectance and magnetic susceptibility via the Section Half Multisensor Logger.
- A significant subset of split cores were not binned or labeled for curation.
- Thin sections of hydrothermally altered peridotite were not made for the majority of cores from Site U1601.
- X-ray diffraction (XRD) was not carried out on samples of any kind for the majority of the recovered cores.
- Shipboard sampling for thin sections, physical properties, and geochemistry was only carried out for a small number of cores from Hole U1601C.
- The preparation of hydrothermally altered peridotite samples for inductively coupled plasma spectroscopy analysis was carried out solely by the Science Party. Because of the restrictions on shipboard sampling, most analyses were performed on the residues of MBIO samples.
- Personal sampling was halted except for MBIO samples and a few additional time-sensitive samples.

As a result of these shipboard challenges, most of the teams were not able to characterize the recovered material with the level of detail and confidence that the community has come to expect from IODP expeditions. Plans are currently under development to address these gaps including splitting WR sections; drying and imaging section halves; recuring unbinned section halves to preserve the long-term integrity of the sections; organizing a small group of scientists to complete “shipboard” sampling for thin sections and physical properties measurements; creating thin sections from hand specimens and billets by a commercial laboratory, with subsequent distribution to Science Party members for initial descriptions; XRD analysis of powders; and a full sampling party for complete description of the cores and personal sampling.

5.2. Scientific objectives

5.2.1. Objective 1: characterizing the life cycle of an oceanic core complex and the links among igneous, metamorphic, structural and fluid flow processes

Hole U1601C is a unique 1268 m section through serpentinized mantle rocks containing numerous gabbroic (“lower crustal”) intrusions. When combined with Hole U1309D (deepened to 1498 mbsf during Expedition 399) the shallow holes of Expedition 357, and seismic data (Figure F1), we have by far the most comprehensive data set on the life cycle of a typical mafic/ultramafic OCC.

The life cycle of a core complex begins with mantle rocks uplifted by corner flow in the spreading environment and affected by high temperature partial melting and porous flow of melts. These processes are evident through observations of dunite and the growth of secondary orthopyroxene in harzburgite. The products of partial melting at deeper levels are seen intruded as a complex network of more than 400 gabbroic intrusions in the section cored in Hole U1601C. Melt-rock reaction textures are also seen in the gabbroic pluton sampled in Hole U1309D, indicating the complexity of the melting and intrusion processes in the Atlantic Massif.

Further unroofing at subsolidus temperatures was accommodated by deformation and hydrothermal alteration over waning temperature conditions. We see strain accommodated by crystal plastic deformation at temperatures $>600^{\circ}\text{C}$ overprinted by brittle faulting, cataclasis, and hydrothermal veining at Site U1601 and recorded a new cataclastic fault zone in Hole U1309D. Hydrothermal fluids infiltrated the rocks, probably in small quantities, at temperatures $>700^{\circ}\text{C}$. Further hydration reactions occurred in amphibolite and greenschist facies in gabbroic rocks, particularly close to contacts with ultramafic rocks. High fluid fluxes in some zones are indicated by intense alteration, including dissolution of minerals to form macroscopic reaction porosity. The most ubiquitous alteration is serpentinization of peridotite, likely occurring at $200^{\circ}\text{--}350^{\circ}\text{C}$ (Klein et al., 2014), probably before complete unroofing of the massif by detachment faulting.

The latest phase in the life cycle of the Atlantis Massif is the uplift of the unroofed massif, hydrothermal circulation forming the LCHF, and low temperature alteration and subsea weathering. Hole U1601C is ideal for investigating the hydrogeology and thermal structure of the massif and preliminary temperature results from logging indicate borehole fluid temperatures $>90^{\circ}\text{C}$ at 1060 mbsf. Because of vigorous fluid circulation at the end of drilling, this is a minimum temperature for the surrounding rock, and metamorphic reactions could be occurring at ambient temperatures well over 100°C in the rocks surrounding the borehole.

5.2.2. Objective 2: accessing the chemical kitchen that preceded the appearance of life on Earth

A major goal of the expedition was to link abundances of H_2 and organic molecules with the physical and chemical conditions that lead to their synthesis. Of particular interest was accessing zones where active serpentinization could lead to the production of H_2 and zones above the temperature limit of life to examine geochemical reactions without a biological overprint.

In Hole U1309D we successfully recovered cores and fluids from zones at temperatures of 140°C , well above the currently recognized limit to life. Olivine gabbro and olivine-bearing gabbro were abundant, and in some cases, olivine was replaced by secondary minerals including serpentine, magnetite, and clay, which can be associated with H_2 production and organic carbon formation. Fluid inclusions in olivine, possibly containing H_2 and/or CH_4 , were locally abundant. The geochemistry of the sampled fluids indicates they were a mix of seawater, formation water, and reacted water from the base of the hole.

Site U1601 was primarily chosen to access an actively serpentinizing environment. The dominant lithology in Holes U1601A and U1601C is harzburgite that has been variably altered to magnetite-bearing serpentinite, suggestive of H_2 formation and reducing conditions. Fluid inclusions, possibly containing H_2 and/or CH_4 , were abundant in the few available thin sections that could be examined from Site U1601. The achieved drilling depths may have accessed a thermal regime above the limit of life because downhole temperature logs recorded a maximum of 91°C within 78 h of flushing with shipboard freshwater, prior to full equilibration of fluids. Elevated concentrations of hydrogen and methane were detected in fluids recovered by the borehole samplers, suggesting serpentinization is active and ongoing, or that pockets of volatile-rich fluids were liberated during drilling. The relationship of volatile distributions with depth, temperature, lithology, and other processes will provide insights into the processes that lead to their formation.

Shore-based analyses will greatly advance this objective. Fluids and rocks will be analyzed for the concentrations and isotopes of organic compounds to identify the forms of reduced carbon present in the subseafloor. Fluid inclusions have been identified in the few peridotite, olivine-gabbro, and troctolite thin sections that were available shipboard; further sampling and analysis will be needed to determine the extent of their distributions and the content of the inclusions. Similarly, shore-based analyses such as Fe-titrations will provide quantitative constraints on the valence of Fe and the formation of H_2 .

A second major goal was to leave both the deepened Hole U1309D and the new peridotite-hosted hole at Site U1601 in a condition such that future expeditions could relog them for temperature and conduct fluid sampling. Prior to our departure, both holes were flushed with seven borehole volumes of seawater to expel drill cuttings and other debris. To the best of our knowledge, no

significant material related to drilling or logging operations was left in the hole, and the camera surveys at the exit of the last bit runs indicated that the reentry cones remained intact.

5.2.3. Objective 3: characterizing the deep biosphere and limits for life in the Atlantis Massif, in particular the impact of lithospheric substrate, porosity, permeability, temperature, fluid chemistry, and reactive gradients

Rocks and fluids were extensively sampled to assess the extent of the deep biosphere and limits of life in Holes U1309D, U1601A, and U1601C. The depth of Hole U1601C provides an opportunity to sample material from near seafloor zones that appear to be more extensively weathered by interaction with oxic seawater, warm anoxic zones in which hydrothermal alteration is extensive and serpentinization appears to be ongoing, and a deep regime that may be at temperatures above the limits of life.

A target for the expedition was to preferentially sample zones of higher porosity and permeability to test whether these regimes are associated with greater microbial biomass and activity. Samples were selected for microbiological analysis in collaboration with a petrologist representing the core description teams so that low(er) temperature alteration phases could be preferentially sampled. Geochemical analyses indicate that the microbiology samples were more carbonate rich than average background samples.

The microbiology samples were extensively documented with general descriptions, 360° imaging, and geochemical analyses including shipboard inductively coupled plasma–atomic emission spectroscopy and coulometry. Because of the absence of other samples available for many shipboard measurements, the exteriors of microbiology samples were also subjected to more extensive analyses than is typically performed, such as porosity and density. The combined data set will allow robust insights into the physical and geochemical properties of locations where higher cellular abundances and indications of active metabolism are identified by shore-based analyses.

6. Outreach

Expedition 399 had a team of two Onboard Outreach Officers (OOO) on board the ship. One was a former teacher and current logistics planner for the United States Arctic Program, and the other was an informal educator and professional science communicator; both OOs were from the United States. The team provided ship-to-shore broadcasts, organized interviews, conducted interviews, and managed the ship social media and blog. They also had individual projects, including postcards sent back to shore and other educational/informative outreach initiatives.

6.1. Webcasts

Using a direct satellite link, the team was able to connect with classrooms and community groups across 16 countries, 15 states in the United States, and 2 remote-based schools (Table T4). This amounted to a total of 60 ship-to-shore tours, reaching over 3 million participants. The age ranges were a complete spectrum from kindergarten classrooms to nursing homes. Teacher workshop presentations generated immediate sign-ups following the presentation for their classrooms. Scientists actively participated in Q&A sessions following the tours. In addition, the team coordinated an “open house” call allowing for anyone who may desire to join in on a tour.

6.2. Social media

The team managed the *JOIDES Resolution* website, in addition to the ship’s Twitter, Facebook, and Instagram accounts (Table T5). Two Twitter chats were hosted, and the team also produced many reels, which are a trending social media genre. Together, the OOs posted 169 posts across all platforms, with over 2 million accounts reached, over 1.5 million accounts engaging, and over 5,000 new followers gained across all the platforms, respectively.

Table T4. Ship-to-shore broadcasts for a total of 60 Zoom tours and 3 million participants.

Country	Quantity	State	Quantity
Antarctica	1	United States	
Australia	4	Arizona	1
Canada	1	California	4
China	2	Colorado	1
France	1	Connecticut	5
Germany	1	Georgia	1
Greece	1	Illinois	2
India	1	Louisiana	1
Ireland	1	Massachusetts	5
Italy	1	Mississippi	2
Japan	3	New York	9
New Zealand	1	North Carolina	1
South Africa	1	Oregon	1
Spain	1	Pennsylvania	1
United Kingdom	1	Virginia	1
United States	See right	Washington, DC	2
		Remote school/Open house	2

Table T5. Readership (post views) and engagement (likes, shares, or replies to posts) of *JOIDES Resolution* social media networks during Expedition 399.

Platform	Time frame (2023)	Accounts reached	Accounts engaged
Facebook	March 9–June 6	1.8 million (+4,000%)	1.3 million (+5,000%)
Twitter	April 12–June 6	240,000	
Instagram	April 12–June 4	18,200 (+354%)	1,169 (+64.4%)

6.3. Media coverage

The outreach team coordinated several media outreaches, including TV, radio, and written publications (Table T6). This included prominent outlets such as The Wall Street Journal, The New Yorker, Science Magazine, The Washington Post, Al Jazeera English, and USA today as of the time of writing. The team also wrote 10 blog posts for the website.

6.4. Additional outreach

500 postcards were sent to 42 states in the United States and 15 other countries. Each postcard was hand-addressed and stamped with the *JOIDES Resolution* stamp as well as a unique stamp made for this expedition with the Expedition 399 logo.

An outreach flag that has traveled to all 7 continents and has now made it to the middle of the Atlantic Ocean was signed by hundreds of students, teachers, and members of the scientific community as well as the general public. A group photo was taken with the flag and the Science Party at the bow of the ship.

Before the expedition, professional educator conferences were attended to promote the expedition with teacher networks about opportunities to engage with their students. Teachers signed up for postcards and signed the outreach flag at these events.

From November 2022 to February 2023 “In Search of Earth’s Secrets” a pop-up museum exhibit featuring *JOIDES Resolution* was hosted at the University of Wisconsin-Whitewater. The exhibit was free and open to the public whenever the community engagement center was open, so full attendance numbers are uncertain. The exhibit had an opening gala drawing in 200 in attendance, including the university chancellor and provost. Students from the geology department were involved in helping to coordinate tours, and an estimated 150 students of various ages from 8 to college age participated in tours. News coverage of the exhibit included local papers, live radio, and University of Wisconsin-Whitewater newspaper publications.

Table T6. Media coverage during Expedition 399. TBD = to be determined.

Outlet	Title	Date	Link
Expedition blogs	Heading to the Atlantis Massif	22 Apr 2023	https://joidesresolution.org/expedition/the-lost-city-hydrothermal-field/
	Testing the Multi-Temperature Fluid Sampler	30 Apr 2023	
	End of an Era	4 May 2023	
	Record Hole in Mantle Rock	21 May 2023	
	Processing Microbiology Samples Onboard	26 May 2023	
	Preparing for Departure	3 Jun 2023	
NewsTalk 590 WVLC	Memorial Day Monday Morning Show with Dave Kesling	30 May 2023	
Wall Street Journal	Drilling Deeper into Ocean Floor in Search for Origins of Life	19 Feb 2023	https://www.wsj.com/articles/drilling-deeper-into-ocean-floor-in-search-for-origins-of-life-fadfcab2
Wall Street Journal (click through)	Looking for Origins of Life Scientists Hit Rock Bottom and Keep Drilling	16 Mar 2023	https://www.wsj.com/story/looking-for-origins-of-life-scientists-hit-rock-bottom-and-keep-drilling-24fc1532
Science	Long Last Ocean Drillers Exhume Bounty of Rocks from Earth's Mantle	25 May 2023	https://www.science.org/content/article/long-last-ocean-drillers-exhume-bounty-rocks-earth-s-mantle
Washington Post	In a Geologic Triumph, Scientists Drill Window into Earth's Mantle	6 Jun 2023	https://www.washingtonpost.com/science/2023/06/06/drill-earth-mantle-rocks/
USA Today	Geoscientists Drill Down into the Ocean for a Record-Breaking Close-up of Earth's Mantle	6 Jun 2023	https://www.usatoday.com/story/news/nation/2023/06/06/scientists-drill-earths-crust-collect-historic-samples-of-mantle/70295164007/
Popular Mechanics	After 60 years of Trying, Geologists Finally Pried Rocks from Earth's Upper Mantle	7 Jun 2023	https://www.popularmechanics.com/science/environment/a44089062/scientists-unearth-upper-mantle-rock/
Al Jazeera English	Television interview by Colin Baker	Story pending	
New Yorker	TBD; interviews with a reporter ongoing	Story pending	
National Geographic	TBD; hosted interviews with reporter, story not yet published	Story pending	

6.5. Postexpedition projects

Both outreach officers will continue to perform outreach to their local communities and in virtual events following the expedition. Additionally, contact information will be forwarded for follow up media inquiries as it is anticipated that more stories will be written and interviews conducted post expedition.

References

- Allen, D.E., and Seyfried, W.E., 2004. Serpentinization and heat generation: constraints from Lost City and Rainbow hydrothermal systems. *Geochimica et Cosmochimica Acta*, 68(6):1347–1354. <https://doi.org/10.1016/j.gca.2003.09.003>
- Allen, D.E., and Seyfried, W.E., 2005. REE controls in ultramafic hosted MOR hydrothermal systems: an experimental study at elevated temperature and pressure. *Geochimica et Cosmochimica Acta*, 69(3):675–683. <https://doi.org/10.1016/j.gca.2004.07.016>
- Andreani, M., Montagnac, G., Fella, C., Hao, J., Vandier, F., Daniel, I., Pisapia, C., Galipaud, J., Lilley, M.D., Früh Green, G.L., Borensztajn, S., and Ménez, B., 2023. The rocky road to organics needs drying. *Nature Communications*, 14(1):347. <https://doi.org/10.1038/s41467-023-36038-6>
- Andreani, M., Muñoz, M., Marcaillou, C., and Delacour, A., 2013. μ XANES study of iron redox state in serpentine during oceanic serpentinization. *Lithos*, 178:70–83. <https://doi.org/10.1016/j.lithos.2013.04.008>
- Beard, J.S., Frost, B.R., Fryer, P., McCaig, A., Searle, R., Ildefonse, B., Zinin, P., and Sharma, S.K., 2009. Onset and progression of serpentinization and magnetite formation in olivine-rich troctolite from IODP Hole U1309D. *Journal of Petrology*, 50(3):387–403. <https://doi.org/10.1093/ptrology/egp004>
- Becker, K., Davis, E.E., Spiess, F.N., and deMoustier, C.P., 2004. Temperature and video logs from the upper oceanic crust, Holes 504B and 896A, Costa Rica Rift flank; implications for the permeability of upper oceanic crust. *Earth and Planetary Science Letters*, 222(3–4):881–896. <https://doi.org/10.1016/j.epsl.2004.03.033>
- Blackman, D., Slagle, A., Harding, A., Guerin, G., and McCaig, A., 2013. IODP Expedition 340T: borehole logging at Atlantis Massif oceanic core complex. *Scientific Drilling*, 15:31–35. <https://doi.org/10.2204/iodp.sd.15.04.2013>
- Blackman, D.K., Cann, J.R., Janssen, B., and Smith, D.K., 1998. Origin of extensional core complexes: evidence from the Mid-Atlantic Ridge at Atlantis Fracture Zone. *Journal of Geophysical Research: Solid Earth*, 103(B9):21315–21333. <https://doi.org/10.1029/98JB01756>
- Blackman, D.K., Ildefonse, B., John, B.E., MacLeod, C.J., Ohara, Y., Miller, D.J., and the Expedition 304/305 Project Team, 2004. Oceanic core complex formation, Atlantis Massif—oceanic core complex formation, Atlantis Massif, Mid-Atlantic Ridge: drilling into the footwall and hanging wall of a tectonic exposure of deep, young oceanic lithosphere to study deformation, alteration, and melt generation. *Integrated Ocean Drilling Program Scientific Prospectus*, 304/305. <https://doi.org/10.2204/iodp.sp.304305.2004>
- Blackman, D.K., Ildefonse, B., John, B.E., Ohara, Y., Miller, D.J., Abe, N., Abratis, M., Andal, E.S., Andreani, M., Awaji, S., Beard, J.S., Brunelli, D., Charney, A.B., Christie, D.M., Collins, J., Delacour, A.G., Delius, H., Drouin, M., Ein-audi, F., Escartin, J., Frost, B.R., Früh-Green, G., Fryer, P.B., Gee, J.S., Godard, M., Grimes, C.B., Halfpenny, A., Hansen, H.E., Harris, A.C., Tamura, A., Hayman, N.W., Hellebrand, E., Hirose, T., Hirth, J.G., Ishimaru, S., John-

- son, K.T.M., Karner, G.D., Linek, M., MacLeod, C.J., Maeda, J., Mason, O.U., McCaig, A.M., Michibayashi, K., Morris, A., Nakagawa, T., Nozaka, T., Rosner, M., Searle, R.C., Suhr, G., Tominaga, M., von der Handt, A., Yamasaki, T., and Zhao, X., 2011. Drilling constraints on lithospheric accretion and evolution at Atlantis Massif, Mid-Atlantic Ridge 30°N. *Journal of Geophysical Research: Solid Earth*, 116(B7):B07103.
<https://doi.org/10.1029/2010JB007931>
- Blackman, D.K., Ildefonse, B., John, B.E., Ohara, Y., Miller, D.J., MacLeod, C.J., and the Expedition 304/305 Scientists, 2006. Proceedings of the Integrated Ocean Drilling Program 304/305: College Station, TX (Integrated Ocean Drilling Program Management International, Inc.). <https://doi.org/10.2204/iodp.proc.304305.2006>
- Blackman, D.K., Karson, J.A., Kelley, D.S., Cann, J.R., Früh-Green, G.L., Gee, J.S., Hurst, S.D., John, B.E., Morgan, J., Nooner, S.L., Ross, D.K., Schroeder, T.J., and Williams, E.A., 2002. Geology of the Atlantis Massif (Mid-Atlantic Ridge, 30°N): Implications for the evolution of an ultramafic oceanic core complex. *Marine Geophysical Research*, 23(5):443–469. <https://doi.org/10.1023/B:MARI.0000018232.14085.75>
- Blackman, D.K., Slagle, A.L., Guerin, G., and Harding, A., 2014. Geophysical signatures of past and present hydration within a young oceanic core complex. *Geophysical Research Letters*, 41(4):1179–1186.
<https://doi.org/10.1002/2013GL058111>
- Boschi, C., Früh-Green, G.L., Delacour, A., Karson, J.A., and Kelley, D.S., 2006. Mass transfer and fluid flow during detachment faulting and development of an oceanic core complex, Atlantis Massif (MAR 30°N). *Geochemistry, Geophysics, Geosystems*, 7(1):Q01004. <https://doi.org/10.1029/2005GC001074>
- Bradley, A.S., Hayes, J.M., and Summons, R.E., 2009. Extraordinary ¹³C enrichment of diether lipids at the Lost City hydrothermal field indicates a carbon-limited ecosystem. *Geochimica et Cosmochimica Acta*, 73(1):102–118.
<https://doi.org/10.1016/j.gca.2008.10.005>
- Brazelton, W.J., and Baross, J.A., 2010. Metagenomic comparison of two *Thiomicrospira* lineages inhabiting contrasting deep-sea hydrothermal environments. *PloS One*, 5(10):e13530.
<https://doi.org/10.1371/journal.pone.0013530>
- Brazelton, W.J., Ludwig, K.A., Sogin, M.L., Andreishcheva, E.N., Kelley, D.S., Shen, C.-C., Edwards, R.L., and Baross, J.A., 2010. Archaea and bacteria with surprising microdiversity show shifts in dominance over 1,000-year time scales in hydrothermal chimneys. *Proceedings of the National Academy of Sciences of the United States of America*, 107(4):1612–1617. <https://doi.org/10.1073/pnas.0905369107>
- Brazelton, W.J., Schrenk, M.O., Kelley, D.S., and Baross, J.A., 2006. Methane- and sulfur-metabolizing microbial communities dominate the Lost City hydrothermal field ecosystem. *Applied and Environmental Microbiology*, 72(9):6257–6270. <https://doi.org/10.1128/AEM.00574-06>
- Canales, J.P., Tucholke, B.E., and Collins, J.A., 2004. Seismic reflection imaging of an oceanic detachment fault: Atlantis megamullion (Mid-Atlantic Ridge, 30°10'N). *Earth and Planetary Science Letters*, 222(2):543–560.
<https://doi.org/10.1016/j.epsl.2004.02.023>
- Canales, J.P., Tucholke, B.E., Xu, M., Collins, J.A., and DuBois, D.L., 2008. Seismic evidence for large-scale compositional heterogeneity of oceanic core complexes. *Geochemistry, Geophysics, Geosystems*, 9(8):Q08002.
<https://doi.org/10.1029/2008GC002009>
- Cann, J.R., Blackman, D.K., Smith, D.K., McAllister, E., Janssen, B., Mello, S., Avgerinos, E., Pascoe, A.R., and Escartin, J., 1997. Corrugated slip surfaces formed at ridge–transform intersections on the Mid-Atlantic Ridge. *Nature*, 385(6614):329–332. <https://doi.org/10.1038/385329a0>
- Cann, J.R., McCaig, A.M., and Yardley, B.W.D., 2015. Rapid generation of reaction permeability in the roots of black smoker systems, Troodos ophiolite, Cyprus. *Geofluids*, 15(1–2):179–192. <https://doi.org/10.1111/gfl.12117>
- Cannat, M., 1996. How thick is the magmatic crust at slow spreading oceanic ridges? *Journal of Geophysical Research: Solid Earth*, 101(B2):2847–2857. <https://doi.org/10.1029/95JB03116>
- Cannat, M., Karson, J.A., Miller, D.J., et al., 1995. Proceedings of the Ocean Drilling Program, Initial Reports, 153: College Station, TX (Ocean Drilling Program). <https://doi.org/10.2973/odp.proc.ir.153.1995>
- Coogan, L.A., Kempton, P.D., Saunders, A.D., and Norry, M.J., 2000a. Melt aggregation within the crust beneath the Mid-Atlantic Ridge: evidence from plagioclase and clinopyroxene major and trace element compositions. *Earth and Planetary Science Letters*, 176(2):245–257. [https://doi.org/10.1016/S0012-821X\(00\)00006-6](https://doi.org/10.1016/S0012-821X(00)00006-6)
- Coogan, L.A., Saunders, A.D., Kempton, P.D., and Norry, M.J., 2000b. Evidence from oceanic gabbros for porous melt migration within a crystal mush beneath the Mid-Atlantic Ridge. *Geochemistry, Geophysics, Geosystems*, 1(9).
<https://doi.org/10.1029/2000GC000072>
- de Ronde, C.E.J., Humphris, S.E., Höfig, T.W., Brandl, P.A., Cai, L., Cai, Y., Caratori Tontini, F., Deans, J.R., Farough, A., Jamieson, J.W., Kolandaivelu, K.P., Kutovaya, A., Labonté, J.M., Martin, A.J., Massiot, C., McDermott, J.M., McIn-tosh, I.M., Nozaki, T., Pellizari, V.H., Reyes, A.G., Roberts, S., Rouxel, O., Schlicht, L.E.M., Seo, J.H., Straub, S.M., Strehlow, K., Takai, K., Tanner, D., Tepley III, F.J., and Zhang, C., 2019. Expedition 376 methods. In de Ronde, C.E.J., Humphris, S.E., Höfig, T.W., and the Expedition 376 Scientists, *Brothers Arc Flux. Proceedings of the International Ocean Discovery Program, 376*: College Station, TX (International Ocean Discovery Program).
<https://doi.org/10.14379/iodp.proc.376.102.2019>
- Denny, A.R., Kelley, D.S., and Früh-Green, G.L., 2016. Geologic evolution of the Lost City Hydrothermal Field. *Geochemistry, Geophysics, Geosystems*, 17(2):375–394. <https://doi.org/10.1002/2015GC005869>
- Detrick, R.S., and Collins, J.A., 1998. Seismic structure of ultramafics exposed at shallow crustal levels in the Mid-Atlantic Ridge rift valley at 15°N. *Eos, Transactions of the American Geophysical Union*, 79:F800.
- Dick, H.J.B., MacLeod, C.J., Blum, P., Abe, N., Blackman, D.K., Bowles, J.A., Cheadle, M.J., Cho, K., Ciazela, J., Deans, J.R., Edgcomb, V.P., Ferrando, C., France, L., Ghosh, B., Ildefonse, B.M., Kendrick, M.A., Koepke, J.H., Leong, J.A.M., Chuangzhou, L., Qiang, M., Morishita, T., Morris, A., Natland, J.H., Nozaka, T., Pluempfer, O., Sanfilippo, A., Sylvan, J.B., Tivey, M.A., Tribuzio, R., and Viegas, L.G.F., 2017. Expedition 360 summary. In MacLeod, C.J., Dick, H.J.B., Blum, P., and the Expedition 360 Scientists, *Southwest Indian Ridge Lower Crust and Moho. Proceedings of*

- the International Ocean Discovery Program, 360: College Station, TX (International Ocean Discovery Program). <https://doi.org/10.14379/iodp.proc.360.101.2017>
- Drouin, M., Godard, M., Ildefonse, B., Bruguier, O., and Garrido, C.J., 2009. Geochemical and petrographic evidence for magmatic impregnation in the oceanic lithosphere at Atlantis Massif, Mid-Atlantic Ridge (IODP Hole U1309D, 30°N). *Chemical Geology*, 264(1):71–88. <https://doi.org/10.1016/j.chemgeo.2009.02.013>
- Drouin, M., Ildefonse, B., and Godard, M., 2010. A microstructural imprint of melt impregnation in slow spreading lithosphere: olivine-rich troctolites from the Atlantis Massif, Mid-Atlantic Ridge, 30°N, IODP Hole U1309D. *Geochemistry, Geophysics, Geosystems*, 11(6):Q06003. <https://doi.org/10.1029/2009GC002995>
- Escartín, J., and Canales, J.P., 2011. Detachments in oceanic lithosphere: deformation, magmatism, fluid flow, and ecosystems. *Eos, Transactions American Geophysical Union*, 92(4):31. <https://doi.org/10.1029/2011EO040003>
- Escartín, J., John, B., Cannat, M., Olive, J.-A., Cheadle, M., Früh-Green, G., and Cotterill, C., 2022. Tectonic termination of oceanic detachment faults, with constraints on tectonic uplift and mass wasting related erosion rates. *Earth and Planetary Science Letters*, 584:117449. <https://doi.org/10.1016/j.epsl.2022.117449>
- Expedition 340T Scientists, 2012. Atlantis Massif Oceanic Core Complex: velocity, porosity, and impedance contrasts within the domal core of Atlantis Massif: faults and hydration of lithosphere during core complex evolution. Integrated Ocean Drilling Program Preliminary Report, 340T. <https://doi.org/10.2204/iodp.pr.340T.2012>
- Ferrando, C., Godard, M., Ildefonse, B., and Rampone, E., 2018. Melt transport and mantle assimilation at Atlantis Massif (IODP Site U1309): constraints from geochemical modeling. *Lithos*, 323:24–43. <https://doi.org/10.1016/j.lithos.2018.01.012>
- Ferrando, C., Lynn, K.J., Basch, V., Ildefonse, B., and Godard, M., 2020. Retrieving timescales of oceanic crustal evolution at oceanic core complexes: insights from diffusion modelling of geochemical profiles in olivine. *Lithos*, 376–377:105727. <https://doi.org/10.1016/j.lithos.2020.105727>
- Foustoukos, D.I., Savov, I.P., and Janecky, D.R., 2008. Chemical and isotopic constraints on water/rock interactions at the Lost City hydrothermal field, 30°N Mid-Atlantic Ridge. *Geochimica et Cosmochimica Acta*, 72(22):5457–5474. <https://doi.org/10.1016/j.gca.2008.07.035>
- Foustoukos, D.I., and Seyfried, W.E., 2004. Hydrocarbons in hydrothermal vent fluids: the role of chromium-bearing catalysts. *Science*, 304(5673):1002–1005. <https://doi.org/10.1126/science.1096033>
- Frost, B.R., Beard, J.S., McCaig, A., and Condliffe, E., 2008. The formation of micro-rodingites from IODP Hole U1309D: key to understanding the process of serpentinization. *Journal of Petrology*, 49(9):1579–1588. <https://doi.org/10.1093/petrology/egn038>
- Früh-Green, G.L., Connolly, J.A.D., Plas, A., Kelley, D.S., and Grobéty, B., 2004. Serpentinization of oceanic peridotites: implications for geochemical cycles and biological activity. In Wilcock, W.S.D., Delong, E.F., Kelley, D.S., Baross, J.A., and Cary, S.C. (Eds.), *The Subseafloor Biosphere at Mid-Ocean Ridges*. Geophysical Monograph, 144: 119–136. <https://doi.org/10.1029/144GM08>
- Früh-Green, G.L., Kelley, D.S., Bernasconi, S.M., Karson, J.A., Ludwig, K.A., Butterfield, D.A., Boschi, C., and Proskurowski, G., 2003. 30,000 years of hydrothermal activity at the Lost City vent field. *Science*, 301(5632):495–498. <https://doi.org/10.1126/science.1085582>
- Früh-Green, G.L., Orcutt, B.N., Green, S., Cotterill, C., and the Expedition 357 Scientists, 2016. Expedition 357 Preliminary Report: Atlantis Massif Serpentinization and Life. International Ocean Discovery Program. <https://doi.org/10.14379/iodp.pr.357.2016>
- Früh-Green, G.L., Orcutt, B.N., Green, S.L., Cotterill, C., Morgan, S., Akizawa, N., Bayrakci, G., Behrmann, J.-H., Boschi, C., Brazelton, W.J., Cannat, M., Dunkel, K.G., Escartín, J., Harris, M., Herrero-Bervera, E., Hesse, K., John, B.E., Lang, S.Q., Lilley, M.D., Liu, H.-Q., Mayhew, L.E., McCaig, A.M., Menez, B., Morono, Y., Quéméneur, M., Rouméjon, S., Sandaruwan Ratnayake, A., Schrenk, M.O., Schwarzenbach, E.M., Twing, K.I., Weis, D., Whattam, S.A., Williams, M., and Zhao, R., 2017. Expedition 357 summary. In Früh-Green, G.L., Orcutt, B.N., Green, S.L., Cotterill, C., and the Expedition 357 Scientists, *Atlantis Massif Serpentinization and Life*. Proceedings of the International Ocean Discovery Program, 357: College Station, TX (International Ocean Discovery Program). <https://doi.org/10.14379/iodp.proc.357.101.2017>
- Früh-Green, G.L., Orcutt, B.N., Rouméjon, S., Lilley, M.D., Morono, Y., Cotterill, C., Green, S., Escartín, J., John, B.E., McCaig, A.M., Cannat, M., Menez, B., Schwarzenbach, E.M., Williams, M.J., Morgan, S., Lang, S.Q., Schrenk, M.O., Brazelton, W.J., Akizawa, N., Boschi, C., Dunkel, K.G., Quéméneur, M., Whattam, S.A., Mayhew, L., Harris, M., Bayrakci, G., Behrmann, J.-H., Herrero-Bervera, E., Hesse, K., Liu, H.-Q., Ratnayake, A.S., Twing, K., Weis, D., Zhao, R., and Bilenker, L., 2018. Magmatism, serpentinization and life: insights through drilling the Atlantis Massif (IODP Expedition 357). *Lithos*, 323:137–155. <https://doi.org/10.1016/j.lithos.2018.09.012>
- Gillis, K., Mével, C., Allan, J., et al., 1993. Proceedings of the Ocean Drilling Program, Initial Reports, 147: College Station, TX (Ocean Drilling Program). <https://doi.org/10.2973/odp.proc.ir.147.1993>
- Gillis, K.M., Snow, J.E., Klaus, A., Guerin, G., Abe, N., Akizawa, N., Ceuleneer, G., Cheadle, M.J., Adrião, Á., Faak, K., Falloon, T.J., Friedman, S.A., Godard, M.M., Harigane, Y., Horst, A.J., Hoshide, T., Ildefonse, B., Jean, M.M., John, B.E., Koepke, J.H., Machi, S., Maeda, J., Marks, N.E., McCaig, A.M., Meyer, R., Morris, A., Nozaka, T., Python, M., Saha, A., and Wintsch, R.P., 2014. Expedition 345 summary. In Gillis, K.M., Snow, J.E., Klaus, A., and the Expedition 345 Scientists, *Proceedings of the Integrated Ocean Drilling Program*. 345: College Station, TX (Integrated Ocean Drilling Program). <https://doi.org/10.2204/iodp.proc.345.101.2014>
- Godard, M., Awaji, S., Hansen, H., Hellebrand, E., Brunelli, D., Johnson, K., Yamasaki, T., Maeda, J., Abratis, M., Christie, D., Kato, Y., Mariet, C., and Rosner, M., 2009. Geochemistry of a long in-situ section of intrusive slow-spread oceanic lithosphere: results from IODP Site U1309 (Atlantis Massif, 30°N Mid-Atlantic-Ridge). *Earth and Planetary Science Letters*, 279(1–2):110–122. <https://doi.org/10.1016/j.epsl.2008.12.034>
- Godard, M., Lagabrielle, Y., Alard, O., and Harvey, J., 2008. Geochemistry of the highly depleted peridotites drilled at ODP Sites 1272 and 1274 (Fifteen-Twenty Fracture Zone, Mid-Atlantic Ridge): implications for mantle dynamics

- beneath a slow spreading ridge. *Earth and Planetary Science Letters*, 267(3):410–425.
<https://doi.org/10.1016/j.epsl.2007.11.058>
- Goordial, J., D'Angelo, T., Labonté, J.M., Poulton, N.J., Brown, J.M., Stepanauskas, R., Früh-Green, G.L., Orcutt, B.N., and Dubilier, N., 2021. Microbial diversity and function in shallow subsurface sediment and oceanic lithosphere of the Atlantis Massif. *MBio*, 12(4):e00490–00421. <https://journals.asm.org/doi/abs/10.1128/mBio.00490-21>
- Grimes, C.B., John, B.E., Cheadle, M.J., and Wooden, J.L., 2008. Protracted construction of gabbroic crust at a slow spreading ridge; constraints from ²⁰⁶Pb/²³⁸U zircon ages from Atlantis Massif and IODP Hole U1309D (30°N, MAR). *Geochemistry, Geophysics, Geosystems*, 9(8):Q08012. <https://doi.org/10.1029/2008GC002063>
- Harding, A.J., Arnulf, A.F., and Blackman, D.K., 2016. Velocity structure near IODP Hole U1309D, Atlantis Massif, from waveform inversion of streamer data and borehole measurements. *Geochemistry, Geophysics, Geosystems*, 17(6):1990–2014. <https://doi.org/10.1002/2016GC006312>
- Henig, A.S., Blackman, D.K., Harding, A.J., Canales, J.-P., and Kent, G.M., 2012. Downward continued multichannel seismic refraction analysis of Atlantis Massif oceanic core complex, 30°N, Mid-Atlantic Ridge. *Geochemistry, Geophysics, Geosystems*, 13(5):Q0AG07. <https://doi.org/10.1029/2012GC004059>
- Heuer, V.B., Inagaki, F., Morono, Y., Kubo, Y., Spivack, A.J., Viehweger, B., Treude, T., Beulig, F., Schubotz, F., Tonai, S., Bowden, S.A., Cramm, M., Henkel, S., Hirose, T., Homola, K., Hoshino, T., Ijiri, A., Imachi, H., Kamiya, N., Kaneko, M., Lagostina, L., Manners, H., McClelland, H.-L., Metcalfe, K., Okutsu, N., Pan, D., Raudsepp, M.J., Sauvage, J., Tsang, M.-Y., Wang, D.T., Whitaker, E., Yamamoto, Y., Yang, K., Maeda, L., Adhikari, R.R., Glombitza, C., Hamada, Y., Kallmeyer, J., Wendt, J., Wörmer, L., Yamada, Y., Kinoshita, M., and Hinrichs, K.-U., 2020. Temperature limits to deep seafloor life in the Nankai Trough subduction zone. *Science*, 370(6521):1230–1234.
<https://doi.org/10.1126/science.abd7934>
- Ildefonse, B., Abe, N., Godard, M., Morris, A., Teagle, D.A.H., and Umino, S., 2014. Formation and evolution of oceanic lithosphere: new insights on crustal structure and igneous geochemistry from ODP/IODP Sites 1256, U1309, and U1415. In Stein, R., Blackman, D.K., Inagaki, F., and Larsen, H.-C. (Eds.), *Earth and Life Processes Discovered from Subseafloor Environments: A Decade of Science Achieved by the Integrated Ocean Drilling Program (IODP)*. R. Stein (Series Ed.). *Developments in Marine Geology*, 7: New York (Elsevier), 449–505.
<https://doi.org/10.1016/B978-0-444-62617-2.00017-7>
- Ildefonse, B., Blackman, D., John, B.E., Ohara, Y., Miller, D.J., MacLeod, C., and the Integrated Ocean Drilling Program Expeditions 304/305 Science Party, 2007. Oceanic core complexes and crustal accretion at slow-spreading ridges. *Geology*, 35(7):623–626. <https://doi.org/10.1130/G23531A.1>
- John, B.E., Cheadle, M.J., Gee, J.S., Grimes, C.B., Morris, A., and Pressling, N., 2009. Data report: spatial and temporal evolution of slow spread oceanic crust; graphic sections of core recovered from IODP Hole U1309D, Atlantis Massif, 30°N, MAR (including Pb/U zircon geochronology and magnetic remanence data). In Blackman, D.K., Ildefonse, B., John, B.E., Ohara, Y., Miller, D.J., MacLeod, C.J., and the Expedition 304/305 Scientists, *Proceedings of the Integrated Ocean Drilling Program 304/305*: College Station, TX (Integrated Ocean Drilling Program Management International, Inc.). <https://doi.org/10.2204/iodp.proc.304305.205.2009>
- Kallmeyer, J., 2017. Contamination control for scientific drilling operations. In Sariaslani, S. and Gadd, G.M., *Advances in Applied Microbiology (Volume 98)*. Cambridge, MA (Academic Press), 61–91.
<https://doi.org/10.1016/bs.aambs.2016.09.003>
- Karson, J.A., Cannat, M., Miller, J., and the ODP Leg 153 Shipboard Scientific Party, 1997. Drilling tectonic windows into the lower crust and upper mantle: ODP Leg 153. *JOIDES Journal*, 23(1):14–15.
http://www-odp.tamu.edu/publications/citations/joides_j/joides_j_23_1.pdf#page=14
- Karson, J.A., Früh-Green, G.L., Kelley, D.S., Williams, E.A., Yoerger, D.R., and Jakuba, M., 2006. Detachment shear zone of the Atlantis Massif core complex, Mid-Atlantic Ridge, 30°N. *Geochemistry, Geophysics, Geosystems*, 7(6):Q06016. <https://doi.org/10.1029/2005GC001109>
- Kelemen, P.B., Kikawa, E., Miller, D.J., et al., 2004. *Proceedings of the Ocean Drilling Program, Initial Reports: College Station, TX (Ocean Drilling Program)*. <https://doi.org/10.2973/odp.proc.ir.209.2004>
- Kelley, D.S., Baross, J.A., and Delaney, J.R., 2002a. Volcanoes, fluids, and life at mid-ocean ridge spreading centers. *Annual Review of Earth and Planetary Sciences*, 30(1):385–491.
<https://doi.org/10.1146/annurev.earth.30.091201.141331>
- Kelley, D.S., and Früh-Green, G.L., 1999. Abiogenic methane in deep-seated mid-ocean ridge environments: Insights from stable isotope analyses. *Journal of Geophysical Research: Solid Earth*, 104(B5):10439–10460.
<https://doi.org/10.1029/1999JB900058>
- Kelley, D.S., and Früh-Green, G.L., 2001. Volatile lines of descent in submarine plutonic environments: insights from stable isotope and fluid inclusion analyses. *Geochimica et Cosmochimica Acta*, 65(19):3325–3346.
[https://doi.org/10.1016/S0016-7037\(01\)00667-6](https://doi.org/10.1016/S0016-7037(01)00667-6)
- Kelley, D.S., Karson, J.A., Blackman, D.K., Früh-Green, G.L., Butterfield, D.A., Lilley, M.D., Olson, E.J., Schrenk, M.O., Roe, K.K., Lebon, G.T., Rivizzigno, P., and the AT3-60 Shipboard Party, 2001. An off-axis hydrothermal vent field near the Mid-Atlantic Ridge at 30°N. *Nature*, 412(6843):145–149. <https://doi.org/10.1038/35084000>
- Kelley, D.S., Karson, J.A., Früh-Green, G., and Schrenk, M.O., 2002b. Ultramafic-hosted hydrothermal systems: the Lost City Field as a possible guide for early life. *Astrobiology*, 2(4):449–450.
- Kelley, D.S., Karson, J.A., Früh-Green, G.L., Yoerger, D.R., Shank, T.M., Butterfield, D.A., Hayes, J.M., Schrenk, M.O., Olson, E.J., Proskurowski, G., Jakuba, M., Bradley, A., Larson, B., Ludwig, K., Glickson, D., Buckman, K., Bradley, A.S., Brazelton, W.J., Roe, K., Elend, M.J., Delacour, A.I., Bernasconi, S.M., Lilley, M.D., Baross, J.A., Summons, R.E., and Sylva, S.P., 2005. A serpentinite-hosted ecosystem: the Lost City hydrothermal field. *Science*, 307(5714):1428–1434. <https://doi.org/10.1126/science.1102556>
- Klein, F., and Bach, W., 2009. Fe–Ni–Co–O–S phase relations in peridotite–seawater interactions. *Journal of Petrology*, 50(1):37–59. <https://doi.org/10.1093/petrology/egn071>

- Klein, F., Bach, W., Humphris, S.E., Kahl, W.-A., Jöns, N., Moskowit, B., and Berquó, T.S., 2014. Magnetite in seafloor serpentinite—some like it hot. *Geology*, 42(2):135–138. <https://doi.org/10.1130/G35068.1>
- Klein, F., Bach, W., Jöns, N., McCollom, T., Moskowit, B., and Berquó, T., 2009. Iron partitioning and hydrogen generation during serpentinization of abyssal peridotites from 15°N on the Mid-Atlantic Ridge. *Geochimica et Cosmochimica Acta*, 73(22):6868–6893. <https://doi.org/10.1016/j.gca.2009.08.021>
- Klein, F., Bach, W., and McCollom, T.M., 2013. Compositional controls on hydrogen generation during serpentinization of ultramafic rocks. *Lithos*, 178:55–69. <https://doi.org/10.1016/j.lithos.2013.03.008>
- Klein, F., Grozeva, N.G., and Seewald, J.S., 2019. Abiotic methane synthesis and serpentinization in olivine-hosted fluid inclusions. *Proceedings of the National Academy of Sciences of the United States of America*, 116(36):17666–17672. <https://doi.org/10.1073/pnas.1907871116>
- Klein, F., and Le Roux, V., 2020. Quantifying the volume increase and chemical exchange during serpentinization. *Geology*, 48(6):552–556. <https://doi.org/10.1130/G47289.1>
- Klein, F., Marschall, H.R., Bowring, S.A., Humphris, S.E., and Horning, G., 2017. Mid-ocean ridge serpentinite in the Puerto Rico Trench: from seafloor spreading to subduction. *Journal of Petrology*, 58(9):1729–1754. <https://doi.org/10.1093/petrology/egx071>
- Lambart, S., Koornneef, J.M., Millet, M.-A., Davies, G.R., Cook, M., and Lissenberg, C.J., 2019. Highly heterogeneous depleted mantle recorded in the lower oceanic crust. *Nature Geoscience*, 12(6):482–486. <https://doi.org/10.1038/s41561-019-0368-9>
- Lang, S.Q., and Brazelton, W.J., 2020. Habitability of the marine serpentinite subsurface: a case study of the Lost City hydrothermal field. *Philosophical Transactions of the Royal Society A: Mathematical, Physical and Engineering Sciences*, 378(2165):20180429. <https://doi.org/10.1098/rsta.2018.0429>
- Lang, S.Q., Butterfield, D.A., Schulte, M., Kelley, D.S., and Lilley, M.D., 2010. Elevated concentrations of formate, acetate and dissolved organic carbon found at the Lost City hydrothermal field. *Geochimica et Cosmochimica Acta*, 74(3):941–952. <https://doi.org/10.1016/j.gca.2009.10.045>
- Lang, S.Q., Früh-Green, G.L., Bernasconi, S.M., Brazelton, W.J., Schrenk, M.O., and McGonigle, J.M., 2018. Deeply-sourced formate fuels sulfate reducers but not methanogens at Lost City hydrothermal field. *Scientific Reports*, 8(1):755. <https://doi.org/10.1038/s41598-017-19002-5>
- Lang, S.Q., Früh-Green, G.L., Bernasconi, S.M., Lilley, M.D., Proskurowski, G., Méhay, S., and Butterfield, D.A., 2012. Microbial utilization of abiogenic carbon and hydrogen in a serpentinite-hosted system. *Geochimica et Cosmochimica Acta*, 92:82–99. <https://doi.org/10.1016/j.gca.2012.06.006>
- Lang, S.Q., Lilley, M.D., Baumberger, T., Früh-Green, G.L., Walker, S.L., Brazelton, W.J., Kelley, D.S., Elend, M., Butterfield, D.A., and Mau, A.J., 2021. Extensive decentralized hydrogen export from the Atlantis Massif. *Geology*, 49(7):851–856. <https://doi.org/10.1130/G48322.1>
- Liebmann, J., Schwarzenbach, E.M., Früh-Green, G.L., Boschi, C., Rouméjon, S., Strauss, H., Wiechert, U., and John, T., 2018. Tracking water-rock interaction at the Atlantis Massif (MAR, 30°N) using sulfur geochemistry. *Geochemistry, Geophysics, Geosystems*, 19(11):4561–4583. <https://doi.org/10.1029/2018GC007813>
- Lissenberg, C.J., and MacLeod, C.J., 2017. A reactive porous flow control on mid-ocean ridge magmatic evolution. *Journal of Petrology*, 57(11-12):2195–2220. <https://doi.org/10.1093/petrology/egw074>
- Lowell, R.P., 2017. A fault-driven circulation model for the Lost City hydrothermal field. *Geophysical Research Letters*, 44(6):2703–2709. <https://doi.org/10.1002/2016GL072326>
- Ludwig, K.A., Shen, C.-C., Kelley, D.S., Cheng, H., and Edwards, R.L., 2011. U–Th systematics and ²³⁰Th ages of carbonate chimneys at the Lost City hydrothermal field. *Geochimica et Cosmochimica Acta*, 75(7):1869–1888. <https://doi.org/10.1016/j.gca.2011.01.008>
- Magenheim, A.J., Spivack, A.J., Alt, J.C., Bayhurst, G., Chan, L.H., Zuleger, E., and Gieskes, J.M., 1995. Borehole fluid chemistry in Hole 504B, Leg 137: formation water or in-situ reaction. In Erzinger, J., Becker, K., Dick, H.J.B., and Stokking, L.B. (Eds.), *Proceedings of the Ocean Drilling Program, Scientific Results, 137/140*: College Station, TX (Ocean Drilling Program), 141–152. <https://doi.org/10.2973/odp.proc.sr.137140.024.1995>
- Malvoisin, B., Zhang, C., Müntener, O., Baumgartner, L.P., Kelemen, P.B., and the Oman Drilling Project Science Party, 2020. Measurement of volume change and mass transfer during serpentinization: insights from the Oman Drilling Project. *Journal of Geophysical Research: Solid Earth*, 125(5):e2019JB018877. <https://doi.org/10.1029/2019JB018877>
- Martin, W., Baross, J., Kelley, D., and Russell, M.J., 2008. Hydrothermal vents and the origin of life. *Nature Reviews Microbiology*, 6(11):805–814. <https://doi.org/10.1038/nrmicro1991>
- Martin, W., and Russell, M.J., 2006. On the origin of biochemistry at an alkaline hydrothermal vent. *Philosophical Transactions of the Royal Society B: Biological Sciences*, 362:1887–1925. <https://doi.org/10.1098/rstb.2006.1881>
- Mason, O.U., Nakagawa, T., Rosner, M., Van Nostrand, J.D., Zhou, J., Maruyama, A., Fisk, M.R., and Giovannoni, S.J., 2010. First investigation of the microbiology of the deepest layer of ocean crust. *PLoS One*, 5(11):e15399. <https://doi.org/10.1371/journal.pone.0015399>
- McCaig, A., Lang, S.Q., and Blum, P., 2022. Expedition 399 Scientific Prospectus: Building Blocks of Life, Atlantis Massif. *International Ocean Discovery Program*. <https://doi.org/10.14379/iodp.sp.399.2022>
- McCaig, A.M., Delacour, A., Fallick, A.E., Castelain, T., and Früh-Green, G.L., 2010. Detachment fault control on hydrothermal circulation systems: interpreting the subsurface beneath the TAG hydrothermal field using the isotopic and geological evolution of oceanic core complexes in the Atlantic. In Rona, P., Devey, C.W., Dymant, J., and Murton, B.J. (Eds.), *Diversity of Hydrothermal Systems on Slow Spreading Ocean Ridges*. *Geophysical Monograph*, 188: 207–239. <https://doi.org/10.1029/2008GM000729>
- McCaig, A.M., and Harris, M., 2012. Hydrothermal circulation and the dike-gabbro transition in the detachment mode of slow seafloor spreading. *Geology*, 40(4):367–370. <https://doi.org/10.1130/G32789.1>

- McCullom, T.M., and Bach, W., 2009. Thermodynamic constraints on hydrogen generation during serpentinization of ultramafic rocks. *Geochimica et Cosmochimica Acta*, 73(3):856–875. <https://doi.org/10.1016/j.gca.2008.10.032>
- McCullom, T.M., Klein, F., Robbins, M., Moskowitz, B., Berquó, T.S., Jöns, N., Bach, W., and Templeton, A., 2016. Temperature trends for reaction rates, hydrogen generation, and partitioning of iron during experimental serpentinization of olivine. *Geochimica et Cosmochimica Acta*, 181:175–200. <https://doi.org/10.1016/j.gca.2016.03.002>
- McCullom, T.M., and Seewald, J.S., 2007. Abiotic synthesis of organic compounds in deep-sea hydrothermal environments. *Chemical Reviews*, 107(2):382–401. <https://doi.org/10.1021/cr0503660>
- McCullom, T.M., and Seewald, J.S., 2013. Serpentinites, hydrogen, and life. *Elements*, 9(2):129–134. <https://doi.org/10.2113/gselements.9.2.129>
- McDermott, J.M., Seewald, J.S., German, C.R., and Sylva, S.P., 2015. Pathways for abiotic organic synthesis at submarine hydrothermal fields. *Proceedings of the National Academy of Sciences of the United States of America*, 112(25):7668–7672. <https://doi.org/10.1073/pnas.1506295112>
- McGonigle, J.M., Lang, S.Q., Brazelton, W.J., and Parales, R.E., 2020. Genomic evidence for formate Metabolism by *Chloroflexi* as the key to unlocking deep carbon in Lost City microbial ecosystems. *Applied and Environmental Microbiology*, 86(8):e02583-02519. <https://doi.org/10.1128/AEM.02583-19>
- Méhay, S., Früh-Green, G.L., Lang, S.Q., Bernasconi, S.M., Brazelton, W.J., Schrenk, M.O., Schaeffer, P., and Adam, P., 2013. Record of archaeal activity at the serpentinite-hosted Lost City hydrothermal field. *Geobiology*, 11(6):570–592. <https://doi.org/10.1111/gbi.12062>
- Ménez, B., Pisapia, C., Andreani, M., Jamme, F., Vanbellingen, Q.P., Brunelle, A., Richard, L., Dumas, P., and Réfrégiers, M., 2018. Abiotic synthesis of amino acids in the recesses of the oceanic lithosphere. *Nature*, 564(7734):59–63. <https://doi.org/10.1038/s41586-018-0684-z>
- Michibayashi, K., Hirose, T., Nozaka, T., Harigane, Y., Escartin, J., Delius, H., Linek, M., and Ohara, Y., 2008. Hydration due to high-T brittle failure within in situ oceanic crust, 30°N Mid-Atlantic Ridge. *Earth and Planetary Science Letters*, 275(3–4):348–354. <https://doi.org/10.1016/j.epsl.2008.08.033>
- Morris, A., Gee, J.S., Pressling, N., John, B.E., MacLeod, C.J., Grimes, C.B., and Searle, R.C., 2009. Footwall rotation in an oceanic core complex quantified using reoriented Integrated Ocean Drilling Program core samples. *Earth and Planetary Science Letters*, 287(1–2):217–228. <https://doi.org/10.1016/j.epsl.2009.08.007>
- Motamedi, S., Orcutt, B.N., Früh-Green, G.L., Twing, K.I., Pendleton, H.L., and Brazelton, W.J., 2020. Microbial residents of the Atlantis Massif's shallow serpentinite subsurface. *Applied and Environmental Microbiology*, 86(11):e00356-00320. <https://doi.org/10.1128/AEM.00356-20>
- Natland, J.H., and Dick, H.J.B., 2002. Stratigraphy and composition of gabbros drilled in Ocean Drilling Program Hole 735B, Southwest Indian Ridge: a synthesis of geochemical data. In Natland, J.H., Dick, H.J.B., Miller, D.J., and Von Herzen, R.P. (Eds.), *Proceedings of the Ocean Drilling Program, Scientific Results*. 176: College Station, TX (Ocean Drilling Program). <https://doi.org/10.2973/odp.proc.sr.176.002.2002>
- Nozaka, T., and Fryer, P., 2011. Alteration of the oceanic lower crust at a slow-spreading axis: insight from vein-related zoned halos in olivine gabbro from Atlantis Massif, Mid-Atlantic Ridge. *Journal of Petrology*, 52(4):643–664. <https://doi.org/10.1093/petrology/egq098>
- Nozaka, T., Fryer, P., and Andreani, M., 2008. Formation of clay minerals and exhumation of lower-crustal rocks at Atlantis Massif, Mid-Atlantic Ridge. *Geochemistry, Geophysics, Geosystems*, 9(11):Q11005. <https://doi.org/10.1029/2008GC002207>
- Pendleton, H.L., Twing, K.I., Motamedi, S., and Brazelton, W.J., 2021. Potential microbial contamination from drilling lubricants into subsurface rock cores. *Scientific Drilling*, 29:49–57. <https://doi.org/10.5194/sd-29-49-2021>
- Pisapia, C., Jamme, F., Duponchel, L., and Ménez, B., 2018. Tracking hidden organic carbon in rocks using chemometrics and hyperspectral imaging. *Scientific Reports*, 8(1):2396. <https://doi.org/10.1038/s41598-018-20890-4>
- Pressling, N., Morris, A., John, B.E., and MacLeod, C.J., 2012. The internal structure of an oceanic core complex: an integrated analysis of oriented borehole imagery from IODP Hole U1309D (Atlantis Massif). *Geochemistry, Geophysics, Geosystems*, 13(9):Q04G01. <https://doi.org/10.1029/2012GC004061>
- Proskurowski, G., Lilley, M.D., Seewald, J.S., Früh-Green, G.L., Olson, E.J., Lupton, J.E., Sylva, S.P., and Kelley, D.S., 2008. Abiogenic hydrocarbon production at Lost City hydrothermal field. *Science*, 319(5863):604–607. <https://doi.org/10.1126/science.1151194>
- Quéménéur, M., Erauso, G., Frouin, E., Zeghal, E., Vandecasteele, C., Ollivier, B., Tamburini, C., Garel, M., Ménez, B., and Postec, A., 2019. Hydrostatic pressure helps to cultivate an original anaerobic bacterium from the Atlantis Massif subsurface (IODP Expedition 357): *Petrocella atlantisensis* gen. nov. sp. nov. *Frontiers in Microbiology*, 10:1497. <https://doi.org/10.3389/fmicb.2019.01497>
- Rouméjon, S., Früh-Green, G., Orcutt, B.N., and the Expedition 357 Science Party, 2017. Alteration heterogeneities in peridotites exhumed on the southern wall of the Atlantis Massif (IODP Expedition 357). *Journal of Petrology*, 59(7):1329–1358. <https://doi.org/10.1093/petrology/egy065>
- Schoolmeesters, N., Cheadle, M.J., John, B.E., Reiners, P.W., Gee, J., and Grimes, C.B., 2012. The cooling history and the depth of detachment faulting at the Atlantis Massif oceanic core complex. *Geochemistry, Geophysics, Geosystems*, 13(10):Q0AG12. <https://doi.org/10.1029/2012GC004314>
- Schrenk, M.O., Brazelton, W.J., and Lang, S.Q., 2013. Serpentinization, carbon, and deep life. *Reviews in Mineralogy and Geochemistry*, 75(1):575–606. <https://doi.org/10.2138/rmg.2013.75.18>
- Schrenk, M.O., Kelley, D.S., Bolton, S.A., and Baross, J.A., 2004. Low archaeal diversity linked to subsurface geochemical processes at the Lost City hydrothermal field, Mid-Atlantic Ridge. *Environmental Microbiology*, 6(10):1086–1095. <https://doi.org/10.1111/j.1462-2920.2004.00650.x>

- Schroeder, T., and John, B.E., 2004. Strain localization on an oceanic detachment fault system, Atlantis Massif, 30°N, Mid-Atlantic Ridge. *Geochemistry, Geophysics, Geosystems*, 5(11):Q11007. <https://doi.org/10.1029/2004GC000728>
- Schroeder, T., John, B., and Frost, B.R., 2002. Geologic implications of seawater circulation through peridotite exposed at slow-spreading mid-ocean ridges. *Geology*, 30(4):367–370. [https://doi.org/10.1130/0091-7613\(2002\)030<0367:GIOSCT>2.0.CO;2](https://doi.org/10.1130/0091-7613(2002)030<0367:GIOSCT>2.0.CO;2)
- Seyfried, W.E., Pester, N.J., Tutolo, B.M., and Ding, K., 2015. The Lost City hydrothermal system: constraints imposed by vent fluid chemistry and reaction path models on seafloor heat and mass transfer processes. *Geochimica et Cosmochimica Acta*, 163:59–79. <https://doi.org/10.1016/j.gca.2015.04.040>
- Sojo, V., Herschy, B., Whicher, A., Camprubí, E., and Lane, N., 2016. The origin of life in alkaline hydrothermal vents. *Astrobiology*, 16(2):181–197. <https://doi.org/10.1089/ast.2015.1406>
- Stüeken, E.E., Anderson, R.E., Bowman, J.S., Brazelton, W.J., Colangelo-Lillis, J., Goldman, A.D., Som, S.M., and Baross, J.A., 2013. Did life originate from a global chemical reactor? *Geobiology*, 11(2):101–126. <https://doi.org/10.1111/gbi.12025>
- Suhr, G., Hellebrand, E., Johnson, K., and Brunelli, D., 2008. Stacked gabbro units and intervening mantle; a detailed look at a section of IODP Leg 305, Hole U1309D. *Geochemistry, Geophysics, Geosystems*, 9(10):Q10007. <https://doi.org/10.1029/2008GC002012>
- Summit, M., and Baross, J.A., 2001. A novel microbial habitat in the mid-ocean ridge seafloor. *Proceedings of the National Academy of Sciences of the United States of America*, 98(5):2158–2163. <https://doi.org/10.1073/pnas.051516098>
- Sylvan, J.B., Estes, E.R., Bogus, K., Colwell, F.S., Orcutt, B.N., and Smith, D.C., 2021. Technical Note 4: Recommendations for microbiological sampling and contamination tracer use aboard the JOIDES Resolution following 20 years of IODP deep biosphere research. *International Ocean Discovery Program*. <https://doi.org/10.14379/iodp.tn.4.2021>
- Tamura, A., Arai, S., Ishimaru, S., and Andai, E.S., 2008. Petrology and geochemistry of peridotites from IODP Site U1309 at Atlantis Massif, MAR 30°N: micro- and macro-scale melt penetrations into peridotites. *Contributions to Mineralogy and Petrology*, 155(4):491–509. <https://doi.org/10.1007/s00410-007-0254-0>
- Teagle, D.A.H., Alt, J.C., Umino, S., Miyashita, S., Banerjee, N.R., Wilson, D.S., and the Expedition 309/312 Scientists, 2006. *Proceedings of the Integrated Ocean Drilling Program, 309/312*: Washington, DC (Integrated Ocean Drilling Program Management International, Inc.). <https://doi.org/10.2204/iodp.proc.309312.2006>
- Ternieten, L., Früh-Green, G.L., and Bernasconi, S.M., 2021. Distribution and sources of carbon in serpentinized mantle peridotites at the Atlantis Massif (IODP Expedition 357). *Journal of Geophysical Research: Solid Earth*, 126(10):e2021JB021973. <https://doi.org/10.1029/2021JB021973>
- Titarenko, S.S., and McCaig, A.M., 2016. Modelling the Lost City hydrothermal field: influence of topography and permeability structure. *Geofluids*, 16(2):314–328. <https://doi.org/10.1111/gfl.12151>
- Wang, D.T., Reeves, E.P., McDermott, J.M., Seewald, J.S., and Ono, S., 2018. Clumped isotopologue constraints on the origin of methane at seafloor hot springs. *Geochimica et Cosmochimica Acta*, 223:141–158. <https://doi.org/10.1016/j.gca.2017.11.030>
- Wheat, C.G., Kitts, C., Webb, C., Stolzman, R., McGuire, A., Fournier, T., Pettigrew, T., and Jannasch, H., 2020. A new high-temperature borehole fluid sampler: the Multi-Temperature Fluid Sampler. *Scientific Drilling*, 28:43–48. <https://doi.org/10.5194/sd-28-43-2020>